Carbon-Carbon Bond Forming Reactions over Metal Oxide Catalysts

---

A Dissertation

Presented to

the faculty of the School of Engineering and Applied Science

University of Virginia

---

in partial fulfillment

of the requirements for the degree

Doctor of Philosophy

by

Joseph Thomas Kozlowski

May

2013

APPROVAL SHEET

The dissertation

is submitted in partial fulfillment of the requirements

for the degree of

Doctor of Philosophy

AUTHOR

The dissertation has been read and approved by the examining committee:

Robert Davis

Advisor

Matthew Neurock

Elizabeth Opila

Gary Koenig, Jr.

Roseanne Ford

Accepted for the School of Engineering and Applied Science:

Dean, School of Engineering and Applied Science

May

2013

Abstract

Alcohol coupling, also known as the Guerbet reaction, is a potentially important process to increase the value of short chain alcohols. Metal oxides, metal phosphates and supported transition metals like copper are some examples of heterogeneous catalysts for the reaction. However, the wide variety of catalyst compositions, reaction conditions, and reactor configurations used to study the reaction complicates a direct comparison of various catalysts. Herein, rates over different catalysts will be compared. One existing gap in the current literature is a thorough comparison of the surface acid and base properties of catalysts employed in the Guerbet coupling of alcohols. In this work, various bifunctional materials were synthesized, characterized, and used in Guerbet alcohol coupling and other probe reactions of acid and base catalysts.

One well-studied reaction catalyzed by acids and bases is transesterification. Two series of Mg:Zr mixed oxides, prepared by either co-precipitation or sol-gel synthesis, were characterized and evaluated in the base-catalyzed transesterification of tributyrin with methanol. A co-precipitated Mg-rich mixed oxide catalyst with Mg:Zr 11:1 was approximately 300% more active than MgO on a surface area basis, whereas pure ZrO_2 was inactive for the reaction. To explore the nature of the activity enhancement, samples were characterized by X-ray diffraction, N_2 adsorption, CO_2 adsorption microcalorimetry and DRIFTS of adsorbed CO_2 and CH_3OH. Although the sol-gel synthesis method provided better atomic-level mixing of Mg and Zr, the resulting catalysts were not as effective as mixed oxides prepared by co-precipitation. The most active mixed oxide (Mg:Zr 11:1) exhibited a high initial heat of CO_2 adsorption and modified modes of methanol adsorption compared to MgO. However, the CO_2 adsorption capacity did not correlate to catalyst activity.

To further examine the promotional effect that zirconia has on magnesia, mixed oxides were prepared by co-precipitation under controlled pH conditions or rising pH conditions. The resulting mixed oxides were characterized using NH_3 and CO_2 adsorption microcalorimetry, X-ray diffraction, and scanning electron microscopy. The samples were also tested as catalysts for transesterification of tributyrin with methanol, coupling of acetone and conversion of ethanol to ethene, ethanal and butanol. Zirconia promoted the activity of MgO for both transesterification and acetone coupling, presumably by exposing new acid-base pairs at the surface. During ethanol conversion, however, zirconia promoted the dehydration reactions. Characterization and reactivity results suggest that a Mg:Zr sample prepared by constant pH precipitation exposes more ZrO_2 than a sample prepared by the rising pH method.

To increase our understanding of MgO as a catalyst for ethanol coupling, steady state isotopic transient kinetic analysis was used in conjunction with in-situ IR spectroscopic measurements. The isotopic transient analysis of ethanol coupling to butanol over MgO in a fixed bed reactor at 673 K revealed a surface coverage of adsorbed ethanol equivalent to about 50% of the exposed Mg-O atomic pairs. Diffuse reflectance IR spectroscopy of the ethanol reaction at 673 K confirmed that the surface was populated primarily with adsorbed ethoxide and hydroxide, presumably from the dissociative adsorption of ethanol. The coverage of reactive intermediates leading to butanol was an order of magnitude lower than that of adsorbed ethanol, and about half the surface base sites counted by adsorption of CO_2. The intrinsic turnover frequency for the coupling reaction at 673 K determined by isotopic transient analysis was 0.04 s^{-1}, which is independent of any assumptions about the nature of the active sites. Although the ethanol coupling reaction appeared to involve aldol condensation of an aldehyde intermediate,

the high coverage of ethanol under steady state conditions apparently inhibited unproductive C-C coupling reactions that deactivate the catalyst at high temperature.

The influence of sodium addition to zirconia on the acid-base properties of the surface and on the catalytic conversion of ethanol and acetone was also investigated. The rates of ethanol dehydration, dehydrogenation and coupling were evaluated in a fixed bed flow reactor operating at temperatures from 613-673 K. The rate of acetone condensation was evaluated in the same reactor operating at 473-573 K.

Addition of 1.0 wt.% Na to ZrO_2 decreased the rate of ethanol dehydration by more than an order of magnitude, which was consistent with a neutralization of acid sites evaluated by ammonia adsorption microcalorimetry. Addition of 1.0 wt.% Na to ZrO_2 also increased the base site density quantified by carbon dioxide adsorption microcalorimetry and the rate of acetone condensation. Although the rate of ethanol coupling was not increased by addition of Na, the overall selectivity of ethanol to butanol was improved over the 1.0 wt.% Na/ZrO_2 sample because of the significant inhibition of ethanol dehydration.

Acknowledgements

I thank my adviser, Robert J. Davis, for his guidance, patience and invaluable constructive criticism throughout my graduate work. I thank all past and present Davis group members that have helped and encouraged me in my work. I would like to specifically thank Dr. Yuanzhou Xi for his guidance and work that provided me with a strong foundation on which to begin my studies. I thank Dr. Sara Davis for her many hours of listening to the difficulties, frustrations and help solving the problems that my research has brought. I thank Ted Birky for his work and collaboration on the SSITKA experiments. I also thank my classmates Adrian Gospodarek, Dr. David Hibbitts, Dr. Ernie Perez, and Dr. Joe Costanzo for their camaraderie and friendship. I am incredibly grateful for Laura's patience and support throughout the last couple years of long hours in lab and with helping me through frustrations and disappointments. I am very grateful for the assistance of the Chemical Engineering staff Vickie Faulconer, Teresa Morris, and Ricky Buchanan. I appreciate the members of the Inorganic Chemistry department at the Fritz-Haber Institute who helped make my time there a valuable and rewarding experience.

I appreciate my brother Matt who has encouraged me and helped keep things in perspective. I thank my parents, Rich and Paula, for their encouragement, advise, love, and dedication to my education which has made everything I have done possible.

I also acknowledge the financial support, which made my work possible, from Chemical Sciences, Geosciences and Biosciences Division, Office of Basic Energy Sciences, Office of Science, U.S. Department of Energy, grant no. DE-FG02-95ER14549 and NSF grant number OISE 0730277.

Table of Contents

Chapter 1: Heterogeneous Catalysts for the Guerbet Coupling of Alcohols and Objectives of This Work

The majority of this chapter has been submitted as: J.T. Kozlowski, R. J. Davis, "Heterogeneous Catalysts for the Guerbet Coupling of Alcohols" Invited Review for ACS Catalysis.

Introduction

The Guerbet reaction involving the coupling of two alcohol molecules is named after Marcel Guerbet, who studied the self-coupling of butan-1-ol to produce the branched saturated alcohol, 2-ethylhexan-1-ol, in the 1890s [1]. Depending on the types of alcohols used in the reaction (primary versus secondary, long chain versus short chain), branched or unbranched products will be formed. In addition, when different alcohols are present in the reaction, self-coupling and cross-coupling reactions can both occur. Typically, reference to "Guerbet Alcohols" is often to highly-branched, saturated alcohols prepared by the condensation of two primary alcohols, and these products are important in the production of surfactants. Much of the work on Guerbet reactions over heterogeneous catalysts, however, focuses on the conversion of short chain alcohols, less than about C_4. Since surfactant production usually involves at least part of the catalyst in the fluid phase, most of that literature is beyond the scope of this review. For a more thorough discussion of the production of Guerbet-alcohol-derived surfactants, please see the review on the topic by O'Lenick [2]. Although, some generalizations regarding the mechanism of alcohol coupling can be obtained from studies involving homogeneous catalysts, this review emphasizes the work on heterogeneous catalysts for the reaction.

Early patents describe mixtures of metal oxides as catalysts for the reaction. In 1931, ethanol coupling in the presence of H_2 was observed over mixtures of MgO, Al_2O_3, and CuO_x between 473 K and 573 K [3]. Self-condensation of ethanol at high pressures (6.1 to 14.2 MPa) and temperatures ranging from 473 to 673 K was also patented over materials containing copper and magnesium oxide in 1933 [4]. Coupling of larger alcohols (C_{4+}) with H_2 over mixtures of MgO, Al_2O_3, and CuO_x received a patent in 1937 [5]. The coupling of various alcohols over soda lime (calcium hydroxide and alkali hydroxides) between 648 K to 853 K was patented in 1953 [6]. Between 1956 and 1970, several patents described how alkali metal salts dissolved in alcohol with the addition of an insoluble dehydrogenation agent like copper or nickel were effective at coupling various alcohols (C_2 to C_{10+}) [7–10]. Subsequent work with methanol and ethanol demonstrated effective coupling reactions catalyzed by γ-Al_2O_3 together with an alkali metal salt and platinum group metal between 473 to 673 K and 6.9 to 13.9 MPa [11]. Soon thereafter, soluble alkali metal or alkali metal salt combined with an insoluble lead salt were reported as alcohol coupling agents in a patent in 1977 [12]. By the mid 1980's, alkali metals were well recognized as important components of alcohol coupling catalysts [13,14]. Indeed, many patents in the field recognize the importance of combining an alkali metal compound with a separate component capable of catalyzing hydrogenation and dehydrogenation such as Cu and Ni [15–23].

A clear picture emerges from the patent literature that two features of the catalyst are required for the alcohol coupling reaction. The first feature is related to the acidity and basicity of the catalyst. Alcohol coupling systems commonly have basic materials in the form of alkali metal, hydroxide, or salt dissolved in the reaction medium or, in the case of heterogeneous catalysts, have a solid base such as magnesia as a critical component. The second feature of a

catalyst needed for alcohol coupling is the ability to facilitate dehydrogenation of the alcohol at the reaction temperature. Some typical metals used as dehydrogenating agents include platinum [11], nickel [13,24,25] and copper [26–29]. Some non-metals, such as the solid base MgO, can catalyze dehydrogenation of alcohols at sufficiently high temperatures.

Many recent publications on Guerbet reactions over heterogeneous catalysts involve the upgrading of short chain alcohols into longer chain saturated alcohols such as the self-coupling of ethanol to produce butan-1-ol. This is an attractive process since the properties of butan-1-ol alleviate some of the problems with ethanol as a fuel or fuel additive. Butan-1-ol has an energy density closer to gasoline than ethanol, and does not have the same propensity as ethanol to absorb water. Unlike ethanol, however, butan-1-ol is mainly produced from fossil resources [30]. Butan-1-ol has many current commercial uses, such as a perfume additive, flavoring agent, solvent, and chemical intermediate [30]. Upgrading of other short chain alcohols is also possible, with the caveat that methanol cannot self-couple through the Guerbet reaction. Methanol can be coupled with alcohols having 2 or more carbon atoms.

The Guerbet reaction involves a complex sequence of many other reactions (dehydrogenation, aldolization, dehydration, and hydrogenation) that could be the legitimate subjects of individual reviews. Nevertheless, the overall reaction path needs to be discussed in light of the various catalysts used for the reaction. While this review is by no means an exhaustive analysis on the topic, hopefully it will provide an introduction to the challenges of Guerbet coupling reactions over heterogeneous catalysts that are in need of more attention.

Reaction Path

Alcohol coupling has been proposed to progress by two different routes. The most commonly-accepted path involves an aldolization reaction as the C-C bond forming step with a non-adsorbed carbonyl-containing intermediate. This route includes 4 different types of reactions: dehydrogenation, aldolization, dehydration, and hydrogenation. This sequence is supported by several pieces of information provided below:

- The intermediates of ethanol self-coupling to produce butan-1-ol included ethanal, but-2-en-1-al and other characteristic aldolization intermediates [29,31–33].
- Aldol intermediates such as but-2-en-1-al, presumably formed during ethanol self-coupling, were hydrogenated in the presence of alcohol at reaction conditions [32].
- Ethanal or but-2-en-1-al each produced butan-1-ol over MgO-CuO-MnO in the presence of H_2 [34].
- Reactions of ^{13}C-labeled ethanal and unlabeled ethanol produced mostly labeled coupling products over a mixed oxide (0.8 wt.% K on Mg_5CeO_x) at low surface residence times [29].
- Aldol condensation occurred readily at the temperatures used in Guerbet reactions [29,32,35].
- The rate of production of the coupled product was proportional to aldehyde concentration [29,33,36].

This generally-accepted sequence of steps, which has been discussed in many publications, is summarized below.

The first step in the alcohol coupling reaction is the dehydrogenation of the reagent alcohol to produce an intermediate aldehyde or ketone. Since aldol condensation occurs between two carbonyl-containing molecules, both alcohols involved in the coupling reaction must be dehydrogenated. Scheme 1.1 and Scheme 1.2 show the dehydrogenation of two primary alcohols. One aspect of this step that remains unclear is the location and chemical state of the hydrogen evolved. In the case of catalysts that include a transition metal like copper, dihydrogen can be released from the surface after the dehydrogenation reaction, and the gas phase dihydrogen and aldehyde are in equilibrium with the alcohol. For mixed oxides, without transition metal co-catalysts, the location of the hydrogen is unclear; it may remain adsorbed on the surface to later hydrogenate products, it may desorb as dihydrogen, or the dehydrogenation imay be coupled to a hydrogenation step by the Meerwin-Ponndorf-Verley (MPV) reaction. Gines and Iglesia [29] observed that a copper-containing mixed metal oxide (K-$CuMg_5CeO_x$) had much higher rates of deuterium incorporation (from gas phase D_2) into the reactant alcohol as well as in the coupled products than the analogous catalyst without copper (K-Mg_5CeO_x). Due to the ambiguity of the fate of the hydrogen atoms, the hydrogen in these schemes will be indicated as (H_2).

Scheme 1.1

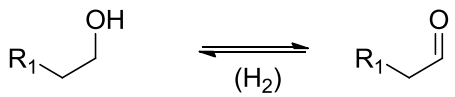

Scheme 1.2

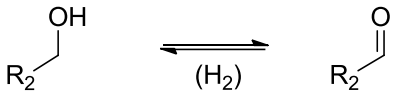

Scheme 1.3 depicts the aldol addition step. Aldol reactions occur readily over basic catalysts and likely proceed through a surface enolate [37]. The enolate acts as a nucleophile and attacks the other aldehyde or ketone present in the system. This addition reaction creates a bond between the α-carbon of one molecule with the carbonyl carbon of another molecule, and is likely responsible for the branched nature of many Guerbet alcohols. For example, if two ethanal molecules undergo an aldol condensation, followed by hydrogenation, then the linear alcohol butan-1-ol is formed since the reactive intermediates are a primary enolate and an aldehyde. If a secondary enolate is formed, or an enolate attacks a ketone, i.e. in the self-condensation of propan-1-ol or the condensation of propan-1-ol with propan-2-ol, a branched alcohol is formed. If the initial reactants are not the same alcohol (excluding methanol) there are four product options, two different cross-coupling products formed from the different enolates, and two self-coupling products. Selectivity to these products will be affected by the relative rates of dehydrogenation and enolate formation.

Scheme 1.3

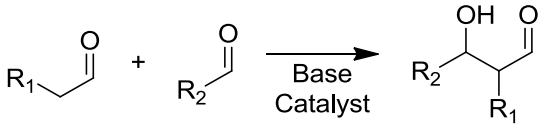

Scheme 1.4 shows the dehydration of the aldol addition product, which presumably occurs quite readily since the aldol addition products are generally not observed. For many of the applications that involve liquid phase condensations with a soluble base, water is removed to

prevent the formation of the undesirable carboxylic acid from the reactant or product aldehyde. Aldehyde oxidation to the acid product is known to occur when base, water and a transition metal catalyst are present at 295 K [38], which is a much lower temperature than that typically used in Guerbet reactions in the liquid phase (>373K). Not only is the carboxylic acid product undesirable in some cases but it also neutralizes the base catalyst. Removal of water to decrease the production of undesired acid is the subject of a patent in which distillation or a desiccant like magnesia or calcium oxide was utilized [17].

Scheme 1.4

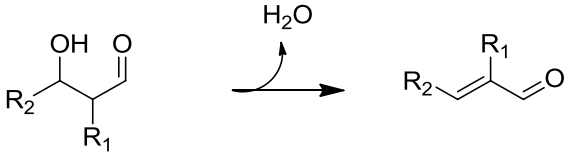

The final two steps in the sequence are represented in Schemes 1.5 and 1.6 as hydrogenation reactions, which might occur in either order. These steps can be accomplished on a hydrogenation catalyst like copper or nickel if it is present on the catalyst or over a metal oxide at sufficiently high temperatures with an adequate hydrogen source such as the reactant alcohol. The unsaturated intermediates have been observed by several groups [29,31,32].

Scheme 1.5

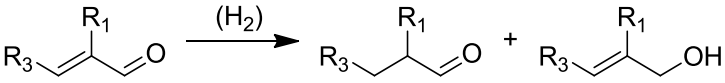

Scheme 1.6

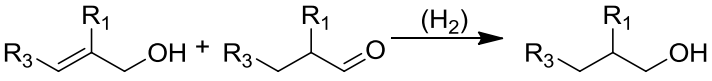

The interrelationships among these steps help explain why some catalysts are more effective than others. Over most basic solids, aldol condensation occurs rapidly and at much lower temperatures than those typically used in Guerbet reactions. For example, Guerbet reactions over MgO are typically performed near 673 K, whereas MgO can easily catalyze the aldol condensation of 2-propanone at room temperature or lower [39–44]. This would suggest that a major hurdle during Guerbet coupling over MgO is the initial dehydrogenation of the alcohol to form the carbonyl intermediate, which explains why addition of a hydrogenation/dehydrogenation catalyst such as copper improves the performance of basic metal oxide catalysts.

A second possible reaction path for Guerbet coupling proposed by Yang and Meng [45] and Ndou et al. [46], involves a direct surface coupling reaction resulting in dehydration from the OH of one alcohol and the hydrogen attached to the α-carbon of a second. Although this proposed reaction (Scheme 1.7) involves two alcohols, the direct reaction of an aldehyde and an alcohol is also considered (Scheme 1.8). This direct coupling mechanism was proposed after addition of reaction intermediates leading to, or produced from, an aldolization-type C-C bond forming step did not increase the rate of butan-1-ol production from ethanol. The analysis did not account for other factors that might affect the conversion of reaction intermediates such as a difference in the amount of surface hydrogen available for reaction. Although the direct coupling route has been proposed, there appears to be a general consensus in most of the literature that Guerbet coupling involves an aldol intermediate.

Scheme 1.7

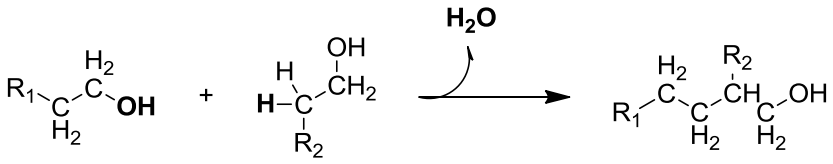

Scheme 1.8

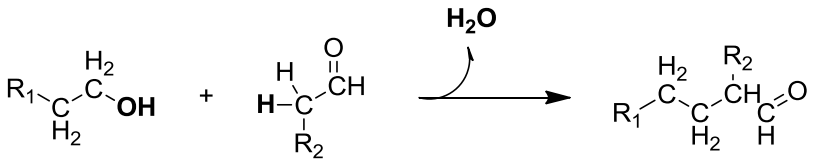

As discussed above, a gas phase a carbonyl species is one likely candidate for the reaction intermediate in Guerbet coupling, but others suggest that the reaction does not necessarily require participation of a gas phase carbonyl. Evidence that some fraction of the final product is not produced from a gas phase carbonyl intermediate is derived from two observations. The first is a kinetic analysis of products observed as the space time of the reactants is changed. For ethanol conversion to butan-1-ol, ethanal and ethene appeared as primary products during the change in space time. However, a low but non-zero slope for butan-1-ol suggests that some of it may also form as a primary product of ethanol conversion [31]. Additionally, Gines and Iglesia [29] added ^{13}C-labeled ethanal to a reaction of unlabeled ethanol over K-CuMg$_5$CeO$_x$ and K-Mg$_5$CeO$_x$ and observed at low contact times that a minority of the C_4 product did not originate from the labeled ethanal [29]. Therefore, Guerbet coupling of ethanol over Mg:Al mixed oxides [31], K-CuMg$_5$CeO$_x$ [29] and K-Mg$_5$CeO$_x$ [29] was proposed to proceed via two different aldehyde intermediates, one involving a gas phase aldehyde and another that is completely surface mediated (without participation of a gas phase aldehyde intermediate). Even for the direct surface route depicted in this mechanism, the C-C bond forming step is still a classical aldolization reaction but with an aldehyde that remains adsorbed

on the catalyst after being formed in the initial alcohol dehydrogenation step. Nagarajan also performed similar kinetic analysis on the products from ethanol coupling but concluded butan-1-ol and but-2-enal were secondary products over a MgO-CuO-MnO catalyst [33]. All of these studies generally support the importance of aldol coupling reactions as intermediate steps in the Guerbet reaction, although the exact details are still subject to debate.

The aldol intermediate produced in the self-coupling of ethanol has many final products that may be derived from it. One example is the production of buta-1,3-diene from the coupling of two ethanol molecules. This reaction has been commercialized in several locations including the US, China, India, Poland, and the former USSR [30]. Two different processes have been used to produce buta-1,3-diene from ethanol; although the Lebedev process is performed in a one step, the Ostromislensky process is a two-step sequence in which ethanol is partially converted to ethanal in the first step, which is followed by aldolization and deoxygenation in the second step.

The single step Lebedev process for the production of buta-1,3-diene from ethanol proceeds via the same reactions as the two step Ostromislensky process, but over a single, multi-functional catalyst. Many of the catalysts that have been used in the single step process contain varying amounts of MgO, SiO_2, and Al_2O_3, with MgO being the majority component [47]. Other materials that have been used to produce buta-1,3-diene from ethanol include tantalum oxide, hafnia, zirconia, or alumina on silica [47], Ni on a magnesium silicate [48], sepiolite [49], aluminated sepiolite [50] and magnesia and silica [51,52]. A recent study by Jones et al. of many different materials supported on silica showed a Zn/Zr oxide on silica to have high activity [53]. Jones et al. concluded that the optimal catalyst needs some acidic sites, but very strong acid sites will increase the selectivity to undesired products like ethene and butane [53]. A thorough review on the topic by Toussaint and Marsh is an excellent resource for more information [47].

Materials exposing acid sites together with base sites, such as Mg:Al mixed oxides or hydroxyapatite, have produced some buta-1,3-diene in the product mixture from ethanol coupling to butan-1-ol [54,55].

The industrially-relevant molecule 2-methylpropene has also been produced from ethanol through a similar proposed aldol intermediate [56]. In this reaction, ethanol is fed to the reactor along with water, which probably facilitates the C-C bond breaking of the aldol products [56]. One potential sequence involves the coupling of ethanol followed by C-C bond cleavage to produce 2-propanone, which can then couple and undergo another C-C cleavage to produce 2-methylpropene. Each of these individual steps, ethanol to 2-propanone [57–61] and 2-propanone to 2-methylpropene [41,62] have been explored, but only recently has the concerted reaction been completed over a Zn/Zr oxide catalyst [56]. As described earlier, a catalyst with appropriately weak acid sites is necessary, being careful to avoid the dehydration of ethanol to the undesired product ethene.

Another example in which alcohol coupling likely plays a role is in higher alcohol synthesis (HAS) from synthesis gas over basic materials. While chain growth to 1 and 2 carbon molecules clearly proceeds in a different fashion it has also been theorized that some of the longer chain alcohols present in the product stream of HAS reactors is due to the aldol-based coupling of two smaller alcohols [63–65]. Alcohol coupling is expected since the reaction conditions of HAS are similar to those of Guerbet coupling and the typical catalysts have all of the functions necessary for coupling to occur.

Basic Metal Oxide and Metal Phosphate Catalysts

MgO

Many different basic oxide materials have been used as catalysts for the Guerbet reaction. In particular, MgO appears to be the standard basic oxide to which many others are compared. Representative results from ethanol and propan-1-ol conversion over MgO are presented in Table 1.1. The rates presented in the table were converted to a consistent units basis and the various examples are placed in order of increasing reaction temperature. Two factors seem to impact the coupling rate to form saturated alcohol. Higher temperatures obviously increase the coupling rate, as well as the dehydrogenation and dehydration rates. The second factor affecting the coupling rate is the intermediate aldehyde concentration. As mentioned above, the Guerbet reaction catalyzed by basic oxides likely occurs by two routes, with the majority of the product being formed from a gas phase aldehyde intermediate. As shown in Table 1.1, the minimum temperature to realize appreciable yields over MgO was apparently 573 K. Table 1.1 also includes the rate of formation of unreported product. Since Ndou et al. [35] do not report dehydration rates, a major component of the rate of unreported products in that case is most likely the result of dehydration of the reactant alcohol.

In addition, the coupling of methanol to higher alcohols can be hard to compare to the self-coupling of ethanol or propanol since rates of dehydrogenation are for both methanal and higher aldehyde production, and since methanal cannot form an enolate, the aldolization rate dependence on the concentrations of the two aldehydes is unclear. Some of the excluded reports involve the coupling of methanol and ethanol [66], the coupling of methanol and C_2 to C_5 primary alcohols [67]. Nevertheless, it is expected the general trends observed in Table 1.1 will

hold for methanol and higher alcohol coupling rates over MgO. Other published works are excluded from the table because of a lack of necessary information for the MgO used in the studies, such as specific surface area.

Many different promoters have been added to MgO to enhance its activity and/or selectivity to butan-1-ol. One common promoter is an alkali metal, such as lithium,[35] sodium [35,66], potassium [35], and cesium [35,66]. The addition of alkali metal salts, which likely imparted additional basicity to the catalyst, increased the selectivity to the dehydrogenation product, but not to the coupled product [35,66]. Unfortunately, there was no discussion of how the surface area might change after the addition of alkali metal promoters in those papers so a direct comparison of areal rates on these materials is not possible. The influence of alkaline earth metals on the reactivity of MgO was also studied by Ndou et al. [46] and Ueda et al. [66]. However, increase in the selectivity to the saturated, coupled alcohol products was observed over these materials.

Table 1.1. Rates for propan-1-ol and ethanol dehydration, dehydrogenation and self-coupling over MgO.

Reactant	Surface Area ($m^2 g^{-1}$)	Temperature (K)	Conversion	Concentration of Aldehyde ($\mu mol\ L^{-1}$)	Dehydrogenation Rate ($nmol\ m^{-2}\ s^{-1}$)	Dehydration Rate ($nmol\ m^{-2}\ s^{-1}$)	Coupling Rate Others ($nmol\ m^{-2}\ s^{-1}$)	Coupling Rate Saturated Alcohol ($nmol\ m^{-2}\ s^{-1}$)	Unreported Product Rate ($nmol\ m^{-2}\ s^{-1}$)	Reference
ethanol	125	573	0.51	0.031	0.078	0.011	NR	0.058	0.0	69
propan-1-ol	50	573	1.5	3.8	0.25	NR	NR	2.2	0.92	35
propan-1-ol	50	623	3.0	6.9	0.50	NR	NR	4.0	2.2	35
ethanol	166	625	10	28	0.62	1.3	0.50	1.1	0.0	55
ethanol	166	658	20	42	1.0	2.9	1.0	2.0	0.10	55
propan-1-ol	50	673	7.5	37	2.9	NR	NR	8.2	5.6	35
propan-1-ol	50	723	28	119	10	NR	1.6	31	12	35
propan-1-ol	50	773	44	82	7.4	NR	NR	38	52	35

Mg:Al Mixed Oxides

Another approach to increase the activity of MgO for the coupling of alcohols is to increase the quantity of appropriate strength acid-base pairs. One method to increase these acid-base pairs is by incorporating Al, a stronger Lewis acid than Mg, into MgO. Preparation of Mg:Al mixed oxides is often accomplished by first synthesizing hydrotalcite layered materials (magnesium aluminum hydroxycarbonate), in which the brucite-like structure of $Mg(OH)_2$ is partially substituted with Al. Thermal decomposition of hydrotalcite gives well mixed oxides of Mg and Al. Mixed oxides prepared from hydrotalcites have been evaluated in a variety of reactions, including aldol condensation. In the aldol self-condensation of propanone and in aldol condensation of 3,7-dimethylocta-2,6-dienal with propanone and butan-2-one, the presence of Al with MgO promoted the rate compared to pure MgO [39,68]. The higher rate is thought to be the result of an increase in the quantity of appropriate acid-base pairs. In particular, the stronger Lewis acid Al may help by stabilizing the adsorbed intermediate.

Table 1.2. Rates for ethanol dehydration, dehydrogenation and self-coupling over Al_2O_3 and Mg:Al mixed oxides.

Material	Surface Area ($m^2 g^{-1}$)	Temperature (K)	Conversion	Concentration of Aldehyde ($\mu mol\ L^{-1}$)	Dehydrogenation Rate ($nmol\ m^{-2}\ s^{-1}$)	Dehydration Rate ($nmol\ m^{-2}\ s^{-1}$)	Coupling Rate Saturated Alcohol ($nmol\ m^{-2}\ s^{-1}$)	Reference
Mg:Al 8.1	114	573	4.4	47	1.3	0.017	0.27	69
Mg:Al 4.6	184	573	3.6	42	0.71	0.019	0.14	69
Mg:Al 3.2	238	573	5.0	23	0.31	0.022	0.28	69
Mg:Al 3	142	523	4.0	2.6	0.20	0	1.0	54
Mg:Al 3	142	573	9.0	11	0.91	0	1.4	54
Mg:Al 3	142	623	21	28	2.7	4.5	2.7	54
Mg:Al 3	142	673	50	110	11	17	3.6	54
Mg:Al 3	142	723	87	242	27	33	2.2	54
Mg:Al 3	142	773	98	340	40	37	1.0	54
Mg:Al 1.1	231	573	9.7	6.0	0.081	0.16	0.51	69
Mg:Al 0.5	298	573	13	6.9	0.072	0.17	0.14	69
Al_2O_3	388	573	86	2.8	0.022	7.9	0	69

Table 1.3. Acid and base properties of MgO, Al_2O_3, and Mg:Al mixed oxides presented in Di Cosimo et al. [31] Adsorption of gas phase probe was completed at room temperature.

Material	Total Evolved CO_2 (μmol m^{-2})	Total Evolved NH_3 (μmol m^{-2})
MgO	1.63	0.48
Mg:Al 8.1	1.17	0.81
Mg:Al 4.6	0.46	0.84
Mg:Al 1.1	0.83	1.57
Mg:Al 0.5	0.73	1.39
Al_2O_3	0.34	1.34

In Table 1.2, rates associated with reactions in ethanol coupling over Mg:Al mixed oxides are presented. The catalyst entries are presented in the order of decreasing Mg content. As Al content in the mixed oxides increased, the rate of dehydration also increased, presumably the consequence of the new acid sites associated with Al. When a pure alumina catalyst or a mixed oxide rich in aluminum was used, the vast majority of the product was the dehydrated reactant, or ethene, because of the high density of strong acid sites [69,70]. Mixed oxides with high concentrations of Al revealed a product distribution that included buta-1,3-diene. For example a Mg:Al mixed oxide (Mg/Al=3) at a conversion of 50% had a 12% selectivity to buta-1,3-diene [54]. Direct comparison of the first two entries in Table 1.1 and Table 1.2 reveals that a Mg:Al mixed oxide had a higher dehydrogenation rate. The observed increase in coupling rate over the mixed oxide is likely due to an increase in the gas phase aldehyde concentration and an increase in the aldol condensation rate over the bifunctional mixed oxide.

The acid and base properties of some of the Mg:Al mixed oxides presented in Table 1.2 have been evaluated with ammonia and carbon dioxide stepwise-temperature programmed desorption, respectively, by Di Cosimo et al. [31] and the results are summarized in Table 1.3. It

should be noted that the acid-base site densities were evaluated by total uptake of the probe molecules at room temperature [31]. As the Al content in the mixed oxides increased, the ammonia uptake also increased. Comparing the rates of dehydration of ethanol and the uptake of ammonia for Mg:Al 8.1 (0.017 nmol m^{-2} s^{-1} and 0.81 μmol m^{-2}) and the Mg:Al 1.1 (0.16 nmol m^{-2} s^{-1} and 1.57 μmol m^{-2}) there appears to be some relationship between the two. Further characterization of the acid character of these samples would shed light on the relationship between Al content and dehydration rate. Likewise, the CO_2 adsorption capacity was correlated to the rate of dehydrogenation [31]. Comparing the rate of dehydrogenation of ethanol to the uptake of carbon dioxide for Mg:Al 8.1 (1.3 nmol m^{-2} s^{-1} compared to 1.17 μmol m^{-2}) and the Mg:Al 1.1 (0.081 compared to 0.83 μmol m^{-2}) a relationship between carbon dioxide adsorption and ethanol dehydrogenation rates is clearly seen.

Hydroxyapatite

Another example of an acid-base bifunctional material used in the coupling of alcohols is hydroxyapatite, $Ca_5(PO_4)_3OH$. Table 1.4 summarizes the reaction rates for ethanol conversion over hydroxyapatites compared to calcium oxide and tricalcium phosphate. The hydroxyapatite materials were more effective at coupling and dehydrogenation compared to calcium oxide. While tricalcium phosphate (β-TCP) showed a higher rate of alcohol coupling compared to the hydroxyapatite, it had a much higher selectivity to the undesired olefin, which may be a

Table 1.4. Rates for ethanol dehydration, dehydrogenation and self-coupling over hydroxyapatite, hydroxyapatite with subsituted strontium and orthovanadate, calcium oxide, and tricalsium phosphate.

Material	Surface Area ($m^2\ g^{-1}$)	Temperature (K)	Conversion	Concentration of Ethanal ($\mu mol\ L^{-1}$)	Dehydrogenation Rate ($nmol\ m^{-2}\ s^{-1}$)	Dehydration Rate ($nmol\ m^{-2}\ s^{-1}$)	Coupling Rate Others ($nmol\ m^{-2}\ s^{-1}$)	Coupling Rate Saturated Alcohol ($nmol\ m^{-2}\ s^{-1}$)	Reference
β-TCP	1.2	678	10	62	77	58	24	54	55
β-TCP	1.2	709	20	105	137	168	40	94	55
Ca:P 1.59	27.5	644	10	15	2.0	35	0	0	55
Ca:P 1.59	27.5	660	20	21	2.9	73	0	0	55
Ca:P 1.62	35.7	593	10	24	2.0	2.2	2.7	7.2	55
Ca:P 1.62	35.7	623	20	31	2.8	9.7	3.0	11	55
Ca:P 1.65	40.3	548	10	11	0.58	0.18	1.8	6.7	55
Ca:P 1.65	40.3	569	20	12	0.68	0.40	3.7	14	55
Ca:P 1.67	37.8	545	10	8.1	0.42	0.10	1.7	6.7	55
Ca:P 1.67	37.8	571	20	12	0.65	0.23	3.5	13	55
Ca:P 1.69	58.7	573	7.1	0.24	0.007	0.00	0.88	2.6	32
CaO	6.4	670	10	79	23	47	0.26	1.1	55
CaO	6.4	694	20	108	32	97	0.94	2.0	55
Sr:P 1.68	26.2	573	7.6	0.78	0.019	0.00	0.58	2.5	32
Ca:V 1.73	26	573	6.6	6.3	0.55	906	0.52	2.1	32
Sr:V 1.69	15.3	573	5.8	56	0.40	75	0.057	0.057	32

consequence of operating at much higher temperatures. Additionally, the selectivity to the dehydrogenation and coupling products increased as the Ca content of the samples increased. Although a direct comparison of the rates in Table 1.4 is complicated by the wide variety of different temperatures used, a complete summary was provided to allow comparison to other materials such as the Mg:Al mixed oxides in Table 1.2.

Table 1.5. Acid and base properties of tricalcium phosphate, hydroxyapatite with different C:P ratios and calcium oxide as presented in Tsuchida et al. [55] Adsorption of gas phase probe was completed at 523 K.

Material	CO_2 Adsorption Site Density ($\mu mol\ m^{-2}$)	NH_3 Adsorption Site Density ($\mu mol\ m^{-2}$)
β-TCP	0.6	0.008
Ca:P 1.59	0.01	0.038
Ca:P 1.62	0.02	0.029
Ca:P 1.65	0.38	0.011
Ca:P 1.67	0.53	0.0006
CaO	0	0

Similar to the Mg:Al mixed oxides, the rates of dehydration and dehydrogenation over hydroxyapatites are impacted by the composition of the catalyst. As the calcium content of the catalysts increased from Ca-deficient materials (Ca/P=1.59) to stoichiometric materials (Ca/P=1.67), the rate of dehydration decreased. The densities of acid and base sites, measured by ammonia and carbon dioxide adsorption at 523 K, respectively, are reproduced from Tsuchida et al. [55] in Table 1.5. The decrease in dehydration rate with increasing Ca content of the samples correlated well to the observed decrease in acid site density and increase in base site density (Table 1.5). A direct comparison of the rates for samples with different Ca content is difficult since the reaction temperatures were not held constant, but a relationship between

dehydration rate and acid site density is apparent and as well as a relationship between dehydrogenation rate and base site density.

Comparing the Mg:Al 8.1 mixed oxide catalyst (Table 1.2) to the Ca:P 1.67 hydroxyapatite catalyst (Table 1.4) at 573 and 571 K, respectively, the hydroxyapatite exhibited about a 50 times higher coupling rate even with a lower gas phase ethanal concentration. Additionally, hydroxyapatite prepared with strontium instead of calcium revealed a slightly higher rate of dehydrogenation than for calcium hydroxyapatite [32].

Hydroxyapatites have been used as catalysts in a variety of other reactions of relevance to alcohol coupling. In particular, they have been used in the MPV hydrogen transfer from 2-butanol to 3-pentanone between 435 K and 552 K [71] and for the dehydrogenation of alcohols [71–73].

Basic Zeolites

Ethanol coupling has been performed over ion-exchanged and rubidium-impregnated zeolite X catalysts and reactivity results are summarized in Table 1.6. The rates are normalized to grams of catalyst instead of surface area since the surface areas were not reported [45]. Although it is unclear how the surface area might be affected by the impregnation of Rb, zeolite 13X has an approximate surface area of 600-700 $m^2 g^{-1}$. The rates in Table 1.6 were determined at 693 K and indicate zeolites have some potential for the reaction, but direct comparisons to MgO, hydroxyapatite and the Mg:Al mixed oxides are not possible since surface area, ethanol concentrations and conversions were not reported.

Table 1.6. Rates for ethanol dehydration, dehydrogenation and self-coupling zeolites published by Yang and Meng [45]

Material	Temperature (K)	Dehydrogenation Rate ($\mu mol\ g_{catalyst}^{-1}\ s^{-1}$)	Coupling Rate Others ($\mu mol\ g_{catalyst}^{-1}\ s^{-1}$)	Coupling Rate Saturated Alcohol ($\mu mol\ g_{catalyst}\ s^{-1}$)
LiX	693	3.5	0	0
NaX	693	2.9	0	0
KX	693	2.4	0	0
Rb-LiX	693	2.4	0.75	4.3
Rb-NaX	693	2.9	1.1	4.0
Rb-KX	693	3.4	0.35	1.7

If a surface area of Rb-NaX is assumed to be 600 $m^2\ g^{-1}$, then estimated rates for dehydrogenation and production of butanol are estimated to be 4.8 and 6.9 nmol $m^{-2}\ s^{-1}$. This calculated rate of coupling is similar to the reported rates of propan-1-ol coupling over MgO at 673 K [74] (8.2 nmol $m^{-2}\ s^{-1}$) and ethanol coupling over MgO at 658 K [55] (2.0 nmol $m^{-2}\ s^{-1}$).

Yang and Meng [45] reported decent selectivity to the coupled product at 693 K. It is important to note that zeolites without excess Rb were active for dehydrogenation but not for alcohol coupling. Evidently the occluded Rb species was required for the aldol condensation step in the coupling sequence. The total rate of ethanol conversion (dehydrogenation rate + coupling rate x 2) for the Rb-promoted samples was reminiscent of the results reported by Hathaway and Davis [75] for dehydrogenation of propan-2-ol over Cs-impregnated CsNaX (cesium acetate impregnated CsNaX) compared to purely ion-exchanged zeolite X (CsNaX). Hathaway and Davis [75] also studied other samples for the dehydrogenation of propan-2-ol and observed that CsAce/CsNaY had a similar activity to MgO and both had higher activity than CsAce/CsNaX. Both Cs impregnated X and Y zeolites were more active dehydrogenation catalysts than the ion-exchanged zeolites (CsNaY or CsNaX).

Dehydrogenation versus Dehydration

To help understand the effect of adding Lewis acid components on the catalysis of alcohol coupling it is necessary to revisit the possible reaction mechanisms of the Guerbet reaction. The first two likely steps convert the reactant alcohol to either an aldehyde (dehydrogenation) or an olefin (dehydration). Dehydrogenation has been proposed to proceed via two different elementary steps on mixed oxides. The first surface intermediate is an adsorbed alkoxide, coordinated to a Lewis acid through the oxygen atom of the alkoxide with the dissociated hydrogen residing on a neighboring surface oxygen atom. The abstraction of hydrogen from an alcohol has been shown to occur over low coordinated Mg and O atoms on MgO [76–78]. These low coordinated sites are present at corner, edge, and defect sites. The adsorbed alkoxide of ethanol and methanol has been observed on MgO by DRIFTS even at room temperature [79,80]. Since the alkoxide is formed easily over basic oxides, it is likely the next step that is limiting the formation of the aldehyde on MgO.

The subsequent step involving the activation of the C-H bond of the adsorbed alkoxide has been proposed to proceed by two slightly different reactions. The two proposed steps include a second hydrogen atom removal with a basic oxygen shown in Scheme 1.9, or the combination of the adsorbed hydrogen from the alcohol group with the second hydrogen on the carbon atom associated with the C-O bond shown in Scheme 1.10. In Scheme 1.9, each hydrogen involved in the reaction is transferred via interaction with the surface oxide anion, whereas in Scheme 1.10 the hydrogen recombination reaction involves direct hydrogen transfer to a surface hydroxyl group.

Scheme 1.9. Proposed mechanisms of alcohol dehydration and dehydrogenation over MgO. This figure is adapted from Diez et al. [81]

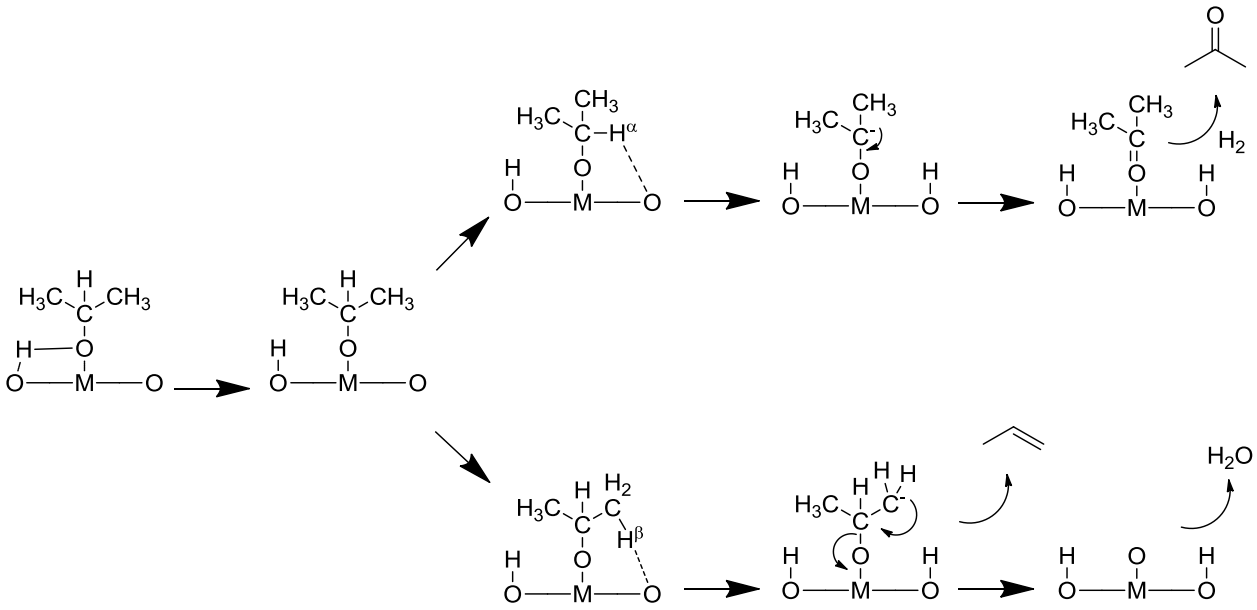

Scheme 1.10. Proposed mechanisms of dehydration and dehydrogenation, adapted from Shinohara et al. [82]

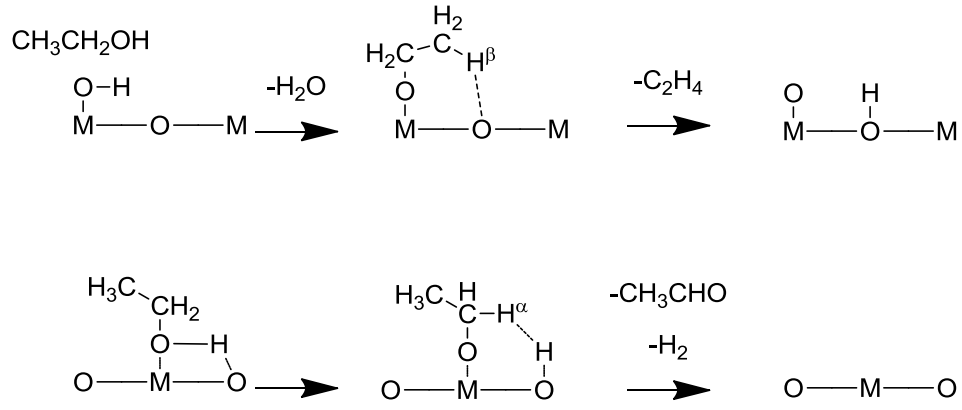

Although the difference between Scheme 1.9 and 1.10 is small, the location of the transferred hydrogen could impact the subsequent hydrogenation steps in the alcohol coupling mechanism. Hydrogen is needed to hydrogenate the products from the aldol condensation and can be derived from three sources: adsorbed hydrogen atoms produced from ethanol dehydrogenation, gas phase dihydrogen produced from ethanol dehydrogenation, or direct H transfer from the ethanol as in the MPV reaction. Interestingly, Gines and Iglesia included gas phase dideuterium in the reactant mixture during alcohol coupling and observed little incorporation of deuterium into the saturated coupled alcohol product formed over a mixed oxide ($K\text{-}Mg_5CeO_x$) [29]. Therefore, gas phase dihydrogen is not the likely source of hydrogen for subsequent hydrogenation steps over mixed oxide samples. The MPV reaction and reactions involving surface hydrogen are more likely to play an important role in the hydrogenation steps over basic oxides or phosphates. Indeed, a surface alkoxide has been proposed to be the key intermediate in the MPV reaction over metal oxides. This proposed intermediate by Ivanov et al. [83] is presented in Scheme 1.11. As expected many of the basic oxide and phosphate catalysts used for alcohol coupling have also been used for MPV reactions at similar conditions. For more information on MPV reactions and the catalysts that perform them, please see a review by Ruiz and Jiménez-Sanchidrián [84]. As discussed previously, the nature of the acid and base pairs on the catalytic surface is likely to play an important role in the dehydrogenation reaction.

Scheme 1.11. Proposed reaction intermediate for the MPV reaction, adapted from Ivanov et al. [83]

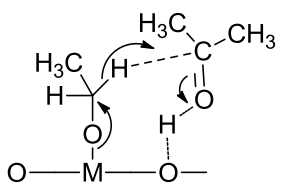

Dehydration reactions on the basic oxides can also occur via two separate pathways. The first proposed mechanism has been called a base-catalyzed dehydration, or more succinctly, an E_{1cB} mechanism. This proposed dehydration mechanism is shown in the bottom half of Scheme 1.9 [81]. The key step is the removal of the β-hydrogen from the adsorbed alkoxide. The intermediate would have to be stabilized with an interaction between the oxygen and the surface Lewis acid ($Mg^{\delta+}$ in MgO). The carbanion intermediate formed with this proposed dehydration mechanism would be quite similar to the carbanion intermediate formed as an intermediate in the base-catalyzed aldolization, the only difference involving an additional hydrogen on the C-O carbon in the case of dehydration.

The second proposed dehydration intermediate, by an E_1-type mechanism, is shown in the top half of Scheme 1.10 [82]. This reaction would also proceed through a stable alkoxide intermediate, which has been confirmed spectroscopically during Brønsted-acid-catalyzed dehydration over zeolites [85]. Obviously the mechanism for dehydration over MgO or other oxides would depend on the reaction temperature and catalyst pretreatment conditions. Although MgO is typically thought to dehydrate alcohols through the E_{1cb} mechanism [86], other basic oxides and mixed metal oxides may have different kinds of Lewis and Brønsted sites available for catalysis.

For both dehydrogenation and dehydration, the nature of the acid-base pair on the surface dictates the selectivity of the products formed. For a more thorough discussion on acid and base pair chemistry in metal oxides, see Iglesia et al. [87].

Aldolization

The aldolization of adsorbed carbonyl-group-containing molecules is represented in Scheme 1.12. This scheme shows how the adsorption of the carbonyl group is associated with an electron accepting or Lewis acid site. This site stabilizes the molecule and allows for the base-catalyzed removal of a hydrogen on the α-carbon. This hydrogen removal step forms a surface enolate in which the carbanion can then attack a nearby adsorbed aldehyde or ketone [62]. The resulting surface aldol product can then desorb, dehydrate and desorb, crack to produce products like 2-propanone from the aldol product of ethanal, perform another aldolization, or continue reacting to produce a completely hydrogenated product as in the Guerbet reaction.

Scheme 1.12. Proposed reaction intermediates for the aldolization of adsorbed carbonyl compounds, adapted from Lippert et al. [62].

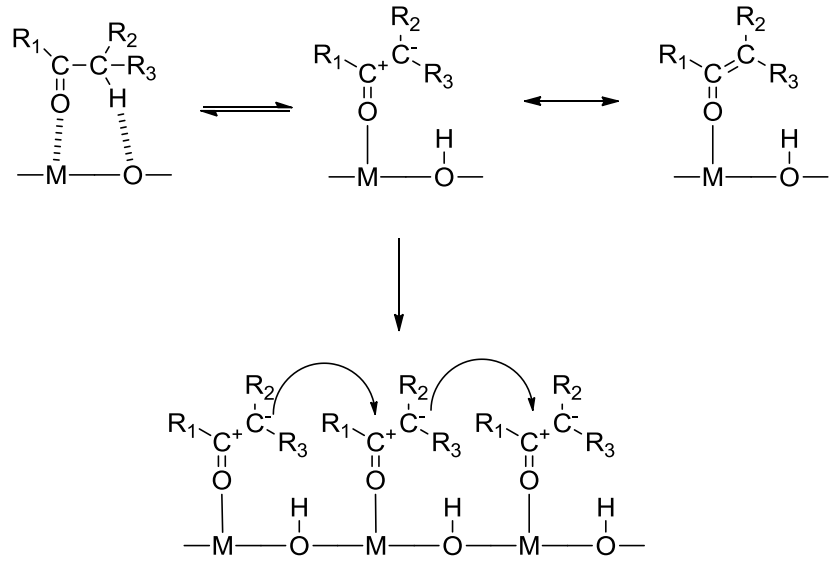

Aldolization has also been shown to be promoted by bifunctional acid-base materials. Examples of bifunctional solids include Y^{3+} added to MgO [88], Mg:Al mixed oxides

[39,41,68,89], amorphous aluminophosphate [40], Cs/ZrO_2 [90] and Mg:Zr mixed oxides [91,92]. The promotion of the reaction on bifunctional catalysts is thought in part to be the result of the stabilization of an intermediate through a Lewis acid interaction. This interaction also allows large networks of aldolization products to form at elevated temperatures, since a strong interaction between the oxygenated intermediates and the Lewis acid sites prevents desorption, especially when multiple functional groups exist in one molecule [88].

There have been many theoretical and experimental studies on aldol condensation over MgO. In particular, 2-propanone condensation has received significant attention. The formation of an enolate on MgO has been shown to occur at room temperature [93] and the rate of 2-propanone condensation can be calculated from the results of Zhang et al. [43] at 273 K to be 54 nmol m^{-2} s^{-1} in liquid acetone (13.8M) based on density [94] at 273 K. This aldol condensation rate over MgO at 273 K is higher than the reported alcohol coupling rates over MgO at temperatures as high as 773 K as summarized in Table 1.1. Since aldol condensation readily occurs at low temperature, it is likely the dehydrogenation step limits the alcohol coupling reaction over basic metal oxides and phosphates.

Catalysts With Transition Metal Components

Catalysts composed of a basic support and a transition metal have an advantage over basic metal oxides for the Guerbet reaction. Use of a metal promoter enhances the ability, in some instances, to operate at lower temperatures because the dehydrogenation of the alcohols occurs much more readily over metals than over metal oxides such as MgO; however, if the

reaction temperature is too high, decomposition of the reactant can cause a decrease in selectivity to the desired saturated alcohol.

Carlini and co-workers [27,95] have studied various metals on the same Mg:Al mixed oxide support for the coupling of methanol with propan-1-ol in a batch reactor at 473 to 493 K and 3 MPa. The metals (Pd, Ni, Rh, and Cu) were either supported on the basic mixed metal oxide or supported on carbon and added as a physical mixture [95]. The researchers observed that the best physical mixture was copper chromite and Mg:Al mixed oxide [95]. Copper chromite and the Mg:Al mixed oxide were better than physical mixtures of a metal (Pd, Ni or Rh) on carbon with the Mg:Al mixed oxide. It was also observed that the metals Pd, Ni and Rh showed no improvement when supported on the Mg:Al oxide compared to the physical mixture of the metal on carbon and the Mg:Al mixed oxide. However, copper supported on the Mg:Al oxide showed an increased rate and selectivity to the coupled product compared to the other physical mixtures and supported metals on Mg:Al mixed oxide catalysts [95].

Nagarajan and Kuloor [34] studied the addition of metal oxides to MgO on ethanol conversion. Their conditions were: 573 and 623 K, 91.3 kPa, gas mixture of 50% H_2 and 50% ethanol in a flow reactor. The lower temperatures were necessary since at higher temperatures, especially over copper-containing materials, they noticed appreciable amounts of reactant decomposition. Among the metal oxides added to MgO (CuO, MnO, Cr_2O_3, ZnO, Al_2O_3, Fe_2O_3, UO_3, CeO_2, ThO_2, ZrO_2) promotional effects were noted after the addition of copper, iron, zinc, uranium and manganese oxide to MgO. Nagarajan and Kuloor [34] also studied three component systems comprised of MgO, a promoter metal oxide (iron, zinc, manganese or uranium) and copper, among which the highest yield of butan-1-ol observed was 36.4 % over a catalyst composition of 65:25:10 (MgO:CuO:MnO). The reactant feed was also varied in this

work to include pure ethanal in one experiment and a 1:1 mixture of dihydrogen to ethanal in another experiment. In both cases, ethanal in the feed caused large amounts of coke to form on the catalyst. In the case without dihydrogen, but-2-enal was obtained at a yield of 10.2% and in the case with dihydrogen, butan-1-ol was formed with a yield of 15.8%. As expected, dihydrogen in the reactant mixture together with copper in the catalyst facilitated hydrogenation of the ethanal condensation product [34].

Another copper-containing material, potassium-promoted magnesia ceria mixed oxide (Mg_5CeO_x) with supported copper, has also been studied for alcohol coupling reactions by Gines and Iglesia [29]. Their experiments were carried out in a recirculating batch reactor at 573 K and 101.3 kPa. They documented the important role of Cu on activity and selectivity. When comparing the rates of ethanol dehydrogenation over catalysts with and without copper, large increases in dehydrogenation rates and coupling products were observed over copper-loaded samples. Initial rates were obtained for ethanol dehydrogenation over Mg_5CeO_x with 0.8 wt.% K and 0 wt.% Cu (3.4 nmol m^{-2} s^{-1}) and a Mg_5CeO_x with 1.0 wt.% K and 7 wt.% Cu (240 nmol m^{-2} s^{-1}). Initial rates of formation of coupling products were also obtained for the same samples, and were reported to be 0.16 nmol m^{-2} s^{-1} and 0.76 nmol m^{-2} s^{-1} for the sample without copper, and with copper, respectively. The increase in dehydrogenation rate for the sample with Cu probably caused the observed increase in the coupling rate through the increased concentration of the aldehyde in the gas phase [29].

Gines and Iglesia [29] also observed that when copper was incorporated into the materials, the dehydrogenation and hydrogenation of alcohol and aldehyde, respectively, occur rapidly, which means that alcohol and aldehyde will both produce the coupled product. They also observed different incorporation rates of gas phase deuterium into the products when co-

feeding dideuterium over materials, with and without copper. For the oxide catalyst without copper, very little deuterium was incorporated into the products, whereas for the copper-containing materials, deuterium was significantly incorporated in the products as well as in the reactants [29]. Both Gines and Iglesia [29] and Nagarajan and Kuloor [34] suggest that copper facilitates the dehydrogenation of the alcohol and promotes the hydrogenation reactions of the adsorbed coupling products.

The temperature and pressure used in Gines and Iglesia's [29] study were similar to the conditions used by Tsuchida et al. [55] for the most active hydroxyapatite catalyst, which allows for some comparisons. While it is not possible to compare the coupling rates since they were reported at drastically different conversions, the dehydrogenation rate of the copper-containing material published by Gines and Iglesia [29] was about 370 times greater than that of hydroxyapatite with a Ca:P ratio of 1.67 [55] or 9 times greater if the coupling rates are also included in the calculation of a total dehydrogenation rate.

Summary and Suggestions

The Guerbet reaction or coupling of alcohols has seen a recent revival of interest especially with the use of heterogeneous catalysts in the upgrading of short chain alcohols. A preponderance of the literature indicates the reaction proceeds through an aldol-type intermediate, which requires the reactant alcohol(s) to first be dehydrogenated. Aldol-type coupling followed by dehydration and hydrogenation produces the Guerbet saturated alcohol product. Side reactions can completely deoxygenate the intermediate to form unsaturated

hydrocarbons like buta-1,3-diene from ethanol or cleave intermediates in the presence of water to form molecules like acetone or 2-methylpropene from ethanol.

Although dehydrogenation of the reactant alcohol is a critical first step, it can be difficult to study at conditions similar to those used in the Guerbet reaction due to rapid conversion of intermediate aldehydes and ketones. However, primary alcohols that do not have an α-hydrogen, like 2,2-dimethylpropan-1-ol, could be used as model reactants to shed light on this step. These dehydrogenation rates could be combined with model aldol condensations to provide an understanding of which steps are promoted over the different materials.

One interesting unresolved question in this area is how metal oxides and metal phosphates catalyze the hydrogenation of the aldol condensation products. Two likely paths include surface hydrogen that remains after alcohol dehydrogenation or from MPV hydrogen transfer from alcohol to the aldol condensation product. On copper, or on some other transition-metal-containing catalysts, there is rapid exchange with gas phase dihydrogen so the hydrogenation and dehydrogenation mechanisms on metal-containing catalysts are likely different than those on metal oxides and phosphates.

The rates of alcohol dehydrogenation, coupling and dehydration appear to be correlated to the acid-base properties of the materials as measured by adsorption of ammonia and carbon dioxide. More direct measurements (i.e. microcalorimetry) of surface affinity and capacity for acid and base probe molecules might provide more insights into the relationship between the acid and base properties and the reaction rates of reactant alcohol for the undesired (dehydration) and desired (dehydrogenation and coupling) products. Additionally, instead of the standard acid site and base site probes, (ammonia and carbon dioxide, respectively), different probe molecules may need to be used to interrogate the types of surface species believed to be active in this reaction.

For example, carbonate (formed by CO_2 adsorption on basic metal oxides) is a very different structure than alkoxide (formed by alcohol adsorption on basic metal oxides). Whereas the overall adsorption capacities of acid and base sites of these materials are certainly part of the picture, additional information is still needed. The most active metal oxide or phosphate catalysts apparently have significant densities of weak acid and medium to strongly basic sites. What is not known is the proximity of the acid and base sites. New probes to study acid-base site pairs need to be developed.

While many materials have been explored for the Guerbet reaction, some of the most promising materials include copper-containing mixed oxides ($K\text{-}CuMg_5CeO_x$) and hydroxyapatite with a stoichiometric ratio of calcium to phosphate. Further investigation of acid-base properties of materials as well as their activity in the individual reaction steps that comprise the overall Guerbet reaction could provide information to further advance these and other materials for alcohol coupling.

Acknowledgements

This work was supported by the Chemical Sciences, Geosciences and Biosciences Division, Office of Basic Energy Sciences, Office of Science, U.S. Department of Energy, grant no. DE-FG02-95ER14549.

Objectives of this Work

Guerbet coupling of alcohols as well as other reactions involving surface acid and base sites, including acetone condensation and transesterification, will be explored in this dissertation. The next two chapters will discuss Mg-Zr mixed metal oxides for transesterification of tributyrin with methanol (Chapters 2 and 3), acetone condensation, acetone coupling, and ethanol coupling (Chapter 3). Chapters 4 and 5 will discuss alcohol coupling with an emphasis on understanding the reactivity of MgO (Chapter 4) and on how modifying the acid and base characteristics of zirconia impact the selectivity and rates for ethanol coupling and acetone condensation (Chapter 5). Throughout this dissertation particular efforts were made to relate catalytic activity to surface acid and base properties of the materials as measured by ammonia and carbon dioxide adsorption microcalorimetry as well as IR spectroscopic studies of adsorbed molecular probes. In particular, this dissertation will address the following research questions:

1. How does Zr affect the catalytic activity of MgO in transesterification, aldol coupling, and alcohol reactions?

2. How does the synthesis procedure affect the reactivity and acid-base characteristics of Mg:Zr mixed oxides?

3. What are the fundamental kinetic parameters (surface coverages, turn over frequencies) for the coupling of ethanol over MgO?

4. How does modification of the surface acid and base properties of ZrO_2 with alkali metal influence catalytic performance in the ethanol coupling reaction?

Chapter 2: Transesterification of Tributyrin with Methanol over Basic Mg:Zr Mixed Oxide Catalysts.

This chapter was previously published as: J.T. Kozlowski, M. Aronson, R. J. Davis, "Transesterification of tributyrin with methanol over basic Mg:Zr mixed oxide catalysts" Applied Catalysis B: Environmental, 96, 508-515 (2010). It was also the basis for my Master's Thesis. It is presented here to provide context for the subsequent chapters.

Introduction

Many different alternatives are being explored to reduce the use of fossil fuels for energy generation and thereby reduce the addition of carbon dioxide to the atmosphere. One of the alternatives for transportation fuel is biodiesel, the common name for fatty acid methyl esters derived from naturally-occurring triglycerides. In one common process to produce biodiesel, triglycerides are transesterified with a short chain alcohol such as methanol to produce monoalkyl esters (biodiesel) and glycerol. The production of biodiesel is generally catalyzed by a homogeneous base catalyst such as sodium methoxide, sodium hydroxide, or potassium hydroxide [96–100]. Due to the separation requirements imposed on production systems that use homogeneous base catalysts, the search for a suitable solid base catalyst is being pursued [100–104]. Metal oxides represent solid catalysts with a high potential for replacing liquid catalysts [96,97,99,100]. Some metal oxides exhibit surface basic properties and high thermal stability, which makes them useful as solid base catalysts and catalyst supports [101,102,105]. Since the transesterification reaction is well-recognized to be catalyzed by solid bases, it serves as an excellent probe reaction for interrogating the nature of metal oxide surfaces [98,103,104,106].

Magnesia is a well-studied solid base metal oxide that catalyzes a variety of reactions, such as 2-propanol decomposition [107–109], Meerwein-Ponndorf-Verley reaction [110], methylbutynol decomposition [111], double bond isomerization [108,112], cycloaddition of CO_2 to epoxides [113], and transesterifcation [103]. Zirconia is of particular interest in this study because it is an amphoteric oxide that exposes both acid and base sites. Indeed, the transesterification of triglycerides occurs in the presence of basic and acidic catalysts, however the rate is orders of magnitude faster with a base catalyst [98–100,114]. Zirconia catalyzes a wide variety of reactions, such as dehydration and dehydrogenation of alcohols, conversion of synthesis gas to higher alcohols, hydrogenation of olefins, as well as hydrocracking, esterification and oxidation reactions [115]. A more complete discussion of the reactions catalyzed by zirconia can be found in Yamaguchi's review article [115].

Recent reports in the literature suggest that mixed oxides of Mg and Zr may exhibit desirable basic properties. The mixed oxide catalysts have been shown to expose more base sites than MgO based on temperature programmed desorption (TPD) of carbon dioxide and high activity for base catalyzed reactions, including 2-propanol to propanone [86,107], 2-methyl-3-butyn-2-ol decomposition [111], transesterification [116], Knoevenagel condensation [117] and bifunctional aldol condensations [92,118]. The nature of the mixed oxide catalysts appears to be affected by their synthesis method. Prior studies have utilized samples prepared by sol-gel chemistry, precipitation and impregnation [86,111,119–123].

In this particular study, several basic mixed oxides of magnesium and zirconium were synthesized, characterized and evaluated for activity in transesterification of tributyrin with methanol, a model reaction for biodiesel synthesis. A comparison of samples prepared by co-precipitation and by a sol-gel method will be presented. The surface character of the basic

oxides has been explored by adsorption of probe molecules. In particular, Diffuse Reflectance Infrared Fourier Transform Spectroscopy (DRIFTS) of adsorbed carbon dioxide and methanol along with carbon dioxide adsorption microcalorimetry were used in this work.

Experimental Methods

Catalyst Preparation

Precipitation Method

The following method, which we will refer to as precipitation or co-precipitation, was used to prepare pure metal oxide or mixed metal oxide, respectively, based on the work of Aramendia et al. [119]. First, 51 g of magnesium nitrate hexahydrate (Acros Organics, 98%) was dissolved in 1 L of deionized water. Zirconyl nitrate hydrate (Acros Organics, 99.50%) was also dissolved in the solution. The amount dissolved depended on the amount of zirconia desired in the catalyst. For example, to prepare a sample with an 11:1 molar ratio of Mg to Zr, 4 g of zirconyl nitrate hydrate was dissolved. The oxide was then precipitated by the dropwise addition of 25 wt.% NaOH solution (Mallinckrodt Chemicals, 98.8%). Sodium hydroxide solution was added until the metal oxide solution reached a pH of 10. The mixture was then allowed to age for 72 h, after which it is was filtered and dried at 413 K. Subsequently, the catalyst was calcined at 773 K in 100 cm^3 min^{-1} of flowing ultra high purity dioxygen (GT&S Welco) for 3 h. After calcination, the catalyst was washed with 20 L of deionized water to remove adsorbed sodium.

A mixed oxide of Mg and Ti was prepared using TiO_2 (Riedel-de Haen, puriss) as the precursor and was mixed into the solution containing magnesium nitrate. The magnesium was then precipitated onto the titania and calcined using the same procedure as described as above.

Catalysts prepared by this precipitation method will be denoted with –P after the catalyst descriptor, such as MgO-P and ZrO_2-P.

Sol-Gel Synthesis Method

The sol-gel procedure was adapted from the work of Liu et al. [122]. Magnesium acetate tetrahydrate (Fisher Chemical, 99.2%) 0 to 80 g, was dissolved in 304 g of absolute ethanol (Sigma-Aldrich >99.5% ACS reagent), together with the non-ionic surfactant Plurionic P-123 (BASF). A solution containing 0 to 25 cm^3 of zirconium (IV) propoxide (70 wt% in 1-propanol, Aldrich) and corresponding amounts of acetylacetone (Sigma-Aldrich ReagentPlus, >99%) 0 to 2.5 cm^3 was added to the ethanol solution, based on the amount of zirconium (IV) propoxide used. This mixture was stirred for 1 h at room temperature and then heated to 323 K, at which point 18 g of deionized water was added dropwise. The mixture was then held at 323 K for 24 h. The resulting slurry was filtered and the recovered solid was refluxed in 500 cm^3 of ammonium hydroxide solution at a pH 10 for 24 h at 373 K. The solid was again removed from solution by filtration. The material was dried in air at 413 K and then calcined by heating at 1 K min^{-1} to 973 K in flowing air at 100 cm^3 min^{-1}.

For comparison, a mixed oxide of 3:1 Mg:Ti was prepared using titanium (IV) propoxide (Fluka) as the metal precursor and was treated exactly as above.

Catalysts prepared by this precipitation method will be denoted with –SG after the catalyst descriptor, such as MgO-SG and ZrO_2-SG.

Catalyst Characterization

The elemental analysis (Zr, Mg, Na) was performed by Galbraith Laboratories (2323 Sycamore Drive, Knoxville, TN 37921) using ICP – OES analysis.

Adsorption of N_2 was performed on a Micromeritics ASAP 2020 automated adsorption system to obtain the BET surface areas and cumulative pore volumes of the catalysts.

The X-ray diffraction patterns were recorded on a Scintag XDS 2000 diffractometer using Cu K α radiation. Scans were collected from 2-theta of 5° to 90° at a rate of 2° min^{-1}.

The DRIFTS experiments were carried out in a Harrick Praying Mantis accessory on a Bio-Rad FTS – 60A FTIR spectrometer. A sample was first mixed with KBr powder (75 wt% KBr, 25 wt% sample) and loaded into the DRIFTS cell. Scans were recorded after heating to 773 K in flowing dinitrogen for 1 h and cooling to ambient temperature. Carbon dioxide (purified by 3 Å molecular sieves) was introduced to the cell at 30 cm^3 min^{-1} for a total of 30 s. In a second set of experiments, anhydrous methanol was introduced to the cell by saturating a flowing N_2 stream at 40 cm^3 min^{-1} and flowing the gas mixture over the sample for 15 min. After purging the cell with N_2, 100 scans of adsorbed CO_2 or CH_3OH were recorded at a resolution of 2 cm^{-1}. A temperature programmed experiment included heating the sample to various temperatures between 303 and 473 K in flowing N_2 and cooling to ambient temperature to acquire spectra.

Adsorption microcalorimetry experiments were carried out on the same home built instrument that has been described previously by Bordawekar et al. [124]. The instrument is a heat flow calorimeter with two cells that are inserted into a large aluminum block maintained at 303 K. One cell functioned as a sample cell and the other one served as a reference. A catalyst sample was first heated to 773 K for 3 h under vacuum to a pressure less than 10^{-2} Pa. The sample was then cooled and allowed to thermally equilibrate with the system for 2 h prior to adsorption of carbon dioxide. Initial dosing pressures of carbon dioxide ranged from 10 Pa to 600 Pa, and each dose was allowed to equilibrate with the sample for 15 min.

Transesterification

The catalytic transesterification reactions were conducted in a round bottom flask at 333 K with an overhead stirrer. The reactor was equipped with a reflux condenser and was continuously purged with flowing N_2 at 40 cm^3 min^{-1}. Unless otherwise indicated, methanol (Fisher, 99.9%) and tributyrin (Acros 98%) were used as reactants. In each run, 136.5 g (4.25 mol) of methanol and 43.8 g (0.14 mol) of tributyrin were loaded into the reactor with 6.5 g (0.5 mol) of dibutyl ether (Aldrich, 99.3%) as an internal standard. After the temperature of the reactants reached 333 K, 0.5 to 1 g of the catalyst, which was first heat treated at 773 K for 1 h in flowing purified N_2, was added to the reactants to initiate the transesterification. After thermal pretreatment, the catalyst was directly transferred to the reactor to avoid CO_2 contamination from air. Liquid samples were removed from the reactor at different time intervals and analyzed for products using the same procedure described in previous work by Xi et al. [103].

Some reaction tests were conducted with purified tributyrin to fully exclude the deactivation due to the possible carboxylic acid impurities from the tributyrin source. To obtain purified tributyrin, a mixture of 100 ml tributyrin and 40 ml saturated sodium carbonate aqueous solution (23.5 wt%) was vigorously stirred for 20 h at room temperature. Then the mixture was allowed to settle and the organic layer was separated. Approximately 16 g of 3A molecular sieves activated at 773 K were added to the organic layer and the mixture was allowed to remain at room temperature overnight. After the tributyrin was separated from the molecular sieves, vacuum distillation was performed to obtain purified tributyrin. In some cases, anhydrous methanol (Aldrich, 99.8%) was used as reactant. The purified reactants were tested in this reaction and had no observable effect on the activity of the mixed oxide catalysts.

To test the effect of catalyst recycling on activity, the used catalyst was separated from the product solution by centrifugation and washed with 200 ml methanol prior to charging back into the reactor with fresh reactants.

Possible leaching was tested by separating the catalyst from the reaction mixture by centrifugation, at approximately 50% conversion. The liquid reactants were reinserted into the reactor and evaluated for any additional conversion.

The transesterification of tributyrin (T) with methanol (M) proceeds in three consecutive steps as shown in the following reaction sequence:

$$T + M \xrightarrow{k_1} D + MB \qquad \textbf{(1)}$$

$$D + M \xrightarrow{k_2} Mo + MB \qquad \textbf{(2)}$$

$$Mo + M \xrightarrow{k_3} G + MB \qquad \textbf{(3)}$$

where D, MB, Mo and G denote dibutyrin, methyl butyrate, monobutyrin and glycerol, respectively. The reaction was assumed to be essentially irreversible and pseudo first order

because of the large of excess of methanol. The pseudo first order kinetic model with respect to the butyrin components was used here to quantify the reaction rate constants on a surface area basis k_1, k_2, k_3 (mol^{-1} L m^{-2} min^{-1}) and the deactivation parameter α (min^{-1}) [103].

Results and Discussion

Influence of Trace Sodium

The effect of washing the precipitated catalysts on the resulting level of trace sodium was investigated. A ZrO_2-P catalyst was first washed with 1 L of water. This sample had a residual loading of Na equal to 3.4 wt.% and was very active in the transesterification reaction (Table 2.1). A second ZrO_2-P catalyst was prepared in the same way except that it was washed with 5 L of water. The resulting catalyst had only 0.19 wt.% Na and a trace level of activity in transesterification. A third sample washed with 20 L of water had only 100 ppm of Na remaining on the catalyst. This zirconia sample had no perceptible activity for the transesterification under our standard conditions. The results from elemental analysis and reactivity tests are summarized in Table 2.1. These experiments confirmed that a pure zirconia sample is ineffective for transesterification of tributyrin with methanol at 333 K and that washing with 20 L of water was needed to remove sodium to levels that would not contribute to the transesterification reaction on the metal oxide surface. All further results presented are for catalysts that have been washed with 20 L of deionized water and have levels of Na that are negligible.

Table 2.1. Influence of trace sodium on the conversion of tributyrin and yield of methybutyrate over ZrO_2-P.

Sodium Concentration weight % (ppm)	Tributyrin Conversion[(a)] (%)	Methylbutyrate Yield[(b)] (%)
3.4 (34,000)	99.9	95.2
0.19 (1,900)	6.7	2.2
0.01 (100)	0	0

(a) Reaction conditions: 1.00 g ZrO_2-P, T=333 K, time = 2.66 h
(b) Methylbutyrate yield is defined as the moles of MB produced divided by the moles of TB reacted divided by 3 (since three moles of MB are produced per mole of TB at complete conversion)

Comparison of Mg:Zr Mixed Oxides Prepared by Co-precipitation and Sol-Gel Synthesis

Figure 2.1 compares the X-ray diffraction pattern of a Mg:Zr-P catalyst with a molar ratio of 11:1 to those of MgO-P and ZrO_2-P. The MgO-P and ZrO_2-P were exclusively in the periclase and tetragonal forms, respectively. The co-precipitated mixed oxide exhibited diffraction peaks associated with both periclase MgO and tetragonal ZrO_2. In general, co-precipitated mixed oxides consisted of a mixture of both pure oxide crystals.

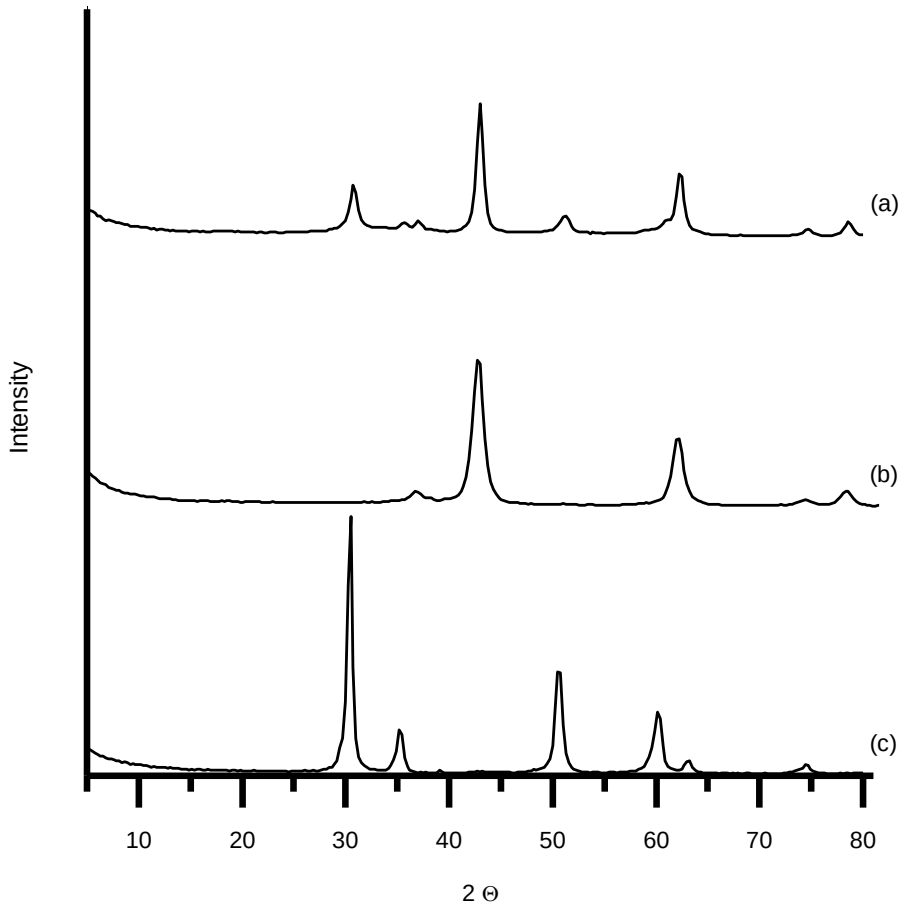

Figure 2.1. Representative X – ray diffraction patterns of catalysts prepared by precipitation. (a) Mg:Zr-P 11:1 (b) MgO-P (c) ZrO_2-P. Patterns are offset for clarity.

Figure 2.2 compares a similar set of diffraction patterns for materials prepared by sol-gel synthesis. In this case, pure ZrO_2-SG had diffraction features associated with both the tetragonal and monoclinic (indicated by arrows) phases. Magnesia prepared by the sol-gel route was in the periclase form, consistent with the precipitated sample. The diffraction pattern of the 5:1 Mg:Zr-SG mixed oxide had very low intensity, broad features associated with periclase MgO. No crystalline form of ZrO_2 was detected. Evidently, sol-gel synthesis results in a sample that was better mixed at the atomic level, thus preventing crystallization of the individual oxides.

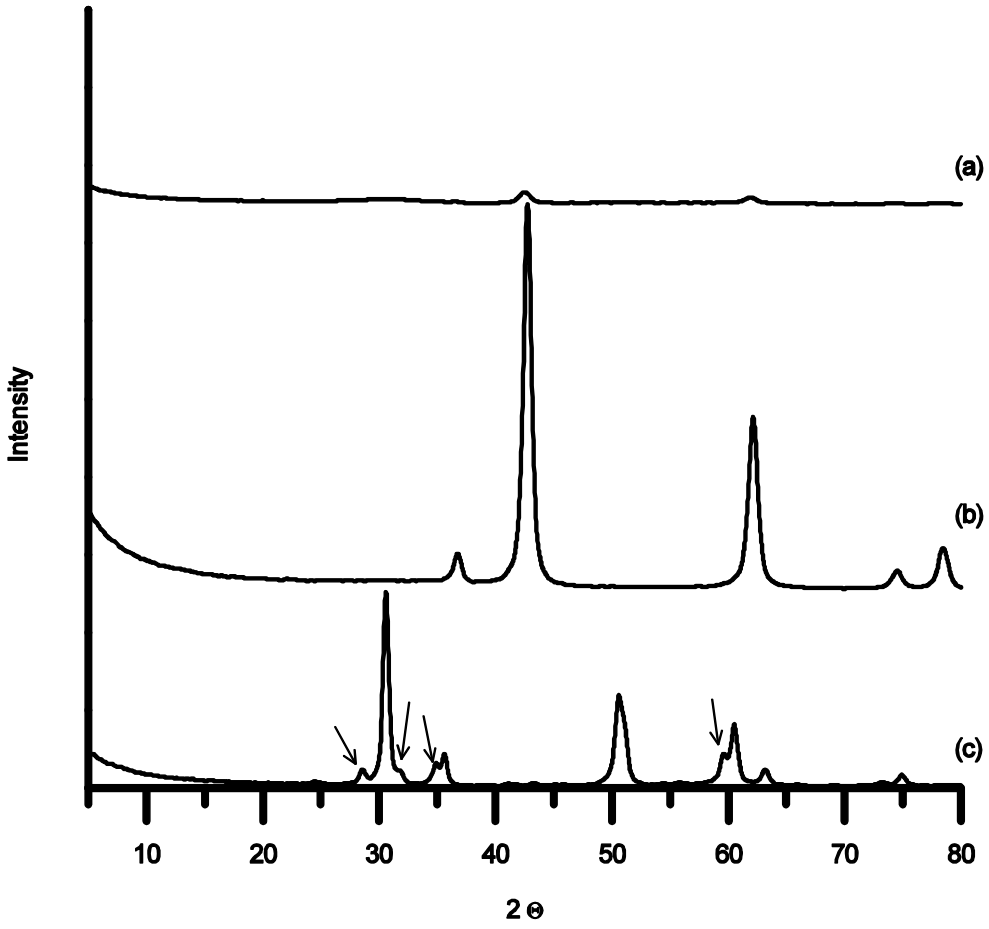

Figure 2.2. Representative X – ray diffraction patterns of catalysts prepared by sol-gel synthesis. (a) Mg:Zr-SG 5:1 (b) MgO-SG (c) ZrO_2-SG (arrows indicate monoclinic ZrO_2). Patterns are offset for clarity.

A typical reaction profile for the transesterification of tributyrin with methanol over a mixed oxide catalyst is presented in Figure 2.3. The lines in the figure are the results from the fitting procedure used with the experimental points. The rate constants derived from the fitting procedure are used to compare the reaction rates over the various materials.

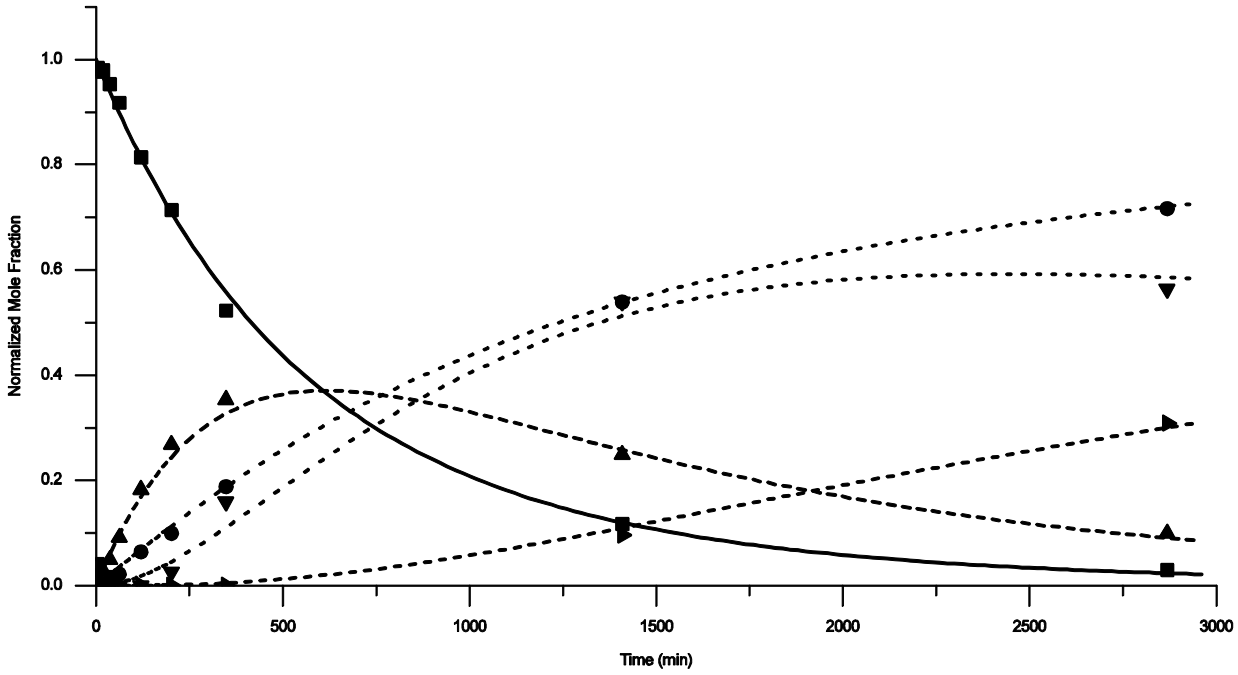

Figure 2.3. Reaction profile from transesterification of tributyrin with methanol at 333 K over 5:1 Mg:Zr-P mixed oxide. The lines are obtained by fitting the model to the experimental data points. The concentrations are normalized to initial tributyrin concentration, where methylbutyrate is divided by 3. ■ Tributyrin ▲Dibutyrin ▼Monobutyrin ►Glycerol ●Methylbutyrate

The rate constants for transesterification of tributyrin with methanol over a series of mixed oxides prepared by co-precipitation are compared to those associated with the pure oxides in Table 2.2. The simplest way to compare specific activity is to examine the rate constant for the consumption of tributyrin as characterized by k_1. In every case the rate constant for dibutyrin conversion to monobutyrin, represented by k_2, confirmed the activity ranking by tributyrin loss. Since the rate of monobutyrin consumption to form glycerol during the sequential reaction could not be reliably quantified (the glycerol level was very low through most of the reaction), it was

not reported. The rate constants were normalized by the exposed surface areas determined by N_2 adsorption.

Table 2.2. Surface areas and transesterification rate constants for catalysts prepared by precipitation and co-precipitation.

Catalyst	Surface Area (m^2 g^{-1})	Cumulative Pore Volume (cm^3 g^{-1})	Catalyst Loading (g)	k_1 ($x10^6$)[(d)] (L mol^{-1} m^{-2} s^{-1})	k_2 ($x10^6$)[(d)] (L mol^{-1} m^{-2} s^{-1})
Mg:Zr-P 1:1 (1.4)[(a)]	176	0.23	0.87	0.37 ± 0.12	0.34 ± 0.15
Mg:Zr-P 5:1 (5.6)[(a)]	223	0.22	0.75	0.50 ± 0.03	0.39 ± 0.09
Mg:Zr-P 8:1 (8.2)[(a)]	256	0.24	0.75	0.73 ± 0.07	0.75 ± 0.22
Mg:Zr-P 11:1 (11.1)[(a)]	173	0.56	0.82	3.00 ± 0.30	3.57 ± 0.85
MgO-P	292	0.46	0.90	0.70 ± 0.02	0.90 ± 0.07
MgO from $Mg(OH)_2$[(b)]	22	-	0.70	1.16 ± 0.34	1.19 ± 0.67
ZrO_2-P	123	0.12	1.00	0	0
MgO:ZrO_2-P 11:1[(c)]	-	-	1.00	1.19 ± 0.31	0.96 ± 0.41

(a) Values in parentheses indicate Mg/Zr molar ratio from elemental analysis
(b) $Mg(OH)_2$, nanopowder (Aldrich, 99.9%)
(c) A physical mixture of MgO-P and ZrO_2-P in a Mg:Zr 11:1 molar ratio.
(d) Errors represent 95% confidence intervals on fitted reaction rate constants

The results in Table 2.2 illustrate the effect of Zr on the reactivity of Mg-rich mixed oxides. Two important conclusions can be drawn from the results. First, decreasing the amount of Zr increased the activity of the mixed oxide for transesterification. Second, a mixed oxide with Mg:Zr-P ratio of 11:1 was 300% more active than pure MgO-P, on a surface area basis. This finding was unusual, but was repeated by re-synthesizing and retesting the mixed oxide catalyst. Moreover, MgO prepared from calcination of $Mg(OH)_2$ exhibited essentially the same activity as MgO-P, although the surface areas of the two MgO samples varied by more than an order of magnitude. As discussed earlier, ZrO_2 was inactive for transesterification under our standard conditions. Moreover, a physical mixture of MgO-P and ZrO_2-P in a ratio of 11:1 converted tributyrin at a rate similar to that of pure MgO-P (Table 2.2).

The rate constants for transesterification over a series of catalysts prepared by sol-gel synthesis are summarized in Table 2.3. As mentioned above, ZrO_2 was not active. Moreover, the activity of MgO-SG (Table 2.3), was similar to that formed by precipitation or calcination of commercial $Mg(OH)_2$ (Table 2.2). A 1:1 Mg:Zr-SG ratio was not active for transesterification which contrasts the result from a 1:1 Mg:Zr-P. Presumably, the atomic level mixing of Mg and Zr as achieved by the sol-gel method was detrimental to base catalysis. The rates observed over the 5:1 Mg:Zr mixed oxides were similar, but less than that of pure MgO. Apparently the synthesis method was not a critical parameter at high Mg contents. Unfortunately, we could not successfully prepare a mixed oxide catalyst with a high ratio of Mg:Zr (11:1) by the sol-gel route.

Table 2.3. Surface areas and transesterification rate constants for catalysts prepared by the sol-gel method.

Catalyst	Surface Area ($m^2\ g^{-1}$)	Cumulative Pore Volume ($cm^3\ g^{-1}$)	Catalyst Loading (g)	k_1 ($x10^6$)[(b)] (L $mol^{-1}\ m^{-2}\ s^{-1}$)	k_2 ($x10^6$)[(b)] (L $mol^{-1}\ m^{-2}\ s^{-1}$)
Mg:Zr 1:1-SG (0.96)[(a)]	118	0.27	0.83	0	0
Mg:Zr 5:1-SG (5.4)[(a)]	120	0.41	0.50	0.32 ± 0.08	0.43 ± 0.77
MgO-SG	134	0.37	0.74	0.87 ± 0.08	0.74 ± 0.16
ZrO_2-SG	120	0.11	1.00	0	0

(a) Values in parentheses indicate Mg/Zr molar ratio from elemental analysis
(b) Errors represent 95% confidence intervals on fitted reaction rate constants

The re-usability of the most active catalyst (11:1 Mg:Zr-P) was also tested. The catalyst was removed by centrifugation, washed with methanol and used for two subsequent reactions. The conversion of tributyrin and the yield of methylbutyrate for each reaction are presented in

Table 2.4. On the basis of tributyrin conversion, the catalyst retained 85% and 75% of its original activity after the first and second recycles, respectively.

Table 2.4. Recycle experiments for transesterification on Mg:Zr-P 11:1.

Reaction[a]	Tributyrin Conversion[b] (%)	Methylbutyrate Yield[c] (%)
1	84	52
2	72	39
3	61	25

(a) Run 1 is for fresh catalyst whereas subsequent runs are after centrifugation and methanol washing.
(b) Reaction conditions: 0.79 g 11:1 Mg:Zr-P, T=333 K, time = 22 h
(c) Methylbutyrate yield is defined as the moles of MB produced divided by the moles of TB reacted divided by 3

A mixed oxide was evaluated for leaching by removal of the catalyst in the middle of the reaction and checking for additional conversion in the reactant mixture. Figure 2.4 shows the reaction profile after removing a Mg:Zr-P 8:1 catalyst at about 180 min. Although there was some conversion of tributyrin after centrifugation, the majority of the rate was attributed to the solid catalyst. The small level of conversion after catalyst removal could be attributed to either a small amount of leaching or incomplete removal of small catalyst particles by centrifugation.

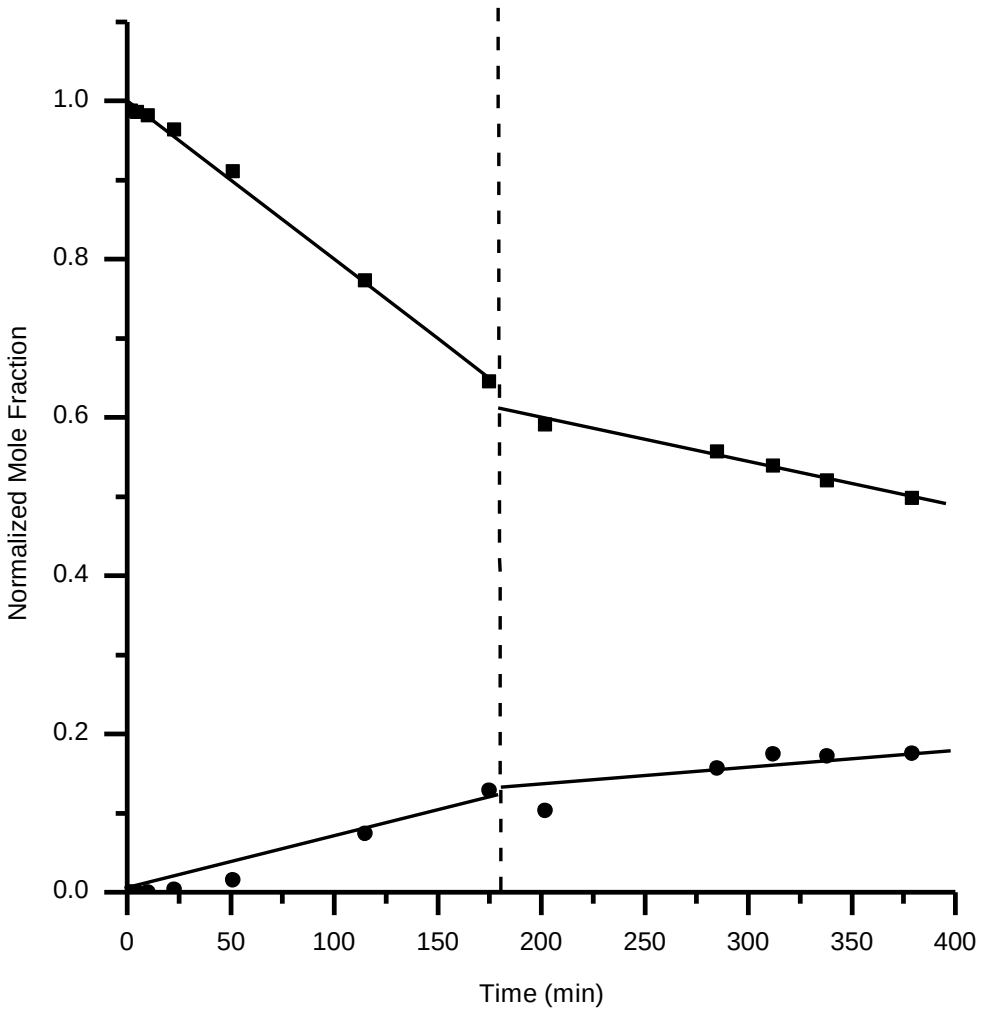

Figure 2.4. Reaction profile from transesterification of tributyrin with methanol at 333 K over 8:1 Mg:Zr-P mixed oxide. The concentrations are normalized to initial tributyrin concentration, where methylbutyrate is divided by 3. The dashed vertical line at approximately 180 minutes corresponds to the removal of the catalyst by centrifugation. ■ Tributyrin ●Methylbutyrate

DRIFTS of Adsorbed CO_2 and CH_3OH

Since the Mg-rich mixed oxide (Mg:Zr-P 11:1) was substantially more active than MgO-P, we attempted to characterize the nature of its surface by FT-IR spectroscopy of adsorbed CO_2

and CH_3OH. Carbon dioxide adsorption on basic oxides has been typically described by three different adsorption modes, bicarbonate, bidentate, and unidentate. Table 2.5 presents the schematic representations of these adsorbate structures and Table 2.6 summarizes the wavenumber positions of features typically associated with each mode. Each of the adsorption modes in Table 2.5 has asymmetric and symmetric O-C-O vibration modes. As indicated in Table 2.6, the bicarbonate structure also exhibits a C-OH bending mode. Figure 2.5 compares the DRIFTS of CO_2 on the pure oxides MgO-P and ZrO_2-P as well as on the highly-active 11:1 Mg:Zr-P mixed oxide. In the spectra associated with MgO-P, three different types of carbonate were detected. The intensities of the IR features decreased with increasing temperature as CO_2 desorbed from the surface. The features that disappeared first appear to originate from bicarbonate; for example, one of the bicarbonate peaks at 1225 cm^{-1} was absent after heating to 373 K. The bands associated with bidentate and unidentate carbonate remained in the spectra of CO_2 on MgO-P even after heating to 473 K. Interestingly, these features appeared to be more intense on the mixed oxide sample. Moreover, the DRIFTS confirmed the same features of CO_2 on both magnesia and zirconia.

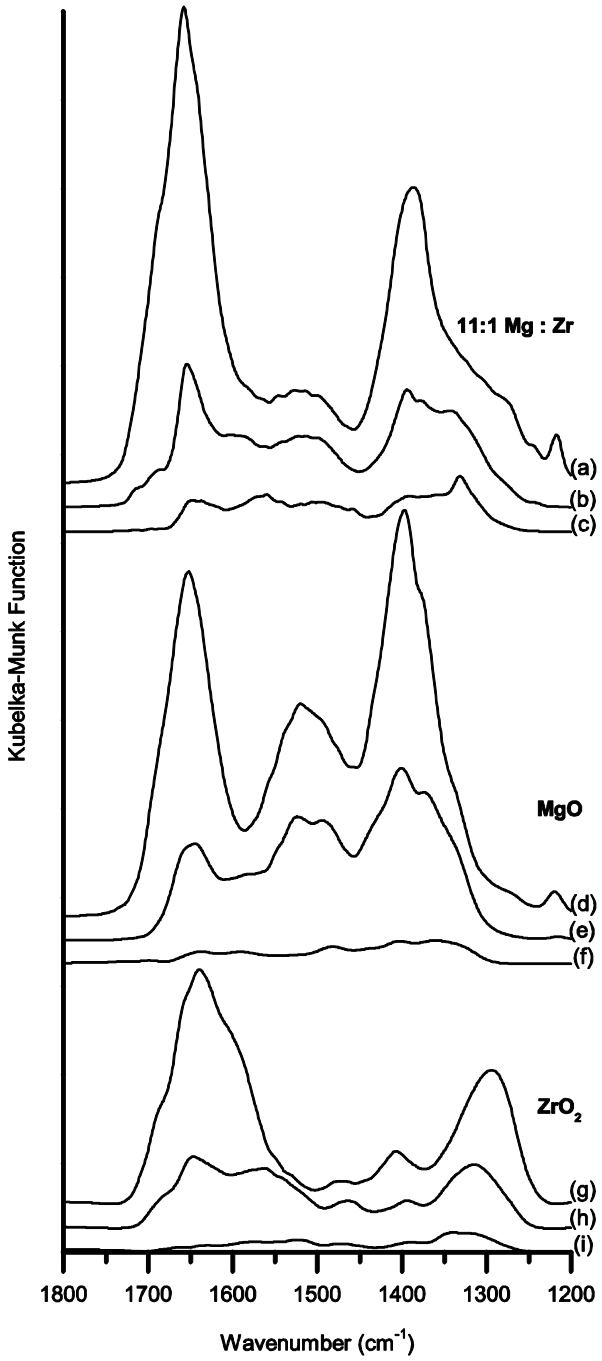

Figure 2.5. DRIFT spectra after adsorption and stepwise desorption of CO_2. Spectra (a), (b) and (c) are associated with CO_2 on Mg:Zr-P 11:1 after heating to 303, 373 and 473 K respectively, and cooling to 303 K. Spectra (d), (e) and (f) are associated with CO_2 on MgO-P after heating to 303, 373 and 473 K respectively, and cooling to 303 K. Spectra (g), (h) and (i) are associated with CO_2 on ZrO_2-P after heating to 303, 373 and 473 K respectively, and cooling to 303 K. Spectra are offset for clarity.

Table 2.5. Representative structures of adsorbed carbon dioxide and methanol [69,79,81,125–130].

Designation	Carbon Dioxide Adsorption Mode	Methanol Adsorption Mode
I	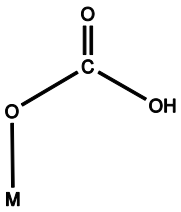	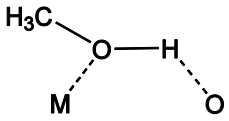
II	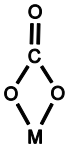	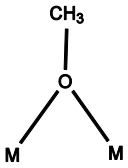
III	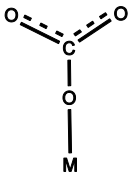	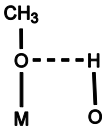

Since DRIFTS of adsorbed CO_2 did not reveal an obvious structural modification of the Mg:Zr-P mixed oxide surface, we explored the adsorption of CH_3OH. This molecule is a logical choice because it was a reagent in the transesterification reaction. In this case, significant differences were observed in the DRIFTS of CH_3OH on the catalysts. Tables 2.5 and 2.7 summarize the various modes of adsorbed CH_3OH and the positions of the IR features associated with those modes, respectively. The DRIFTS for CH_3OH on the representative catalyst samples are presented in Figure 2.6. Zirconia appears to have the largest relative amount of methanol adsorbed in the deprotonated form (Type III, Table 2.5) but the bands are broader and shifted in position to higher wavenumbers from the type III features on MgO-P and the Mg:Zr-P mixed

oxide. The MgO-P and Mg:Zr-P 11:1 samples have three modes of CH_3OH adsorption: molecularly-adsorbed (type I), bidentate (type II), and unidentate (type III). The unidentate and bidentate forms appears to be fairly stable since they were observed on the surface after heating to 473 K. Although the mixed oxide and magnesia had similar features in the DRIFTS of CH_3OH, the relative intensity of the bidentate mode compared to the unidentate mode was higher on the mixed oxide. Moreover, the IR spectra of methanol adsorbed on a physical mixture of MgO-P and ZrO_2-P in a ratio of 11:1 revealed features that were nearly identical to the spectra associated with MgO-P in Figure 2.6. At this point, we cannot state whether any of these structures are relevant to the transesterification reaction of tributyrin with methanol.

Table 2.6. Representative values for the IR shifts for carbon dioxide adsorption in the range of 1200-1800 cm^{-1} [69,81,125–128].

	ν_{as} OCO (cm^{-1})[(a)]	ν_s OCO (cm^{-1})[(b)]	ν COH (cm^{-1})[(c)]
Bicarbonate (MgO)	1646-1650	1405-1480	1220-1225
Bidentate (MgO)	1610-1691	1320-1362	N/A
Unidentate (MgO)	1360-1405	1510-1560	N/A
Bicarbonate (t-ZrO_2)[(d)]	1620	1450	1225-1230
Bidentate (t-ZrO_2)[(d)]	1550-1570	1325-1350	N/A
Unidentate (t-ZrO_2)[(d)]	1425-1430	1450-1460	N/A

(a) Asymmetric O-C-O stretching vibration
(b) Symmetric O-C-O stretching vibration
(c) COH bending mode only associated with bicarbonate
(d) t-ZrO_2 is tetragonal zirconia

Table 2.7. Representative values for the IR vibration modes for methanol adsorption in the range of 1200-1000 cm^{-1} [79,129,130]**.**

	ν H_3C-O (cm^{-1})[(a)]
Molecularly Adsorbed (MgO)	1033-1060
Bidentate (MgO)	150-192
Unidentate (MgO)	1090-1115
Bidentate (t-ZrO2)[(b)]	1070
Unidentate (t-ZrO2)[(b)]	1154

(a) C-O vibrations of adsorbed methanol
(b) t-ZrO_2 is tetragonal zirconia

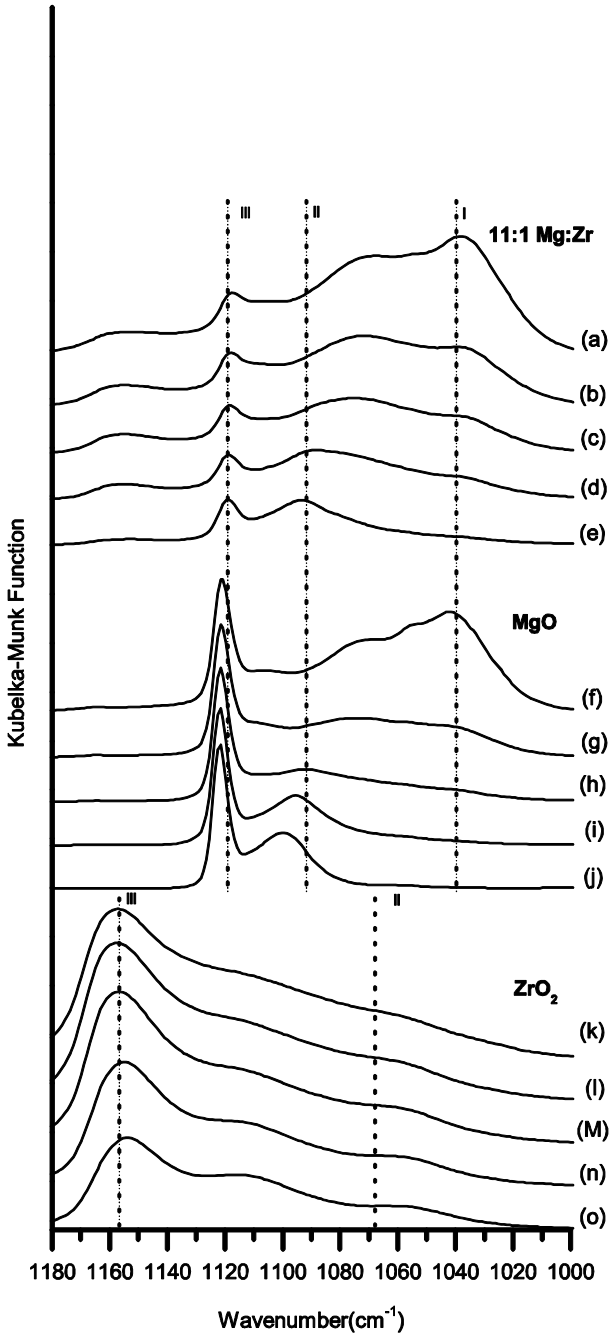

Figure 2.6. DRIFT spectra after adsorption and stepwise desorption of CH_3OH. Spectra (a), (b), (c), (d), and (e) are associated with CH_3OH on Mg:Zr-P 11:1 after heating to 303, 333, 373, 423 and 473 K respectively, and cooling to 303 K. Spectra (f), (g), (h), (i) and (j) are associated with CH_3OH on MgO-P after heating to 303, 333, 373, 423 and 473 K respectively, and cooling to 303 K. Spectra (k), (l), (m), (n) and (o) are associated with CH_3OH on ZrO_2-P after heating to 303, 333, 373, 423 and 473 K respectively, and cooling to 303 K. Spectra are offset for clarity.

CO2 Adsorption Microcalorimetry

Figure 2.7 presents the CO_2 adsorption isotherms obtained from the adsorption microcalorimetry experiments. The total CO_2 capacity was derived from extrapolating the saturation portion of the isotherm to zero pressure as depicted by the solid lines in the plots. Although the uptakes were similar on the materials (1-2 μmol CO_2 m^{-2}), ZrO_2-P had the largest adsorption capacity, followed by the Mg:Zr-P 11:1 mixed oxide, and MgO-P. A comparison of the CO_2 uptakes as summarized in Table 2.8 to the rate constants presented in Table 2.2 indicates that there is no correlation between the CO_2 capacity and the activity for transesterification. This is rather surprising since CO_2 is often used as a measure of surface basicity.

Table 2.8. Summary of results from CO_2 adsorption microcalorimetry on Mg and Zr oxide samples, prepared by precipitation.

Catalyst	Catalyst Loading (g)	CO_2 Uptake (μmol m^{-2})	Initial Heat of Adsorption (kJ mol^{-1})	Heat at 1/2 Coverage (kJ mol^{-1})
Mg:Zr-P 1:1 (1.4)[(a)]	0.14	1.6	145	117
Mg:Zr-P 5:1 (5.6)[(a)]	0.13	1.2	154	126
Mg:Zr-P 8:1 (8.2)[(a)]	0.16	1.0	154	106
Mg:Zr-P 11:1 (11.1)[(a)]	0.20	1.3	170	104
MgO-P	0.12	1.2	127	101
t-ZrO_2-P	0.30	1.7	114	98

(a) Values in parentheses indicate Mg/Zr molar ratio from elemental analysis

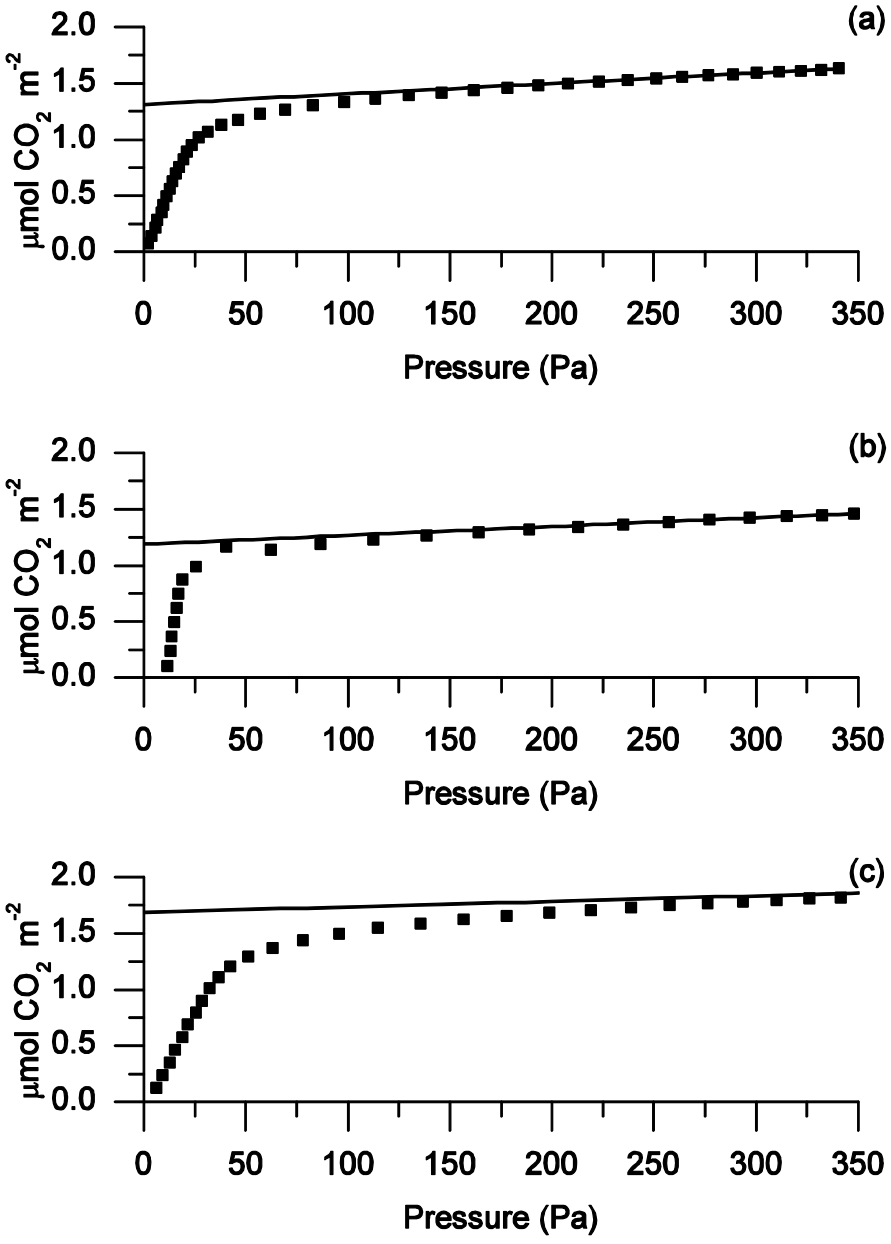

Figure 2.7. Representative CO_2 adsorption isotherms, on (a) Mg:Zr-P 11:1 (b) MgO-P, and (c) ZrO_2-P prepared by precipitation obtained from the microcalorimetry experiment. The lines represent the extrapolation of saturation conditions to zero pressure to obtain the total CO_2 adsorption capacity.

Figure 2.8 compares the heat of adsorption as a function of CO_2 adsorption on the precipitated materials. The initial heat of adsorption represented by the first point at low coverage is reported in Table 2.8 along with the heat of adsorption at a surface coverage equal to half the saturation coverage. As with CO_2 adsorption capacity, there was no apparent correlation of the heat of CO_2 adsorption with the catalytic activity. However, it is interesting to note that the highest initial heat of adsorption (170 kJ mol^{-1}) was associated with the mixed oxide with the greatest catalytic activity. More work is needed to understand the role of the strongest of basic sites on the catalytic activity. One hypothesis for the exceptional activity of the 11:1 Mg:Zr-P mixed oxide is that a few basic sites with a high affinity for CO_2 are created by adding small amounts of Zr to MgO. The rest of the surface appears to expose sites similar to those on MgO-P, according to DRIFTS of CO_2 and CH_3OH.

These results suggest that perhaps a minor fraction of modified surface adsorption sites might account for the promotional effect of Zr on catalysis by MgO. These special minority sites could be located at grain boundaries between the Mg and Zr oxide crystallites. Recent work by Viduk et al. suggests that modification of grain boundaries in MgO creates strong base sites that are responsible for an approximately 4-fold increase in activity for transesterification [131]. Altered grain boundaries could explain the results we obtained for Mg:Zr-P 11:1 mixed oxide. Modified MgO-like base sites were observed by CO_2 adsorption microcalorimetry, DRIFTS of adsorbed methanol, and enhanced transesterification activity. Extensive characterization work is needed to confirm this idea.

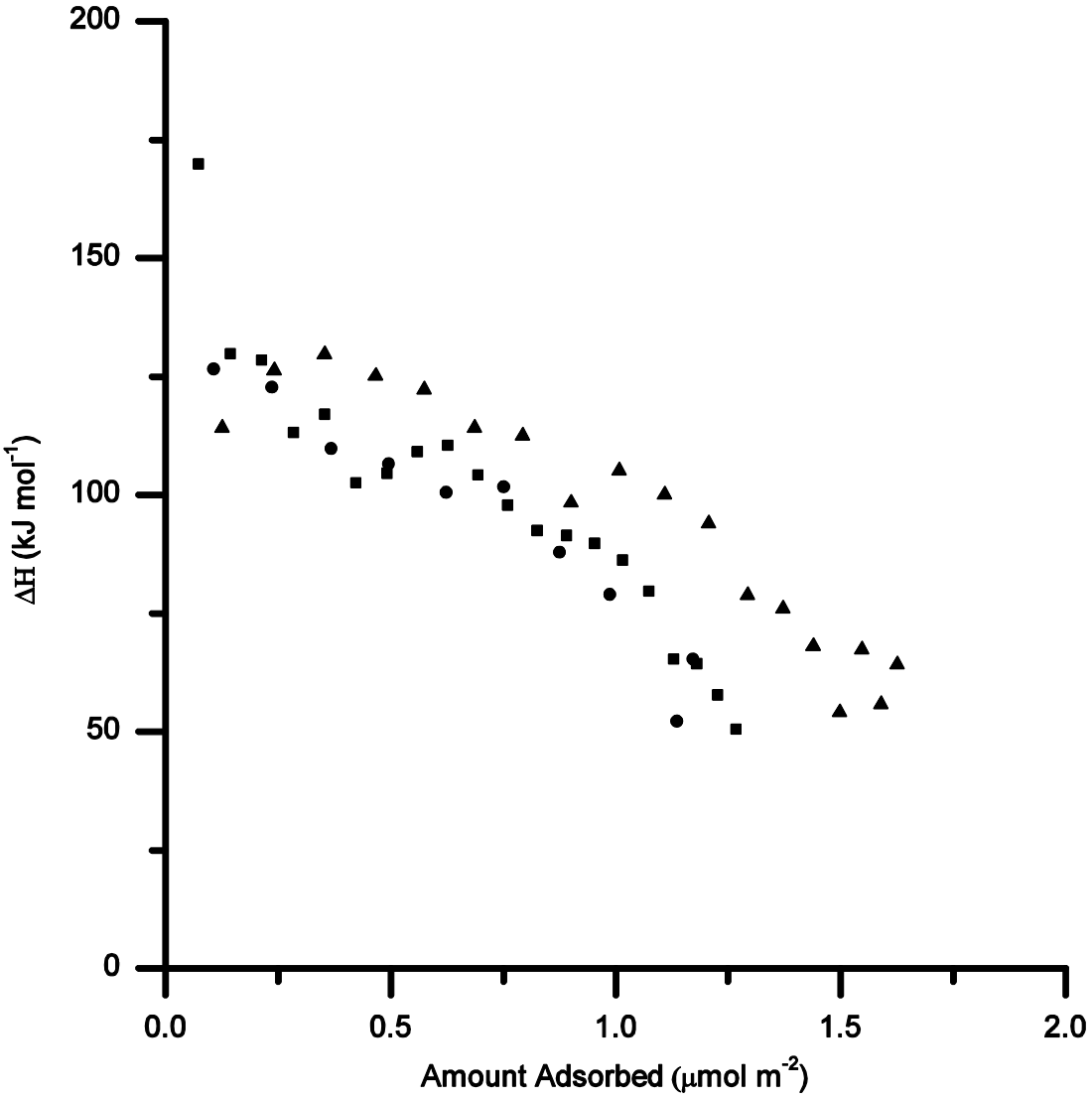

Figure 2.8. Heat of CO_2 adsorption as a function of the amount adsorbed, normalized by surface area, on samples prepared by precipitation. ■ Mg:Zr-P 11:1, ● MgO-P, and ▲ ZrO_2-P.

Comparison to a Mixed Oxide of Ti and Mg

Mixed oxides of magnesia and titania have also been reported to exhibit enhanced surface basicity compared to pure MgO [111,119]. Therefore, a mixed oxide prepared by precipitation of Mg onto TiO_2 with a Mg:Ti ratio of 14:1 was synthesized and determined to have a k_1 for transesterification of 0.4 L mol^{-1} m^{-2} s^{-1} with a surface area of 293 m^2 g^{-1}. This observed rate was approximately 50% of that associated with pure MgO-P on a surface area basis. A mixed oxide of Mg:Ti-SG ratio of 3:1 was also synthesized. Results from x-ray diffraction of the calcined material failed to reveal any crystalline phases. This sol-gel derived catalyst as well as pure titania obtained from precipitation, sol-gel synthesis, and Evonik (Aeroxide P25) were inactive for transesterification at our standard conditions.

Conclusions

Mixed oxides of magnesia and zirconia have great potential for base catalyzed reactions. First, mixed oxides prepared by sol-gel synthesis were better mixed at the atomic level since the x-ray diffraction patterns revealed poor crystallinity compared to samples prepared by co-precipitation. However, the only significant promotional effect for transesterification was observed on a magnesia-rich mixed oxide (Mg:Zr-P 11:1) prepared by co-precipitation. The x-ray pattern of this sample revealed phases of both MgO and ZrO_2, suggesting that perhaps the promotional effect occurred at the interface between phases. The influences of trace sodium and catalyst leaching on activity were ruled out by control experiments. In an attempt to relate surface properties to catalysis, DRIFTS of adsorbed CO_2 and CH_3OH were recorded on the most

active mixed oxide, standard MgO-P and inactive ZrO_2-P. The DRIFTS of adsorbed CO_2 was not effective at distinguishing between the samples. However, DRIFTS of adsorbed CH_3OH showed very significant differences among the samples. Although the mixed oxide sample was primarily composed of magnesia, the DRIFTS of CH_3OH showed a different ratio of unidentate to bidentate modes. Moreover, the initial heat of CO_2 adsorption on the mixed oxide was greater than that on MgO-P. Initial attempts to promote magnesia with Ti were unsuccessful.

Acknowledgement

This work was supported by the Chemical Sciences, Geosciences and Biosciences Division, Office of Basic Energy Sciences, Office of Science, U.S. Department of Energy, grant No. DE-FG02-95ER14549.

Chapter 3: Influence of Precipitation Method on Acid-Base Catalyzed Reactions over Mg-Zr Mixed Oxides

This chapter was accepted for publication in ChemCatChem as: J.T. Kozlowski, M. Behrens, R. Schlögl, R.J. Davis, "Influence of Precipitation Method on Acid-Base Catalyzed Reactions Over Mg-Zr Mixed Oxides".

Introduction

Promotion of the classical solid base catalyst MgO by addition of amphoteric ZrO_2 has been recognized for many years [80,91,116,119,122,132–134]. For example, mixed oxides of MgO and ZrO_2 have been employed as catalysts and catalyst supports for reactions such as aldol condensation [91,92], transesterification [80,116], alcohol dehydration and alcohol dehydrogenation [111,135]. Both aldol condensation [40,90,91] and alcohol dehydrogenation [31,87] are claimed to be accelerated over materials with acid-base pairs (amphoteric materials) compared to traditional solid bases, which may account for the catalytic effectiveness of Mg:Zr mixed oxides. To properly investigate mixed oxides for reactions involving acid-base pairs, materials need to be properly prepared to expose the desired components. In this work, two different methods of synthesizing Mg:Zr mixed oxides will be compared for both sample uniformity and surface functionality.

The common solid base MgO has been explored extensively using many different techniques, including IR spectroscopy of adsorbed molecular probes [93,136–139], adsorption microcalorimetry [80,140,141], temperature-programmed desorption [79,122,131,142,143],

catalytic probe reactions [79,139,142,144], electron microscopy [131,143,145,146], and quantum chemical calculations [37,76–78,137,147–150]. These experimental and theoretical methods have provided a thorough understanding of the surface basicity and its structural origins in MgO. Many of these same techniques can also be used to probe the properties of Mg:Zr mixed oxides.

One way to quantify the acid and base sites on a material is to measure the heat of adsorption and the chemisorption capacity of ammonia and carbon dioxide, respectively, by adsorption microcalorimetry [80,124,141,151]. In this work, we will attempt to correlate the acid-base properties of the mixed oxides with structural features evaluated by the electron microscopy and X-ray diffraction. Although the physical characteristics are good indicators of surface reactivity, the ultimate test is performance in a catalytic reaction. Therefore, multiple catalytic reactions will be used to probe Mg:Zr mixed oxides.

As mentioned earlier, transesterification has been widely studied over magnesia and magnesia-containing materials [80,106,116,145,152,153], and prior work in our lab has confirmed the positive influence of Zr on MgO-catalyzed transesterification of tributyrin with methanol. Since MgO is well understood and has been evaluated thoroughly for transesterification, it is a reaction that can be used to probe the surface acid-base properties of related materials.

Acetone coupling, or aldol condensation of two acetone molecules, has also been studied over a wide variety of materials with particular attention paid to MgO. As with transesterification, acid-base bifunctional materials appear to be more effective catalysts than traditional solid bases for aldol condensation [39,40,90]. Some examples of acid-base bifunctional catalysts for aldol condensation include: Y/MgO [88], Mg:Al mixed oxides

[39,41,68,89], amorphous aluminophosphate [40], Cs/ZrO_2 [90], and Mg:Zr mixed oxides catalysts [91,92]. In many of these studies, a goal of the preparation was to locate a Lewis acid center in proximity to a strong base site. It is important to recognize, though, an increase in reactivity may not be exclusively the result of acid-base bifunctionality, but also may arise from a change in base site density and base site strength.

The reactions of alcohols can also be used to probe the acid-base character of mixed oxides [88,135,139,154]. Although alcohols can both dehydrate and dehydrogenate, the carbonyl product of dehydrogenation can also couple to form a heavier alcohol over suitable catalysts. Ethanol is of interest since the coupling product is butanol, which is of higher value [27,29,31,35,46,55,66,95,155]. While MgO has been studied quite extensively for ethanol reactivity [31,35,46,55,66], the relative rates of ethene, ethanal, and butanol formation can provide information on the surface acid and base properties of the Mg:Zr mixed oxide catalysts.

In this study, a Mg:Zr mixed oxide is synthesized via a constant pH precipitation method with the intent of producing a highly uniform sample that can be compared to a traditionally-precipitated Mg:Zr mixed oxide formed by increasing the pH during precipitation. Scanning electron microscopy and X-ray diffraction were performed on the mixed oxide catalysts to compare how the synthesis method impacted the sample morphology. Results from ammonia and carbon dioxide adsorption microcalorimetry, as well as rates from tributyrin transesterification with methanol, acetone coupling, and ethanol conversion, were correlated to morphological properties to elucidate how sample preparation can influence surface reactivity.

Experimental Methods

Catalyst Synthesis

Rising pH Precipitation

The following method, which is based on the work of Aramendia et al. [119], was used to prepare pure metal oxide and mixed metal oxide. First, 51 g of magnesium nitrate hexahydrate (Acros Organics, 98%) was dissolved in 1,000 cm^3 of distilled, deionized water. An appropriate amount of zirconyl nitrate hydrate (Acros Organics, 99.50%) was also dissolved in the solution to give the desired ratio of Mg:Zr. For example, to prepare a sample with a nominal 11:1 molar ratio of Mg to Zr (Mg:Zr 11:1), 4 g of zirconyl nitrate hydrate was dissolved. The oxide was then precipitated by the dropwise addition of 25 wt.% NaOH solution (Mallinckrodt Chemicals, 98.8%). Sodium hydroxide solution was added until the metal oxide solution reached a pH of 10. The mixture was then allowed to age for 72 h, after which it is was filtered and dried in air at 413 K. Subsequently, the catalyst was washed with water to remove Na, and calcined at 773 K in 100 cm^3 min^{-1} of flowing ultra-high purity dioxygen (Praxair, ultra-high purity) for 3 h.

Controlled pH Precipitation

Two separate aqueous solutions were fed to a continuously-stirred Labmax reactor. The first solution contained 1M NaOH solution, whereas the second one contained magnesium nitrate

hexahydrate and zirconyl nitrate hydrate in appropriate concentrations. For example, to prepare a sample with a nominal 11:1 ratio of Mg:Zr (Mg:Zr 11:1), a solution of 76.47 g of magnesium nitrate and 6.05 g of zirconyl nitrate dissolved in 500 cm^3 of distilled, deionized water was used. This mixed metal salt solution was fed to the Labmax reactor at a rate of 4.5 g min^{-1}, which had an initial volume of 400 cm^3 of distilled, deionized water and NaOH at an initial pH of 11. The solution was fed continuously until 390 grams had been pumped into the reactor. The NaOH solution was used to maintain the solution pH in the reactor at a constant value of 10.5 (This was the lowest value of pH that could be accurately controlled in this precipitation). The resulting solid was aged for 72 h, filtered, dried at in air 403 K, washed with water to remove Na, and calcined at 773 K in 100 cm^3 min^{-1} of flowing dioxygen.

Magnesia Supported onto Zirconia

An additional set of catalysts was prepared to investigate the role of zirconia as a support for magnesia. First, zirconia was precipitated using the rising pH method, dried, washed, and calcined as described above. Second, a specified amount of zirconia was added to a solution with 51 g of magnesium nitrate. Sodium hydroxide was then added to the solution until a pH of 10 was achieved. The resulting solid was then aged for 72 h, filtered, dried, calcined and washed identically to the metal oxides described above.

Catalyst Characterization

The elemental analysis (Zr, Mg, and Na) was performed by Galbraith Laboratories (2323 Sycamore Drive, Knoxville, TN 37921) using inductively coupled plasma optical emission spectrometry (ICP-OES).

Adsorption of N_2 was performed on a Micromeritics ASAP 2020 automated adsorption system to obtain the BET surface areas of the catalysts after evacuation at 723 K for 4 h.

The X-ray diffraction patterns were recorded on a PANalytical X'pert diffractometer using Cu K-α radiation.

Adsorption microcalorimetry experiments were completed on the same home built instrument that has been described previously by Bordawekar et al. [109,124,151,156]. The instrument is a heat flow calorimeter with two cells that are inserted into a large aluminum block maintained at 303 K. One cell functioned as a sample cell and the other one served as a reference. A catalyst sample was first heated to 773 K under vacuum to a pressure less than 10^{-2} Pa. The sample was then cooled and allowed to thermally equilibrate with the system for 2 h prior to adsorption of carbon dioxide or ammonia. Initial dosing pressures of adsorbate ranged from 10 Pa to 600 Pa, and each dose was allowed to equilibrate with the sample for 15 min.

Scanning electron microscopy (SEM) and energy dispersive X-ray analysis (EDX) were performed with a Hitachi S-4800 (FEG) equipped with an EDAX Sapphire detector on an EDAX Genesis 4000 system. The samples were loosely dispersed on an Al-stub with conductive carbon glue to preserve the as-prepared morphology as much as possible. The micrographs were taken in secondary electron and low angle back scattered electron mode with an accelerating voltage of 2 kV or 15 kV.

Transesterification of Tributyrin with Methanol

The catalytic transesterification reactions were performed in a round bottom flask at 333 K with an overhead stirrer. The reactor was equipped with a reflux condenser and was continuously purged with flowing N_2 (Praxair, ultra-high purity and additionally purified by passage through a Supelco OMI-2 purifier) at 40 cm^3 min^{-1}. Methanol (Fisher, 99.9%) and tributyrin (Acros 98%) were used as reactants. In each run, 136.5 g of methanol and 43.8 g of tributyrin were loaded into the reactor with 6.5 g of dibutyl ether (Aldrich, 99.3%) as an internal standard. After the temperature of the reactants reached 333 K, 0.5 to 1 g of the catalyst, which was first heat treated at 773 K for 1 h in flowing purified N_2, was added to the reactants to initiate the transesterification. The catalyst was directly transferred to the reactor to avoid CO_2 contamination from air. Liquid samples were removed from the reactor at different time intervals and analyzed for products using an Agilent 5890 gas chromatograph equipped with a DB-5 capillary column.

The transesterification of tributyrin (T) with methanol (M) proceeds in three consecutive steps as shown in the following reaction sequence:

$$T + M \xrightarrow{k_1} D + MB \qquad \textbf{(1)}$$

$$D + M \xrightarrow{k_2} Mo + MB \qquad \textbf{(2)}$$

$$Mo + M \xrightarrow{k_3} G + MB \qquad \textbf{(3)}$$

where D, MB, Mo and G denote dibutyrin, methyl butyrate, monobutyrin and glycerol, respectively. The reaction was assumed to be essentially irreversible and pseudo first order

because of the large of excess of methanol. The pseudo first order kinetic model with respect to the butyrin components was used here to quantify the reaction rate constants on a surface area basis k_1, k_2, k_3 (L mol^{-1} m^{-2} min^{-1}) and the deactivation parameter α (min^{-1}). This is the same procedure that has been described in detail in previous works [80,152,153,157], however, only k_1 is reported here.

Acetone Coupling

Acetone coupling was carried out in a round bottom flask maintained at 299 K. The 150 cm^3 reactant solution consisted of 95 wt.% acetone (Sigma-Aldrich, $\geq$99.9%) and 5 wt.% hexane (Sigma-Aldrich, $\geq$97%) as an internal standard. The acetone solution was rapidly stirred with a magnetic stir bar. After the temperature of the reactant reached 299 K, a thermally-pretreated catalyst (773 K for 1 h in flowing purified N_2) was added to the reactor without exposure to air to initiate the coupling reaction. The amount of catalyst used was adjusted to give 40 m^2 of surface area and the reactor was initially purged for 10 minutes with 100 cm^3 min^{-1} of purified dinitrogen prior to addition of the catalyst. Samples of the product were taken at different time intervals and analyzed with an Agilent gas chromatograph equipped with a DB-WAX column. The initial rates of acetone coupling were calculated by producing a linear fit to the production of diacetone alcohol over the first 30 minutes of reaction. The selectivity to diacetone alcohol was >99% and conversion of acetone was between 1 and 2%. The rates presented here were normalized to surface area of catalyst added to the reaction.

Acetone Condensation

Acetone condensation was carried out in a gas phase, downward flow, fixed bed reactor. The feed to the reactor, 95 wt.% acetone (Sigma-Aldrich, ≥99.9%) and 5 wt. % hexane (Sigma-Aldrich, ≥97%) as an internal standard, was pumped to a vaporizer at a rate of 0.02 cm^3 (liquid) min^{-1}. The acetone/hexane vapor was then mixed with 100 cm^3 min^{-1} flowing He to give 5.5 % acetone in the vapor stream. All gas lines were maintained at 473 K to avoid condensation of reactants and products. The feed mixture flowed through the catalyst bed and then into a gas sampling valve for online gas chromatography. This reaction was performed at less than 103.4 kPa gauge and at 573 K. A constant surface area of metal oxide catalyst, 14 m^2 g^{-1}, was loaded into the fixed bed reactor. Product analysis was carried out with an Agilent 7890 GC equipped with a DB-WAX column.

Dehydration and Dehydrogenation of Ethanol

Conversion of ethanol was carried out in a gas phase, downward flow, fixed bed reactor. A reactant stream of ethanol (Sigma-Aldrich, 99.5% purity anhydrous) and 5 wt.% octane (Sigma-Aldrich, 99.9% purity anhydrous) as an internal standard was fed to a vaporizer that contained glass beads and 3 Å molecular sieves to remove water from the ethanol feed. The ethanol and octane mixture was vaporized and mixed with flowing N_2 to give 6.8 % ethanol in the vapor stream. The vaporizer was maintained at 333 K and all gas lines were maintained at 473 K to avoid condensation of reactants and products. The feed mixture flowed through the catalyst bed and then into a gas sampling valve for online gas chromatography. The GC column

was a Varian CP-Poraplot column, 25 m in length with an internal diameter of 0.32 mm. The reaction was performed between 136 to 170 kPa absolute and at 673 K. The flow rate of N_2 and reactant liquid was 100 cm^3 min^{-1} and 0.02 cm^3 min^{-1} respectively.

Results

Catalyst Characterization

Synthesis of Mg:Zr mixed oxides by the rising pH precipitation method can create non-uniform distributions of the two oxides in the final material [91]. Therefore, we desired to compare the physical properties and catalytic effectiveness of the materials prepared at constant pH to those prepared by the rising pH method. Figure 3.1 shows the pH in a Labmax reactor throughout the synthesis of a Mg:Zr 11:1 mixed oxide and confirmed that the precipitation occurred at a constant pH of 10.5.

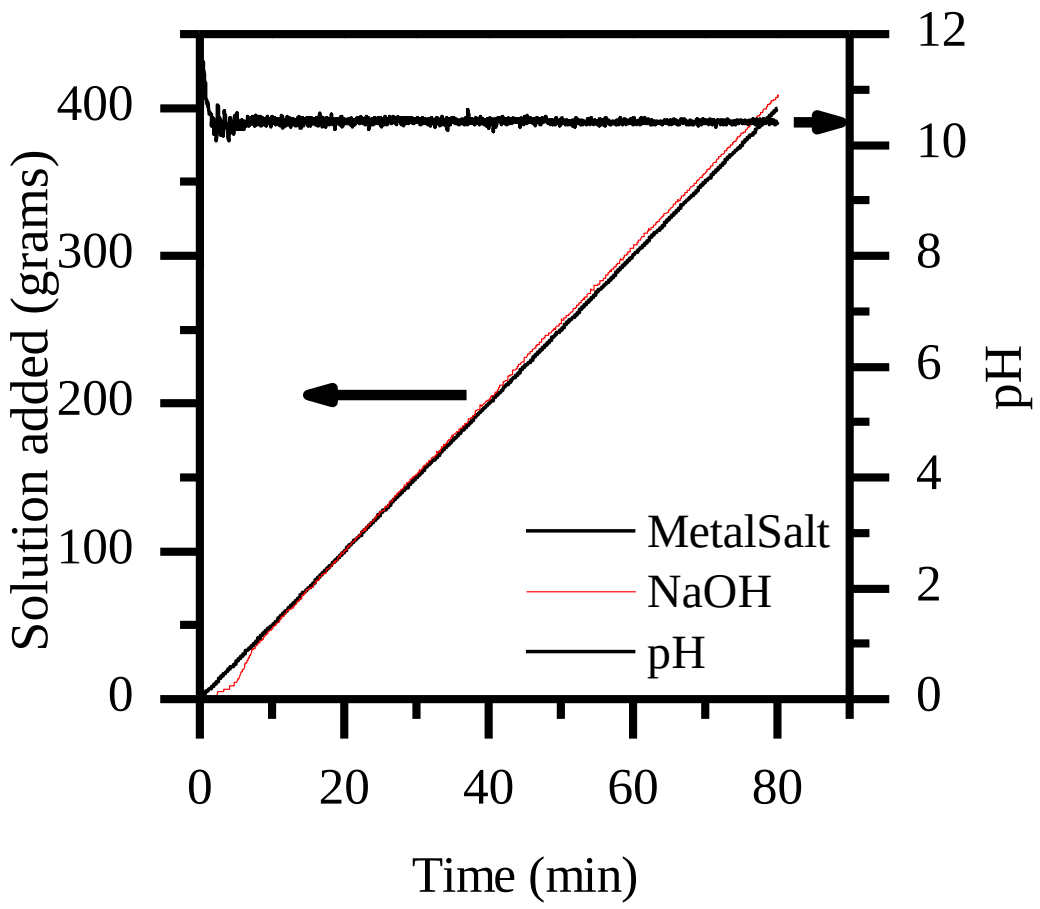

Figure 3.1. The pH of the slurry containing precipitate (Mg:Zr 11:1) as sodium hydroxide and metal precursor were continuously added to the Labmax reactor. (--) grams of 1 M NaOH(aq) solution added, (-) grams of metal salt precursor solution added, (-) pH of solution

Table 3.1 summarizes the compositions of all the materials prepared in this work. It should be noted that all the materials prepared by the rising pH precipitation method, except for the Mg on Zr 11:1 sample, are the same ones presented in Kozlowski et al. [80]. Residual Na levels were evaluated since alkali metals will influence the acid-base properties of the solids. In

all cases, the Na level was lower than 350 ppm, with the majority of samples having less than 100 ppm Na. In prior work, Na loadings below 1,000 ppm had a negligible effect on reactivity in the transesterification of tributyrin with methanol. Measured ratios of Mg:Zr were close to the nominal values, illustrating the effectiveness of the precipitation.

Table 3.1. Results from N_2 adsorption and elemental analysis.

Catalyst	Synthesis Method or Source	Surface Area (m^2 g^{-1})	Mg Content on a Metals Basis (Mg/(Mg+Zr))	Na Content (ppm)
Mg:Zr 1:1[a]	Rising pH Precipitation	176	0.58	<100
Mg:Zr 5:1[a]	Rising pH Precipitation	223	0.85	<100
Mg:Zr 8:1[a]	Rising pH Precipitation	256	0.89	<100
Mg:Zr 11:1[a]	Rising pH Precipitation	173	0.92	<100
Mg:Zr 11:1	Controlled pH Precipitation	194	0.94	<100
Mg on Zr 11:1	Rising pH Precipitation	291	0.93	340
MgO[a]	Rising pH Precipitation	292	1.00	<100
MgO	Controlled pH Precipitation	162	1.00	<100
MgO[a]	from $Mg(OH)_2$ Sigma Aldrich	22	1.00	-
MgO	Ube MgO 500 Å	35	1.00	-
ZrO_2[a]	Rising pH Precipitation	123	N/A	100
ZrO_2	Controlled pH Precipitation	70	N/A	340
ZrO_2	Sigma Aldrich	13	N/A	220

[a] Results presented in Kozlowski et al.[80]

In Figure 3.2, diffraction patterns are presented for the Mg:Zr 11:1 samples prepared by controlled pH precipitation and rising pH precipitation, as well as for MgO supported on ZrO_2 (11:1). The MgO on ZrO_2 sample shows peaks for both crystalline magnesia and zirconia (tetragonal and monoclinic). A Scherrer analysis of the tetragonal zirconia phase for the rising and controlled pH samples gave crystallite sizes of about 10 and 8.6 nm respectively.

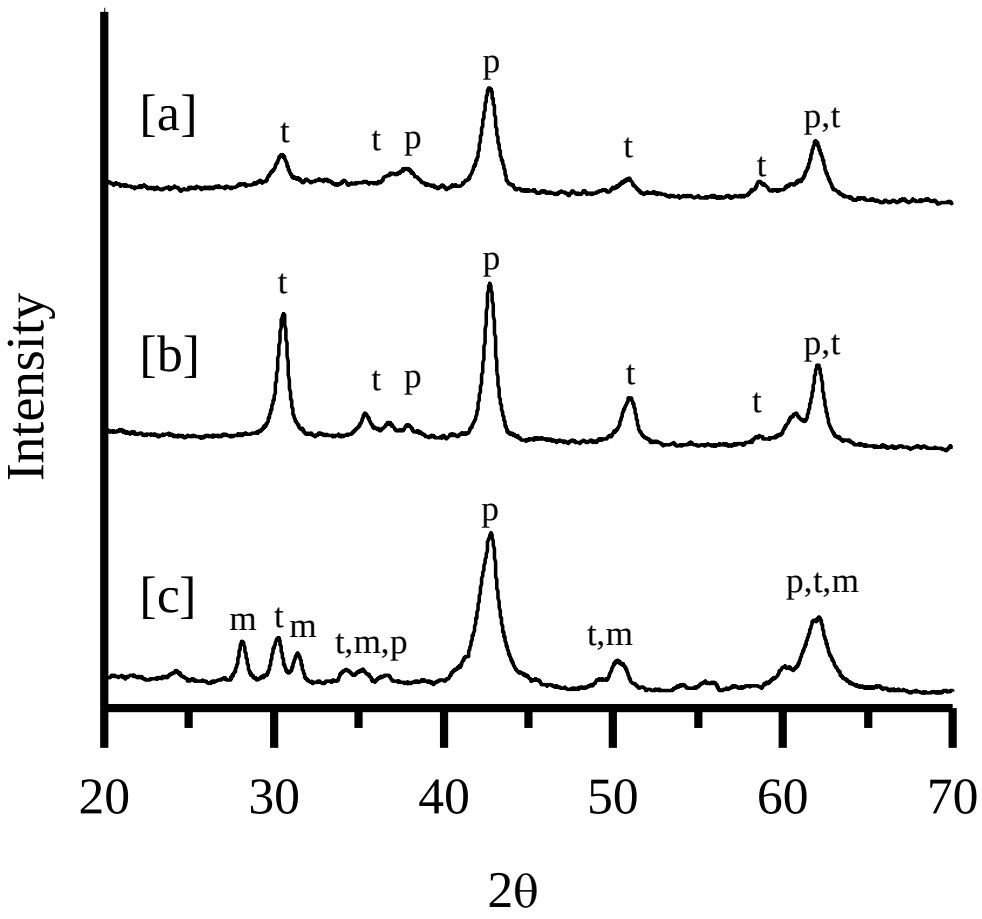

Figure 3.2. X-ray diffraction patterns of: [a] controlled precipitated 11:1 Mg:Zr mixed oxide, [b] rising pH precipitated 11:1 Mg:Zr mixed oxide, and [c] Mg on Zr 11:1 mixed oxide. The peaks associated with periclase magnesia, tetragonal zirconia and monoclinic zirconia are marked with p, t and m, respectively.

The XRD results indicated that the controlled pH precipitated material had slightly smaller crystallites of zirconia compared to the rising pH precipitated catalyst, which was confirmed by microscopy. Scanning electron microscopy was performed on both the controlled pH precipitation and rising pH precipitation samples and a few example images and line scans for the two materials are shown in Figures 3.3 and 3.4. The difference in the uniformity between the two samples is quite apparent in the SEM images and in the EDX line scans of the two

samples. The sample prepared by the rising pH method had larger domains of zirconia, and these domains appeared to be highly concentrated within each particle. The controlled precipitation sample showed a more uniform particle size and smaller domains of zirconia. These observations are consistent with the expected increase in sample uniformity achieved by the controlled pH precipitation method. While we were able to observe the morphology and size of zirconia domains by SEM, we could not distinguish if large regions of zirconia were exposed on the surface or if they were covered with thin layers of MgO. To help quantify the surface concentration of zirconia (which is more acidic and less basic than MgO) the acid and base properties of the materials were evaluated.

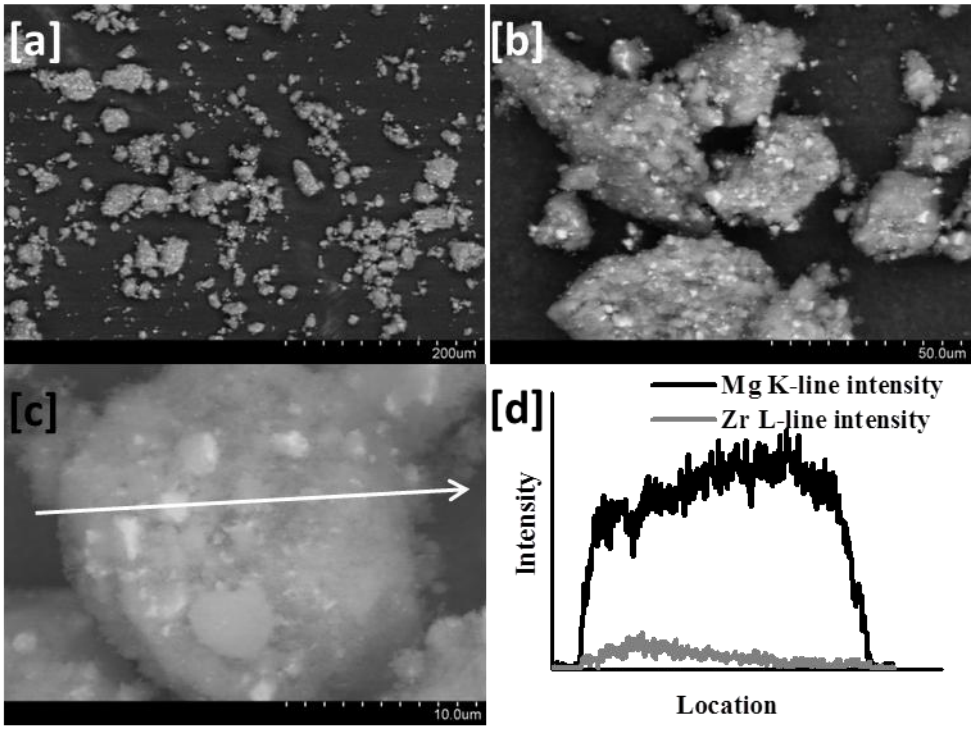

Figure 3.3. SEM images [a], [b] and [c] of the controlled precipitation material. [d] EDX of the line scan whose direction is shown on image [c].

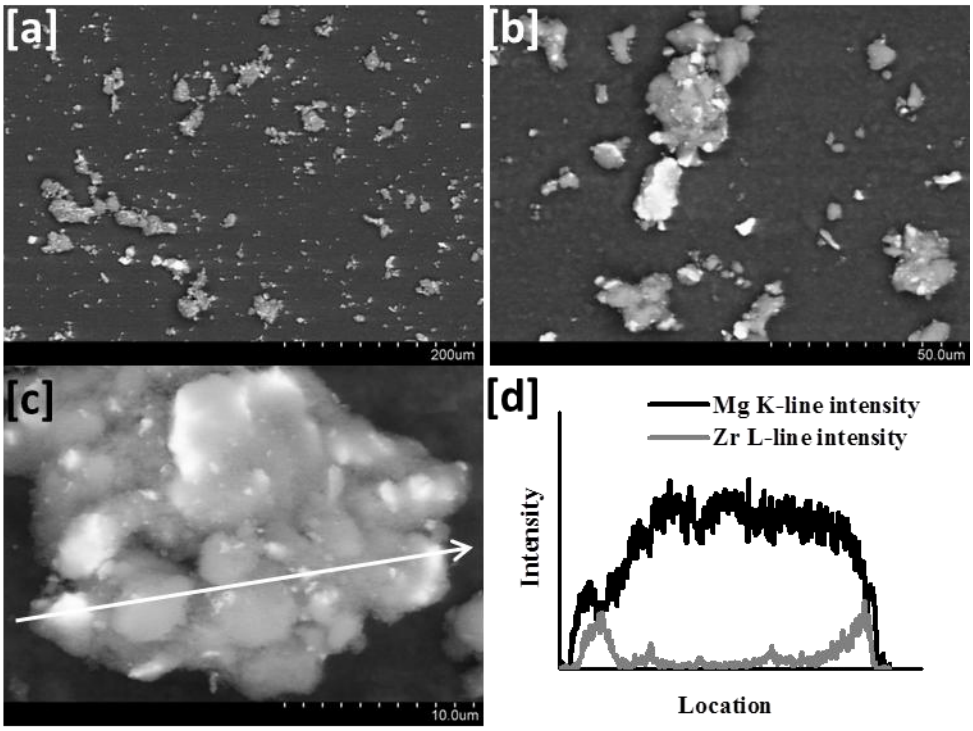

Figure 3.4. SEM images [a], [b] and [c] of the rising pH precipitation material. [d] EDX of the line scan whose direction is shown on image [c].

The acid and base sites were probed by adsorption microcalorimetry of ammonia and carbon dioxide on the two Mg:Zr 11:1 samples as well as on zirconia and magnesia prepared by controlled pH precipitation. The adsorption isotherms and differential heats of adsorption are shown in Figures 3.5 and 3.6 for carbon dioxide and ammonia, respectively. A summary of the initial heats of adsorption and saturation coverages is presented in Table 3.2.

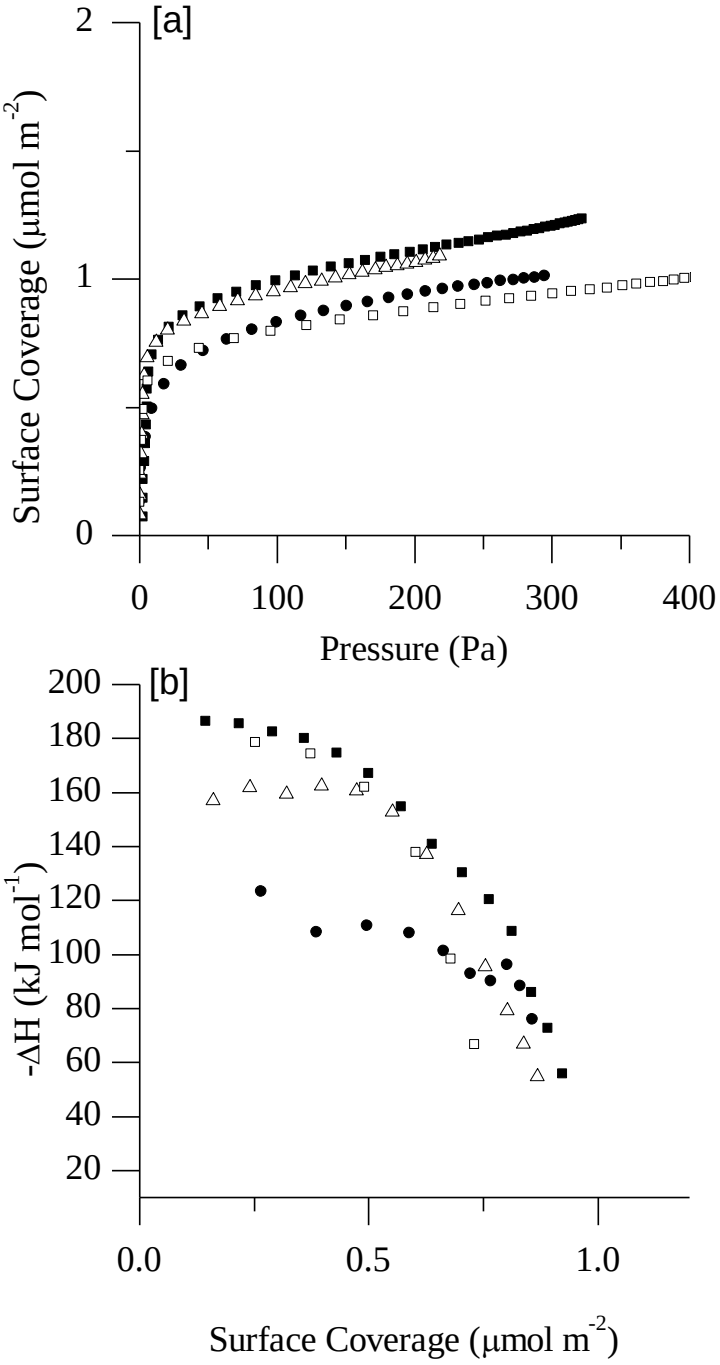

Figure 3.5. CO_2 adsorption microcalorimetry on controlled pH precipitated MgO (Δ), ZrO_2 (●) and Mg:Zr 11:1(■) with rising pH precipitation Mg:Zr 11:1 (□). [a] adsorption isotherm and [b] differential heats of adsorption

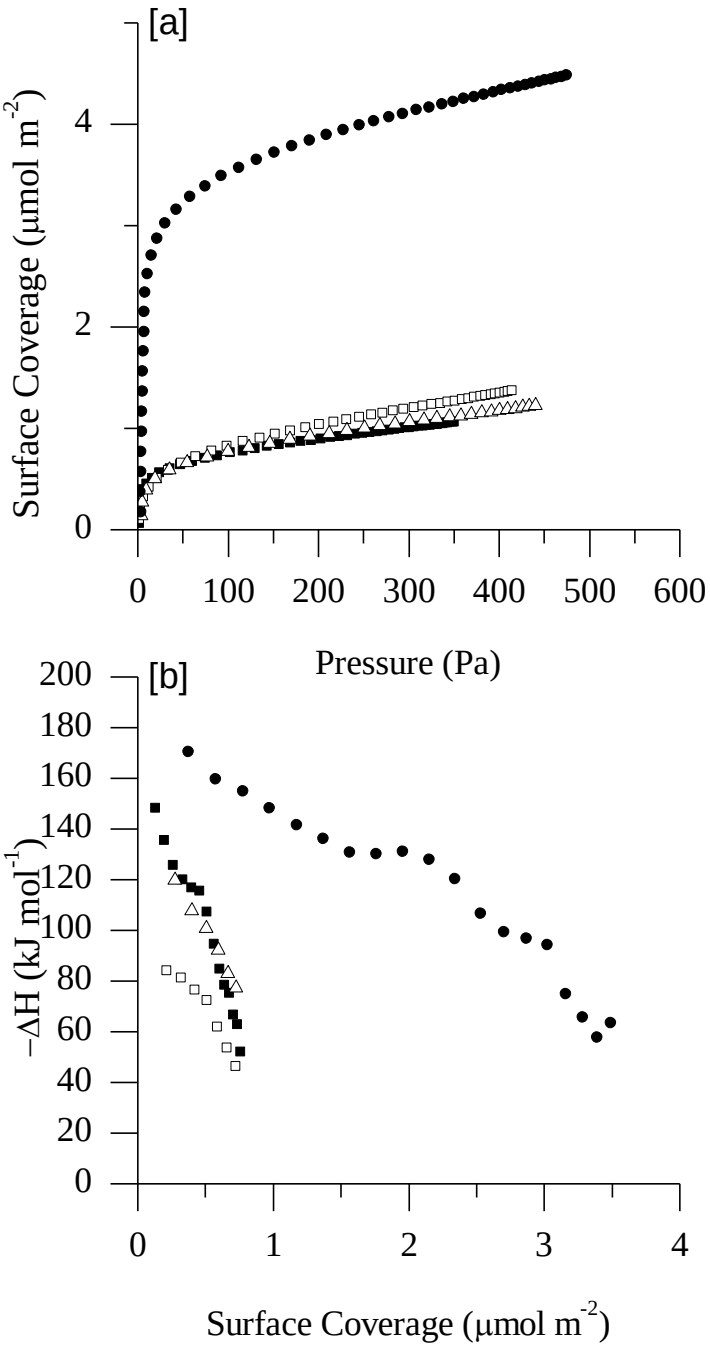

Figure 3.6. NH_3 adsorption microcalorimetry on controlled pH precipitated MgO (Δ), ZrO_2 (●) and Mg:Zr 11:1(■) with rising pH precipitation Mg:Zr 11:1 (□). [a] adsorption isotherm and [b] differential heats of adsorption

Although zirconia and magnesia have similar uptakes of CO_2, MgO exhibited stronger interactions with the weakly acidic probe molecule as indicated by the higher heat of adsorption (162 vs 123 kJ mol^{-1}). Very different results were found with NH_3 adsorption microcalorimetry. Figure 3.6 and Table 3.2 clearly illustrate the much higher capacity of ZrO_2 surfaces for NH_3 compared to MgO (3.5 vs 0.70 μmol m^{-2}) and a much higher initial heat of adsorption (170 vs 120 kJ mol^{-1}).

Table 3.2. Summary of results from adsorption microcalorimetry of ammonia and carbon dioxide on Mg and Zr containing oxides.

	NH_3 Adsorption		CO_2 Adsorption	
Catalyst	Initial -ΔH (kJ mol^{-1})	Coverage (μmol m^{-2})	Initial -ΔH (kJ mol^{-1})	Coverage (μmol m^{-2})
MgO[a]	120	0.70	162	0.83
Mg:Zr 11:1[b]	84	0.73	185	0.74
Mg:Zr 11:1[a]	141	0.73	187	0.91
Mg:Zr 5:1[b][c]	-	-	154	1.2
Mg on Zr 11:1[b]	-	-	153	1.0
ZrO_2 [a]	170	3.5	123	0.81

[a] Sample prepared by controlled pH precipitation
[b] Sample prepared by rising pH precipitation
[c] Result presented in Kozlowski et al. [80]

Even though zirconia was present in the Mg:Zr 11:1 mixed oxide sample in low concentration (8.2 at.% in the rising pH sample and 5.8 at.% in the controlled precipitation sample), exposed Zr cations are still anticipated to significantly influence the ammonia adsorption isotherms since zirconia has a much stronger interaction and overall capacity for NH_3 compared to magnesia. For zirconia, 3.5 μmol m^{-2} of ammonia was adsorbed on exposed Zr cations present at a maximum surface density of 16.6 μmol m^{-2} based on the (111) surfaces of tetragonal zirconia [158]. We assume that the quantity of ammonia adsorbed on Brønsted acid sites is much lower than that on Lewis acid sites because of the high temperature used in the

sample pretreatment. Prior work on a tetragonal zirconia with a thermal pretreatment similar to the samples in this study revealed only Lewis acid sites evaluated by IR spectroscopy of adsorbed pyridine [158]. The maximum theoretical capacity for ammonia based on crystallographic parameters can be used to compare MgO and ZrO_2. For magnesia, 0.7 μmol m^{-2} of ammonia was adsorbed. Since MgO is a solid base, the interaction of NH_3 with the surface likely arises from hydrogen-bonding interactions and possibly NH_3 dissociation by strongly basic oxygen atoms. For example, Tsyganenko et al. reported that ammonia adsorbed on MgO evacuated at greater than 723 K was either hydrogen bonded to surface O^- anions or dissociated into surface bound amide and hydroxyl groups [159], indicating ammonia adsorption on MgO is likely to involve surface oxygen groups. Based on the (100) surface in MgO there are 9.37 μmoles m^{-2} of O ions. This would indicate that zirconia has higher capacities per maximum theoretically exposed adsorption site and much stronger affinity for ammonia than magnesia. The Mg:Zr 11:1 sample prepared by rising pH presents few acid sites, with none having $-\Delta H_{ads}$ greater than about 85 kJ mol^{-1} (Figure 3.6). The mixed oxide sample prepared by controlled precipitation also exhibited few sites for ammonia adsorption, but nearly half of the adsorption sites had a $-\Delta H_{ads}$ greater than 100 kJ mol^{-1}, with some sites having $-\Delta H_{ads}$ greater than those on MgO. Evidently, the controlled pH precipitation method formed a sample exposing surfaces with a higher density of zirconia compared to a sample prepared by the traditional rising pH method.

Transesterification of Tributyrin with Methanol

The rate of transesterification of tributyrin with methanol was used to compare a sample prepared by controlled pH precipitation to that prepared by increasing the pH. A summary of the rate constants for the initial transesterification of tributyrin to dibutyrin (k_1) is provided in Table 3.3. The Mg:Zr 11:1 sample prepared by controlled precipitation catalyzed the rate of transesterification similar to that over Mg:Zr 11:1 prepared by the rising pH method, which was several times greater than the rate over MgO. It should be noted that ZrO_2 was not active for the reaction under these conditions. Mixed oxide samples containing greater amounts of ZrO_2 were similar to, or less active, than pure MgO.

Table 3.3. Rate constants for transesterification of tributyrin with methanol at 333 K over pure and mixed oxides of zirconia and magnesia.

Catalyst	k_1 ($x10^6$)[e] ($L\ mol^{-1}\ m^{-2}\ s^{-1}$)
Mg:Zr 1:1[a][b]	0.37 ± 0.12
Mg:Zr 5:1[a][b]	0.50 ± 0.03
Mg:Zr 8:1[a][b]	0.73 ± 0.07
Mg:Zr 11:1[a][b]	3.0 ± 0.30
Mg:Zr 11:1[c]	3.2 ± 0.35
Mg on Zr 11:1[b]	0.66 ± 0.13
MgO[a][b]	0.70 ± 0.02
MgO from $Mg(OH)_2$[a][d]	1.2 ± 0.34
ZrO_2[b]	0

[a] Result presented in Kozlowski et al. [80]
[b] Sample prepared by titration precipitation
[c] Sample prepared by controlled pH precipitation
[d] $Mg(OH)_2$, nanopowder (Aldrich, 99.9%)
[e] Rate constant for consumption of tributyrin (or rate of dibutryrin production) normalized to surface area of catalyst

To further explore how the interface between the two phases (MgO and ZrO_2) might be involved in the promotion of the reaction, a sample in which MgO was deposited onto ZrO_2 was synthesized. This sample showed both MgO and ZrO_2 by XRD, however it did not promote the transesterification of tributyrin with methanol because the surface area normalized rate constant was below that of pure MgO.

A likely explanation for the observed promotional influence of Zr is that appropriate strength acid-base pairs are present on the mixed oxide surface. To evaluate these materials for acid-base bifunctionality, a reaction such as acetone coupling was performed since it has been proposed to occur faster over bifunctional materials [87].

Acetone Coupling and Condensation

Table 3.4. Rates of diacetone production over the pure oxides, the controlled pH precipitation and the rising pH precipitation samples.

Catalyst	Rate of Diacetone Alcohol Production (mol s^{-1} m^{-2})(x10^7) [c]	TOF (s^{-1})[d]
Mg:Zr 11:1[a]	1.6	0.21
Mg:Zr 11:1[b]	1.7	0.19
Mg:Zr 5:1[a]	1.2	0.10
Mg on Zr 11:1[a]	1.2	0.12
MgO[b]	0.81	0.10
ZrO_2[b]	0.00	N/A

[a] Mixed oxides prepared by rising pH precipiation
[b] Samples prepared by controlled pH precipitation
[c] Rates were calculated from the first 30 minutes of reaction.
[d] TOF was calculated by normalizing the rate by the CO_2 adsorption capacity.

The pure and mixed oxide materials were used in acetone coupling at 299 K to produce diacetone alcohol. The rates of diacetone alcohol production, normalized to the total surface area of a sample, are presented in Table 3.4. Similar to the results from transesterification, the Mg:Zr 11:1 mixed oxides showed a higher rate (nearly double) compared to MgO, whereas ZrO_2 was inactive. The inactivity of zirconia at 299 K is consistent with the work of Zaki et al. [160]. Using IR spectroscopy, they observed acetone adsorbed on Lewis acid sites, but found little evidence for acetone coupling products. The lack of coupling products on the surface at room temperature is likely the results of zirconia's rather weak basicity since higher temperatures are needed to activate acetone [160]. To address this issue, we studied acetone condensation reactions at elevated temperature. The reactivity results from acetone conversion at 573 K are reported in Table 3.5. Mesityl oxide was the major condensation product observed over all of the catalysts.

Table 3.5. Conversion and selectivities for acetone condensation in a flow reactor at 573 K.

Catalyst	Initial Conversion[e]	Conversion at 12 hours [e]	Mesityl Oxide Selectivity	Isophorone Selectivity	Mesitylene Selectivity
ZrO_2 (S.A.)[a]	10%	9%	80%	8%	12%
Mg:Zr 1:1[b]	7%	3%	82%	14%	4%
Mg:Zr 5:1[b]	5%	3%	78%	6%	16%
Mg:Zr 11:1[c]	5%	2%	85%	4%	11%
MgO[d]	12%	5%	80%	19%	trace

[a] ZrO_2 obtained from Sigma-Aldrich
[b] Mixed oxides prepared by rising pH precipitation, same materials discussed in Kozlowski et al. [80]
[c] Controlled pH precipitation sample
[d] MgO obtained from Ube Material Industries Ltd. (Ube MgO 500Å)
[e] Conversion calculated by the sum of all products that were identified and quantified (diacetone alcohol, mesityl oxide, isophorone, and mesitylene).

A prior report has indicated that addition of Y^{3+} to MgO increases deactivation since the more Lewis acidic metal ion helps stabilize reaction intermediates that lead to acetone coupling products [88]. In our study with MgO and ZrO_2 mixed oxides, all samples containing MgO deactivated quickly. In fact, initial conversions reported in Table 3.5 are quite likely influenced by the rapid deactivation at very short times on stream. On the other hand, acetone condensation over zirconia proceeded without substantial deactivation, revealing only a 10% decrease in rate over 12 h of reaction (Table 3.5).

Ethanol Reactivity

Table 3.6. Ethanol reaction rates to ethene, ethanal and butanol at 673 K.

Catalyst	Ethene Formation Rate (mol m^{-2} s^{-1}) x10^9	Ethanal Formation Rate (mol m^{-2} s^{-1}) x10^9	Butanol Formation Rate (mol m^{-2} s^{-1}) x10^9
MgO[a]	6.6	15	1.1
Mg:Zr 11:1[b]	12	15	0.8
Mg:Zr 11:1[a]	19	19	N.O.(c)
ZrO_2[a]	180	10	N.O.(c)

[a] Sample prepared by controlled pH precipitation
[b] Sample prepared by rising pH precipitation
[c] Butanol was not detected in the products

The observed promotion of transesterification and low temperature coupling of acetone over Mg:Zr mixed oxides compared to MgO led us to explore their potential for Guerbet coupling of alcohols. Therefore, ethanol conversion at 673 K was evaluated in a flow reactor. Ethanol can dehydrate to ethene, dehydrogenate to ethanal and couple to heavier products such as butanol and higher alcohols. The rates at 683 K for dehydration, dehydrogenation and

Guerbet coupling of ethanol are presented in Table 3.6. As expected, zirconia catalyzed dehydration faster than MgO or Mg:Zr 11:1 mixed oxides by more than an order of magnitude, presumably because of the stronger acidity of ZrO_2 compared to MgO. Thus, ethanol dehydration should be a very sensitive probe for Zr^{4+} at the surface of the mixed oxide. The Mg:Zr 11:1 sample prepared by the rising pH method exhibited a lower rate of dehydration compared to the mixed oxide prepared by controlled precipitation. This is consistent with the results presented earlier that suggested the sample prepared by the rising pH method exposed less zirconia than the mixed oxide prepared by the controlled pH precipitation method. In Table 3.7, the TOFs for ethanol dehydration, normalized by the ammonia uptake (Table 3.2), and ethanol dehydrogenation, based on the carbon dioxide uptake (Table 3.2), are presented. The substantial variation in TOF for dehydration indicates that total ammonia uptake is not a good basis for normalizing dehydration rates. The rate appears to also depend on the strength of the acid sites. In contrast, the relatively constant value of TOF for dehydrogenation suggests that CO_2 adsorption capacity might be a reasonable basis for normalization.

Table 3.7. Turnover frequencies for ethanol dehydration and dehydrogenation to ethene and ethanal, respectively.

Catalyst	Ethene TOF (s^{-1})[c]	Ethanal TOF (s^{-1})[d]
MgO[a]	0.009	0.018
Mg:Zr 11:1[b]	0.016	0.021
Mg:Zr 11:1[a]	0.025	0.020
ZrO_2[a]	0.051	0.012

[a] Sample prepared by controlled pH precipitation
[b] Sample prepared by rising pH precipitation
[c] Rate of ethene production divided by ammonia uptake measured by adsorption microcalorimetry
[b]Rate of ethanal production divided by carbon dioxide uptake measured by adsorption microcalorimetry

Discussion

Results from several physical and chemical probes reveal the complex nature of the mixed oxides of Mg and Zr. Although controlled pH precipitation of Zr and Mg gave a more even distribution of Zr throughout the sample and smaller ZrO_2 crystallites, compared to a mixed oxide prepared by a rising pH method, the fraction of exposed ZrO_2 was greater with controlled precipitation. Since Zr precipitates at a lower pH than Mg, the rising pH method would favor the initial precipitation of the zirconium followed by subsequent precipitation/deposition of magnesium. This sequence of reactions would give particles that are more MgO-rich at the surface, which is consistent with adsorption and reaction results. Additionally, mixed oxides prepared by a rising pH method have been shown to expose an MgO like surface based on DRIFTS of methanol and carbon dioxide adsorption [80].

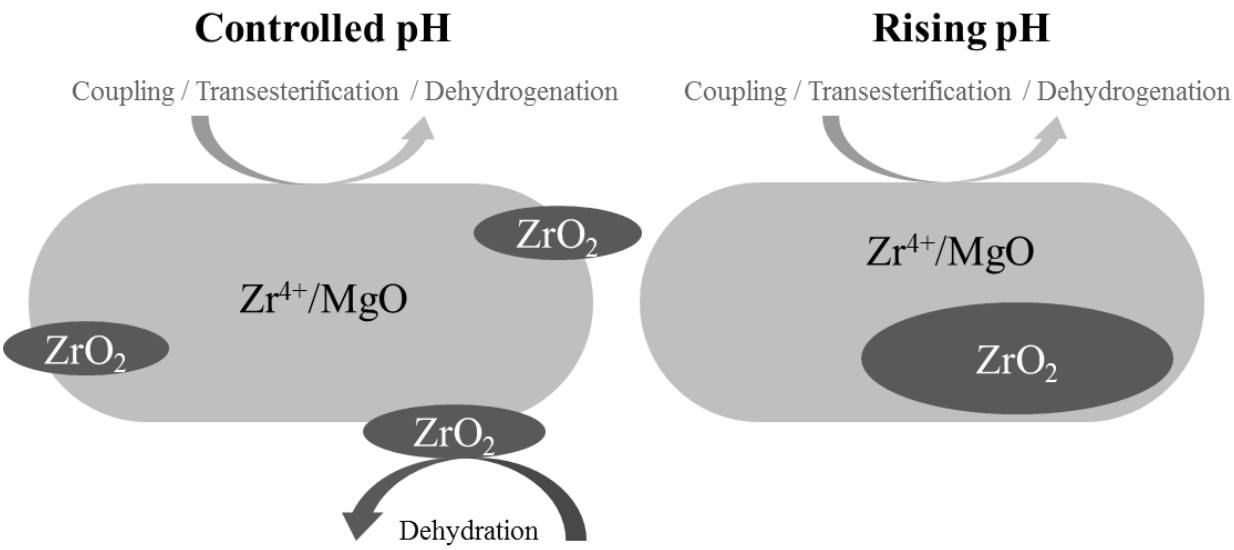

Figure 3.7. An illustration of the Mg:Zr 11:1 catalyst particles prepared using controlled pH (left) and rising pH (right) precipitation methods. The Zr^{4+}/MgO phase accelerates the rates of acetone coupling and tributyrin transesterification with methanol compared to unpromoted MgO. Although ethanol dehydrogenates on both ZrO_2 and MgO, dehydration is favored over ZrO_2.

A proposed simple diagram of the surface of these materials is shown in Figure 3.7. For the controlled precipitation method, two regions are exposed, 1. small zirconia crystallites, although inactive for aldol condensation and transesterification, can be probed by ammonia microcalorimetry and higher ethanol dehydration rates, and 2. crystallites of mostly magnesia with small amounts of zirconium. The presence of isolated Zr with MgO could account for the increase in reactivity as well as the increase in the heat of carbon dioxide adsorption and would be consistent with the work of Sádaba et al. [91]. While the sample prepared with rising pH would also have these domains of isolated Zr with MgO, it would have less exposed crystalline zirconia and therefore a lower heat of ammonia adsorption and a lower ethanol dehydration rate.

Conclusions

A mixed oxide of Mg:Zr 11:1 that was prepared in a controlled precipitation had a higher surface exposure of zirconia than a material prepared traditionally by increasing the pH. Although the controlled precipitation method produced a more uniform distribution of zirconia, the larger surface exposure of zirconia caused an undesirable increase in the rate of ethanol dehydration, which is detrimental to the Guerbet coupling reaction. Since ZrO_2 was inactive for transesterification and low temperature coupling of acetone, the presence of small amounts of crystalline ZrO_2 on the surface of Mg:Zr 11:1 was not detrimental to those reactions. In contrast, Mg:Zr 11:1 mixed oxides prepared by either method were substantially more active for transesterification and low temperature acetone coupling compared to MgO (on a surface area basis). The promotion of MgO-catalyzed reactions by the addition of Zr^{4+} was presumably the result of additional acid-base surface sites that facilitate those reactions.

In summary, both methods of preparation, i.e. controlled precipitation and rising pH precipitation, produced highly active mixed oxides for transesterification and acetone coupling. However, if crystalline ZrO_2 at the surface of the oxide is detrimental to a reaction, the rising pH method of precipitation is the preferred synthesis procedure since crystalline ZrO_2 is buried below the interface.

Acknowledgements

This work was supported by the Chemical Sciences, Geosciences and Biosciences Division, Office of Basic Energy Sciences, Office of Science, U.S. Department of Energy, grant no. DE-

FG02-95ER14549 and NSF grant number OISE 0730277. Scanning electron microscopy was performed by Gisela Weinberg.

Chapter 4: Isotopic Transient Analysis of the Ethanol Coupling Reaction over Magnesia

This chapter was published as: T.W. Birky, J.T. Kozlowski, R. J. Davis, "Isotopic Transient Analysis of the Ethanol Coupling Reaction over Magnesia" Accepted, Journal of Catalysis DOI:10.1016/j.jcat.2012.11.014. It was a collaborative effort in which I completed the DRIFTS, adsorption microcalorimetry, background kinetic studies and mentored T.W. Birky on his SSITKA work.

Introduction

Although numerous synthetic routes exist to produce saturated long chain alcohols, a particularly attractive one involves the so-called Guerbet reaction or coupling of two shorter chain alcohols over basic catalysts. The Guerbet reaction has historically been used for the production of long chain branched alcohols due to the plethora of available primary and secondary alcohols that can be used as reactants. However, recently it has received attention for the possible upgrading of short, readily available linear alcohols. For example, the small molecule ethanol is an oxygenated transportation fuel additive that is produced in large quantities by fermentation of sugars, but has a significantly lower energy density than gasoline and is readily soluble with water. Butanol, on the other hand, has a higher energy density than ethanol and is less hydrophilic, thus making it an attractive oxygenated fuel additive that can be produced from ethanol via the Guerbet reaction over solid base catalysts.

The Guerbet reaction or alcohol coupling was first investigated over a century ago after its namesake Marcel Guerbet published the original paper in the field on the conversion of 1-butanol into 2-ethylhexan-1-ol in 1899 [1]. The reaction is generally believed to occur through a

series of elementary steps that include alcohol dehydrogenation to form an aldehyde or ketone intermediate, aldol condensation of the aldehyde or ketone intermediates to form a C-C bond, and hydrogenation of the resulting unsaturated product [2,28,29,31,35,69,87]. Although alternative mechanisms have been proposed [24,45,46], the Guerbet reaction likely requires a catalyst that is multifunctional since O-H, C-H and C-C bonds are transformed in the sequence. Catalysts such as magnesia [35,46,66], hydroxyapatite [32,55,155], Mg-Al mixed oxides [27,31,69,95,161], alkali-metal-loaded zeolites [45], and transition metals in the presence of basic compounds [25–29,46,95,162–164] have demonstrated activity in the Guerbet coupling of alcohols.

A quantitative basis for evaluating activity for the Guerbet reaction is lacking since there is no good method to independently count the actual active sites on the catalysts. Calculating a rate based on the surface area of a solid catalyst is usually a good way to begin quantifying activity, but it is quite likely that only a small fraction of the catalyst surface is involved in such a complex reaction as Guerbet coupling. One of the most common methods to quantify the basic site density on a solid catalyst is to adsorb a gas phase acid such as CO_2. However, it is not clear that sites titrated by CO_2 at low temperature would be involved in a reaction that occurs at temperatures several hundreds of kelvins higher. Moreover, a distribution of affinities for adsorption usually exists on a solid catalyst so that not all sites counted by a probe such as CO_2, which is known to adsorb in different modes, would have the same likelihood for participating in the Guerbet reaction.

To overcome these limitations, we have chosen to use an isotopic transient method to quantify the turnover frequency for ethanol coupling to butanol over a commercially available MgO catalyst at 673 K. In this technique, often referred to as steady state isotopic transient

kinetic analysis (SSITKA), a catalytic reaction that is running at steady state experiences a step change in the isotopic content of the reactant. After the step change, the isotopically-labeled reactant will gradually appear in the product, without disturbing the steady state rate of reaction. By evaluating the time dependence of the isotope incorporation into the product, the coverage of reactive intermediates and the intrinsic turnover frequency of the catalytic cycle can be determined. The SSITKA technique was developed several decades ago [165–168] and a complete description of the method can be found in a review on the topic by Shannon and Goodwin [169]. The goal of this study is to determine fundamental parameters from SSITKA (steady state coverages and intrinsic turnover frequency) for ethanol coupling and relate these to adsorption microcalorimetry of CO_2 and IR spectroscopy of adsorbed ethanol.

Experimental Methods

Reactor System

The reactor system is a slightly modified version of the one used in prior work to perform isotopic transient experiments during ammonia synthesis and CO oxidation [170–176]. A schematic illustration of the modified system is provided in Figure 4.1. Prior to loading 200 mg of the MgO catalyst (UBE Industries, Grade 500 Å, BET surface area = 34.9 $m^2\ g^{-1}$) into the reactor, the sample was pressed, crushed and sieved to give particles between 106 and 180 μm. The sample was supported on a quartz wool plug in the stainless steel reactor and heated in situ at 10 K min^{-1} to 773 K in flowing N_2 (50 $cm^3\ min^{-1}$) and held at 773 K for 1 h before cooling to the reaction temperature of 673 K. To initiate the reaction, unlabeled anhydrous ethanol (Sigma

Aldrich, 99.5%) was added to the flowing N_2 stream (ultrahigh purity from Praxair, additionally purified by passage through a Supelco OMI-2 purifier) via a saturator maintained at 299 K in a temperature-controlled water bath. A small flow of argon gas (1 cm^3 min^{-1}, ultrahigh purity from Praxair) was added to the reactant stream to monitor the gas phase hold up of the system, as illustrated in Figure 4.1. A separate saturator was loaded with ^{13}C-labeled ethanol ($^{13}CH_3{}^{13}CH_2OH$, from Cambridge Isotopes) and placed in the same water bath as the unlabeled ethanol saturator. The ^{13}C-labeled ethanol was received with a substantial amount of water (5.89 wt.%) so 3A molecular sieves (Sigma Aldrich), dehydrated at 523 K in N_2, were used to remove the water. Additional dehydrated 3A molecular sieves were added to both of the saturators to ensure the heat transfer and gas-liquid contacting profiles were the same. The back pressure regulators on both the reactor line and the vent line were adjusted to give a total system pressure 1.3 atm, with a mole fraction of ethanol equal to 6%. Three different reactant flow rates were used (25, 50 and 75 cm^3 min^{-1}) to explore the influence of reactant and product re-adsorption on the isotopic transient responses. It should be noted that there was some small conversion of ethanol to acetaldehyde in an empty reactor tube at 673 K, but no butanol was ever detected in the absence of catalyst.

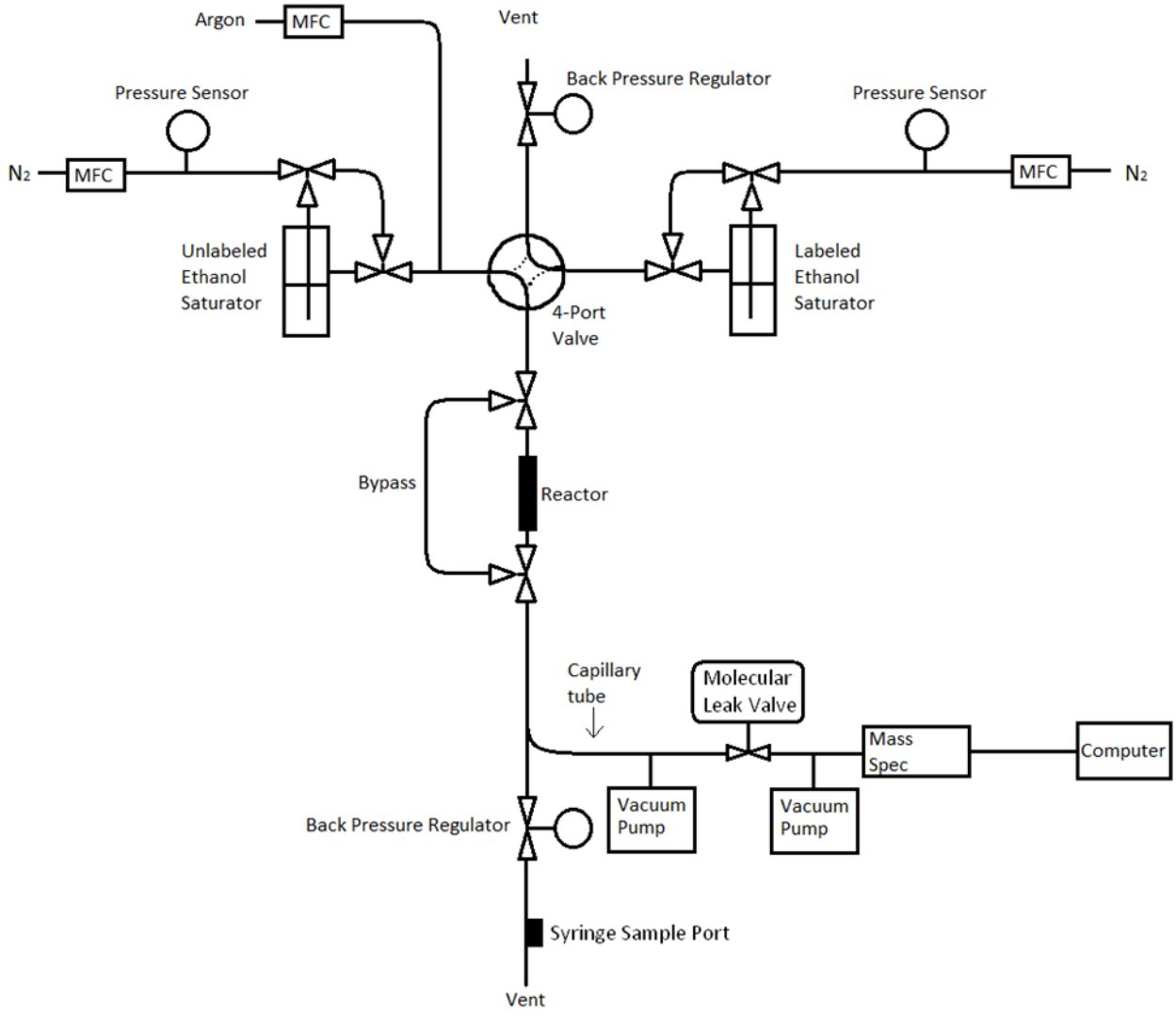

Figure 4.1. Schematic of the reactor system used for isotopic transient analysis of ethanol reactions on MgO.

The reactor was operated differentially (low ethanol conversion) at a stationary state, which allowed for an isotope jump in the reactants and products to be monitored with time. The rate of reaction and selectivity to different products was evaluated from a sample of gas removed from a sample port located after the catalyst bed and injecting it into a gas chromatograph (Agilent 7890A, equipped with a PoraPLOT Q-HT 25m, 320 micron ID, column connected to a

flame ionization detector). The major products from the reaction were acetaldehyde (from ethanol dehydrogenation), butanol (from ethanol coupling) and ethene (from ethanol dehydration). Since crotonol is sometimes reported as a product from Guerbet coupling of ethanol and the PoraPLOT column used for determination of reaction rate did not separate crotonol from butanol, we used a GC equipped with an Agilent DB-WAX 30m, 530 micron ID, column to check for crotonol formation. At 673 K and 50 cm^3 min^{-1} reactant flow, the butanol to crotonol ratio was 8.0. Since the amount of crotonol formed was low under the conditions of the study, we ignored its presence in the mass spectrometer. The selectivity to various products reported in this work is a carbon-based selectivity. For example, the selectivity to butanol, $S_{Butanol}$, is defined as

$$S_{butanol} = \frac{4 \times Rate_{butanol}}{4 \times Rate_{butanol} + 2 \times Rate_{Acetaldehye} + 2 \times Rate_{Ethene}}$$

where *Rate* is defined as moles of product formed per unit time per unit surface area.

The ethanol, argon and butanol concentrations were continuously monitored by an on-line mass spectrometer (Balzers-Pfeiffer Prisma 200) during the reaction. After the steady state reaction was achieved, the four-port valve (see Figure 4.1) rapidly switched the reactant stream from unlabeled ethanol to labeled ethanol. Since the Ar tracer was not added to the labeled ethanol steam, the evolution of the Ar signal in the mass spectrometer (m/e = 40) with time was used to quantify the overall gas-phase response of the system. The complexity of the fragmentation patterns of unlabeled and labeled ethanol, acetaldehyde (a primary product) and butanol prevented the resolution of all products in the mass spectrometer. After comparing the fragmentation patterns of ethanol (MW = 46) and acetaldehyde (MW=44), we chose to follow the most intense peak of ethanol, which was a fragment at m/e= 31. Thus, the labeled ethanol

was monitored at m/e = 32. Acetaldehyde was not followed because of the large signal from the N_2 carrier gas at m/e=28 and other overlapping peaks with ethanol and other products. Butanol was the main coupling product and was followed at m/e = 56 and 60 for unlabeled and completely labeled butanol, respectively. We also tried to follow m/e = 58 to derive information on bi-labeled butanol formation (product of coupling between labeled and unlabeled ethanol), but we were unable to derive any useful results.

Adsorption Microcalorimetry of CO_2 on MgO

Adsorption microcalorimetry experiments were completed on the same home built instrument that has been described previously by Bordawekar et al. and used in previous work [80,109,124,151]. The instrument is a heat flow calorimeter with two cells that are inserted into a large aluminum block maintained at 303 K. One cell functioned as a sample cell and the other one served as a reference. A catalyst sample was first heated to 773 K and evacuated to a pressure less than 10^{-2} Pa. The sample was then cooled and allowed to thermally equilibrate with the system for 2 h prior to adsorption of carbon dioxide (GT&S Welco, Scientific Grade). Initial dosing pressures of adsorbate ranged from 10 Pa to 250 Pa, and each dose was allowed to equilibrate with the sample for 15 min.

Diffuse Reflectance FT-IR Spectroscopy of Adsorbed Ethanol

The vibrational spectrum of ethanol adsorbed on MgO after various treatments was collected on a BioRad FTS-60A FT-IR spectrometer equipped with a Harrick Praying Mantis accessory and high temperature reaction chamber for diffuse reflectance infrared Fourier transform spectroscopy (DRIFTS) studies of catalysts. The MgO sample was first mixed with KBr powder (5 wt% MgO) and loaded into the DRIFTS cell. Prior to adsorption of ethanol, the sample was heated at 10 K min^{-1} in He (ultrahigh purity, Praxair, further purified by passage through a Supelco OMI-2 purifier) flowing at 30 cm^3 min^{-1} to a temperature of 773 K and held at that temperature for 1 h prior to cooling to the adsorption temperature. The He stream (30 cm^3 min^{-1}) was then passed through a saturator containing anhydrous ethanol (Sigma Aldrich, 99.5%) maintained at 295 K and the He/ethanol mixture passed over a bed of 3A molecular sieves prior to entering the DRIFTS cell. All spectra were averaged from 100 scans collected at a resolution of 4 cm^{-1}.

The adsorption of ethanol was studied in two different modes, 1. adsorption followed by stepwise temperature-programmed desorption (STPD), and 2. reaction at high temperature. For the STPD experiment, the pretreated MgO catalyst was cooled to 303 K, exposed to the flowing He/ethanol stream for 15 min, and purged with pure He for 15 min prior to acquisition of spectra. The temperature was then increased stepwise while flowing He and waiting 15 minutes at each new temperature prior collection of the IR spectra. The averaged spectrum collected at each temperature was referenced to a background spectrum of MgO collected at that same temperature. In this manner, the progressive desorption of ethanol from MgO could be followed

by DRIFTS. For the evaluation of DRIFTS during reaction of ethanol, a spectrum of the sample was collected after the ethanol/He mixture flowed over a pretreated MgO sample at 673 K for 1 h. In this case, ethanol was not purged from the cell, but was continually fed to the heated catalyst during the collection of the spectra. Two background spectra were used in this case, one of flowing ethanol at 673 K in the sample cell containing only KBr was used to remove the contribution of gas phase species, and another which was MgO in KBr at 673 K with no ethanol in the gas phase.

Results and Discussion

Steady State Reaction

Table 4.1. Product Distribution during Steady State Reaction of Ethanol over MgO at 673 K.

Total Flow Rate (cm^3 min^{-1})	Ethanol Conversion (%)	Rate of Ethanol Conversion (mol m^{-2} s^{-1})	Selectivity (%)		
			Acetaldehyde	Butanol	Ethene
25	23	4.7×10^{-8}	52	34	14
50	13	5.3×10^{-8}	66	20	14
75	7	4.6×10^{-8}	73	13	13

The ethanol coupling reaction over MgO produces three main products under the conditions used here, acetaldehyde, butanol and ethene. Table 4.1 summarizes the influence of flow rate on the conversion of ethanol and the distribution to various products over the MgO catalyst. The fractional conversion of ethanol from Table 4.1 is plotted in Figure 4.2 as a

function of the inverse flow rate, which is proportional to the reactor space time. The linearity of the plot, which passed through the origin, confirmed that the reactor was operated differentially with respect to ethanol. Since the mass of the catalyst was held constant, the slope of the line in Figure 4.2 (conversion versus 1/F) is directly proportional to the reaction rate. Acetaldehyde was the major product with all three flow rates, but its selectivity decreased as the conversion of ethanol increased. This behavior is consistent with the sequential nature of the Guerbet reaction in which acetaldehyde is produced directly from ethanol whereas butanol is produced from reaction of acetaldehyde. Ethene appears to be a minor side product of ethanol conversion over MgO at all of the flow rates examined.

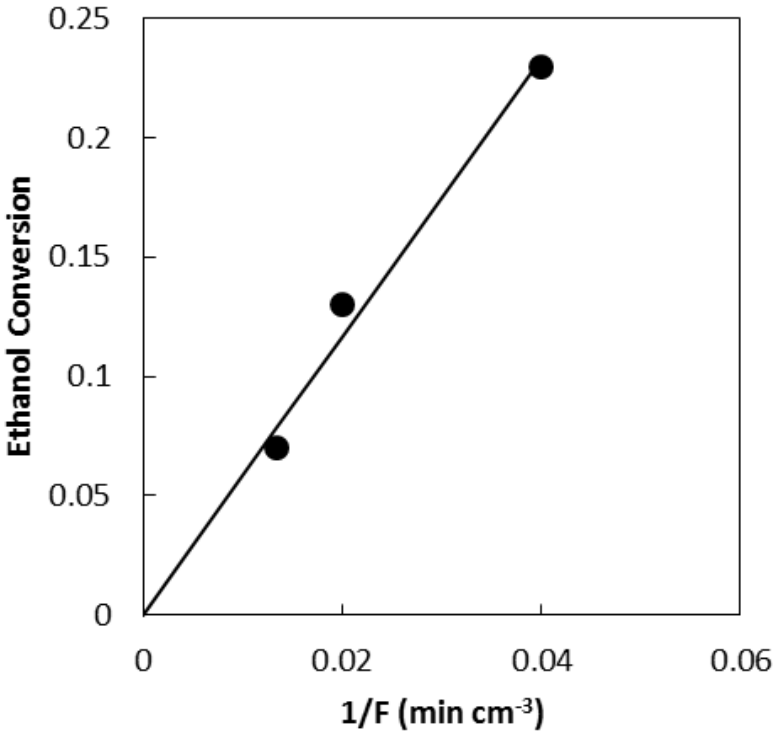

Figure 4.2. Linear relationship of the fractional ethanol conversion as a function of the inverse of the reactant flow rate (proportional to reactor space time) confirmed differential reactor behavior.

Small amounts of the expected intermediates of acetaldehyde condensation were also observed in the product mixture. For example, crotonol was seen exiting the reactor at 673 K and 50 cm^3 min^{-1} reactant flow, but its concentration was less than 15% of that for butanol. Trace amounts of crotonaldehyde were also detected at the conditions of the study. Since crotonol and crotonaldehyde were insignificant side products of the reaction, the selectivity and rate associated with these intermediates were not explicitly quantified at the various flow conditions and were ignored in the isotopic transient analysis.

Switch of $^{12}CH_3{}^{12}CH_2OH$ to $^{13}CH_3{}^{13}CH_2OH$

During the steady-state reaction, the unlabeled ethanol feed stream was switched to a doubly ^{13}C labeled ethanol feed stream without disturbing the steady state. Figure 4.3 presents the normalized isotopic transients in the ethanol concentration measured at the exit of the reactor following the switch. The curves for the labeled and unlabeled ethanol are inverted from each other and intersect at a relative concentration of 0.5, which indicates the concentration of ethanol in the reactor (both labeled and unlabeled) was constant throughout the switch. The argon tracer that was included in the feed stream, with unlabeled ethanol, is also included in the figure to illustrate the gas phase hold-up of the system. Since Ar is assumed to pass through the packed bed reactor without adsorbing on the catalyst, the difference in normalized transients between the unlabeled ethanol and argon is attributed to adsorption of ethanol on the catalyst surface. The integral between the normalized unlabeled ethanol transient, $F_{ethanol}$, and the argon transient, F_{Ar}, in Figure 4.3 is the characteristic time constant for ethanol adsorption, $\tau_{ethanol}$, at a particular flow

rate. The value of $\tau_{ethanol}$ can be combined with the molar flow rate of ethanol exiting the reactor to determine the total amount of ethanol residing on the surface of MgO at steady state conditions, $N_{ethanol}$, according to the following equations:

$$\tau_{ethanol} = \int_0^{\infty} (F_{ethanol} - F_{Ar})\, dt \qquad \textbf{(1)}$$

$$N_{ethanol} = Flow\ Rate_{ethanol} * \tau_{ethanol} \qquad \textbf{(2)}$$

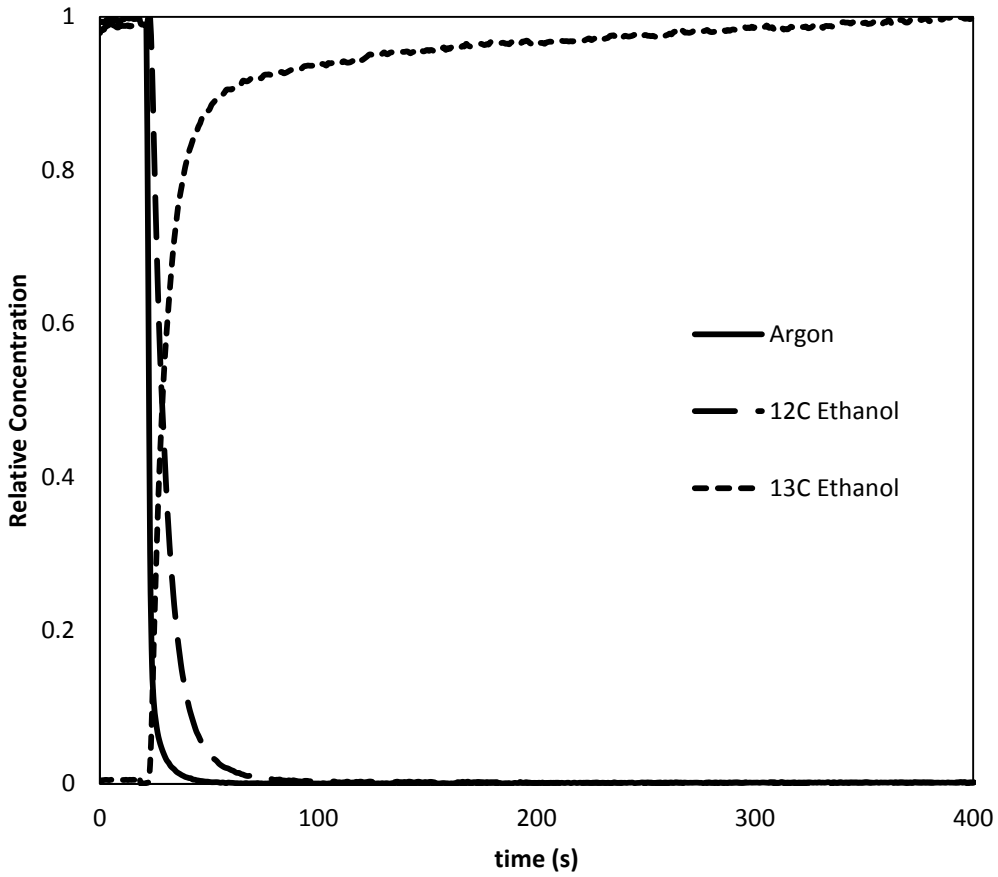

Figure 4.3. Isotopic transient results following the switch from unlabeled ethanol to doubly labeled ^{13}C-labeled ethanol at a total flow rate of 75 cm^3 min^{-1} during reaction of 6% ethanol in N_2 over 0.2 g of MgO at 673 K and 1.3 atm. The transient for the argon tracer in the unlabeled ethanol stream illustrates the gas phase hold up the reactor.

Table 4.2 summarizes the values of $\tau_{ethanol}$ and $N_{ethanol}$ for the three volumetric feed rates used in this study. The ethanol coverage varied from 4.6×10^{-6} mol m^{-2} to 5.1×10^{-6}, which is a fairly narrow range given a factor of three difference in flow rate. Based on the periclase structure of MgO and its known lattice parameter 4.21Å, the maximum density of Mg-O atomic pairs exposed on the (100) surface is calculated to be 9.37×10^{-6} m^{-2}, suggesting that about half of the available Mg-O adsorption sites are covered by ethanol under steady-state Guerbet coupling conditions.

Table 4.2. Coverage of ethanol on MgO during steady state Guerbet reaction at 673 K determined from isotopic transient analysis.

Total Flow Rate (cm^3 min^{-1})	$\tau_{ethanol}$ (s)	Coverage of Ethanol $N_{ethanol}$ (mol m^{-2})
25	32	5.1×10^{-6}
50	13	4.7×10^{-6}
75	7.8	4.6×10^{-6}

Analysis of Product Transients

The mass spectrometer at the reactor exit was also programmed to monitor the isotopic transients associated with the butanol product. An example set of transients, for the decay of unlabeled butanol and the rise of labeled butanol in the product stream, after a switch from unlabeled to labeled ethanol feed is provided in Figure 4.4. The transient curves for the unlabeled and labeled butanol product are similar in shape to those for the ethanol signals (Figure 4.3), but the butanol transient is significantly delayed from that of ethanol. Butanol is a

product of reaction so the characteristic time for producing butanol, $\tau_{butanol}$, and the surface coverage of reactive intermediates that lead to butanol, $N_{butanol}$, can be derived from the transient results. In particular, the characteristic time for butanol production is calculated from the following integral in Figure 4.4:

$$\tau_{butanol} = \int_0^\infty (F_{butanol} - F_{Ar})\, dt \qquad \textbf{(3)}$$

where $F_{butanol}$ and F_{Ar} are the normalized transient responses of the butanol and Ar tracer, respectively. The surface coverage of reactive intermediates is given by:

$$N_{butanol} = Rate_{butanol} * \tau_{butanol} \qquad \textbf{(4)}$$

where $Rate_{butanol}$ is the formation rate of butanol in units of mol m^{-2} s^{-1} so that the units of $N_{butanol}$ are mol m^{-2}.

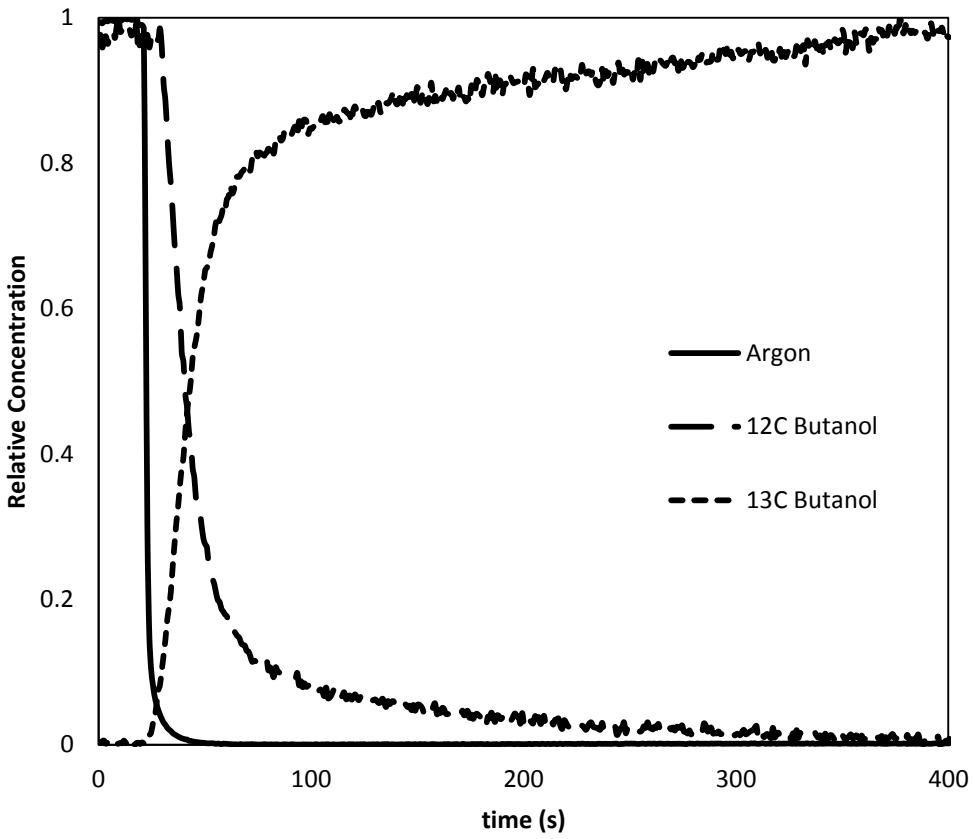

Figure 4.4. Isotopic transient results of the product butanol following the switch from unlabeled ethanol to doubly labeled ^{13}C-labeled ethanol at a total flow rate of 75 cm^3 min^{-1} during reaction of 6% ethanol in N_2 over 0.2 g of MgO at 673 K and 1.3 atm. The transient for the argon tracer in the unlabeled ethanol stream illustrates the gas phase hold up the reactor.

Table 4.3 summarizes the values of $\tau_{butanol}$ and $N_{butanol}$ for the three flow rates used in this study. The value of $\tau_{butanol}$ varied with flow rate, similar to the case of $\tau_{ethanol}$ as given in Table 4.2. Figure 4.5 compares the flow rate dependence of $\tau_{ethanol}$ and $\tau_{butanol}$, which reveals that both alcohols (reactant and product) experienced re-adsorption on the MgO catalyst prior to exiting the reactor. As the flow rate increased, the influence of alcohol re-adsorption decreased and therefore lowered the values of τ derived from the isotope switches. Extrapolation of the line for $\tau_{ethanol}$ to infinite flow rate (origin of the *x*-axis in Figure 4.5) passes nearly through the origin

demonstrating the expected lack of re-adsorption of reactant molecules at exceedingly high flow rates.

Table 4.3. Coverage of reactive intermediates leading to butanol on MgO during steady state Guerbet reaction of ethanol at 673 K determined from isotopic transient analysis.

Total Flow Rate ($cm^3\ min^{-1}$)	Rate of Butanol Formation (mol $m^{-2}\ s^{-1}$)	$\tau_{butanol}$ (s)	Coverage of Intermediates to Butanol $N_{butanol}$ (mol m^{-2})
25	8.1×10^{-9}	60	4.9×10^{-7}
50	5.2×10^{-9}	36	1.9×10^{-7}
75	3.1×10^{-9}	32	1.0×10^{-7}

In isotopic transient experiments, linear extrapolation of the τ values for product molecules to infinite flow rate (zero space time) is often used to find the intrinsic time constant for the reaction, free of artifacts from re-adsorption. A complete description of how to minimize the influence of product readsorption in the analysis of isotopic transients can be found in the review by Shannon and Goodwin [28] and the work of McClaine and Davis [34].

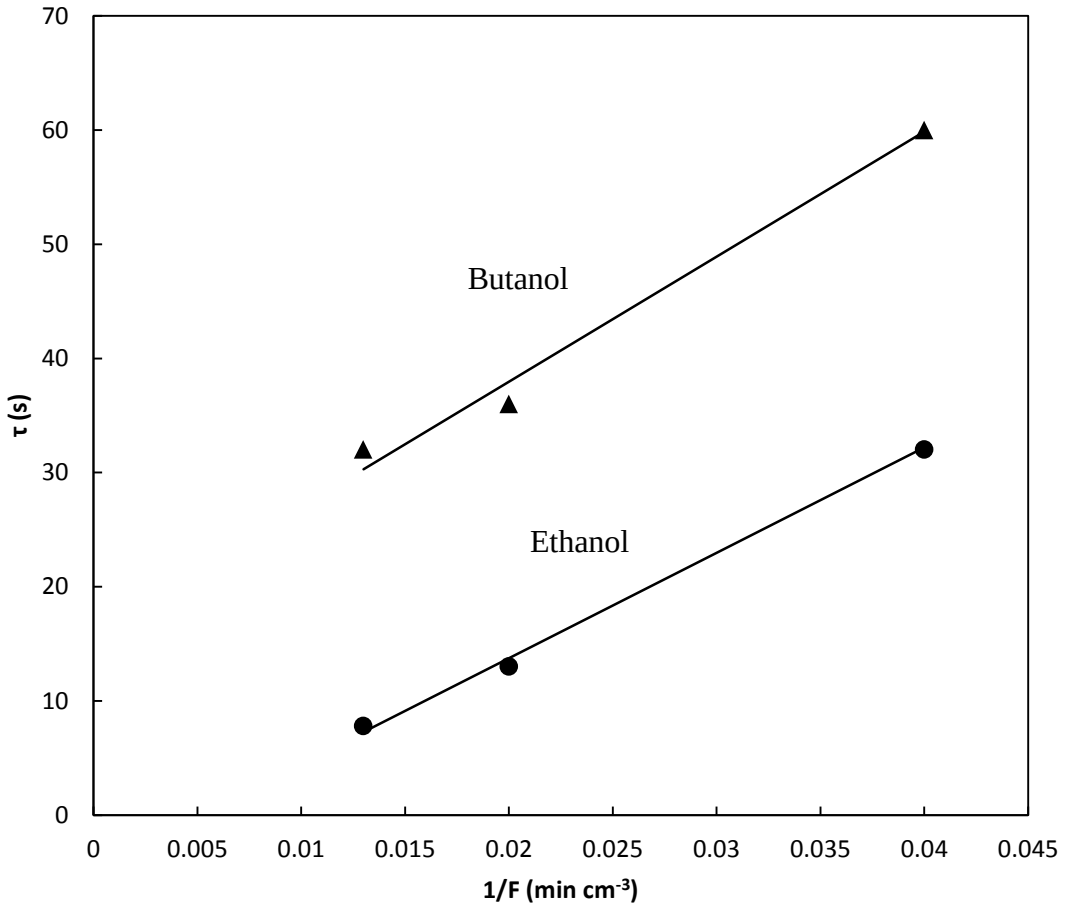

Figure 4.5. Influence of the volumetric flow rate of the feed stream on the measured values of τ for butanol production (solid triangles) and ethanol adsorption (solid circles) on MgO at 673 K and 1.3 atm during Guerbet coupling of ethanol.

In the results reported here, extrapolating $\tau_{ethanol}$ to infinite flow rate (zero space time) gave a slightly negative value, suggesting that a linear extrapolation might not be the best method in this case. Moreover, the product butanol is not actually a primary reaction product and its rate of formation depends on the level of intermediate concentration of acetaldehyde in the reactor. Table 4.3 shows the significant change in the coverage of reactive intermediates leading to butanol at the different flow rates (i.e. different levels of conversion), and Figure 4.6

illustrates the nearly pseudo-first order dependence of butanol formation on the acetaldehyde concentration during these experiments. The similarity of the slopes of the two lines in Figure 4.5 is consistent with the fact that both ethanol and butanol are short chain primary alcohols that would likely interact with the MgO in a similar manner. Thus, we assumed the influence of alcohol re-adsorption is nearly equivalent for the two molecules and simply subtracted the corresponding values of $\tau_{ethanol}$ (only alcohol re-adsorption) from $\tau_{butanol}$ (reaction plus re-adsorption) at each flow rate to arrive at an average intrinsic time constant, $\tau_{butanol}^{0}$, of 25 s for the ethanol coupling reaction at 673 K on MgO. This value of $\tau_{butanol}^{0}$ is similar to that obtained by simple linear extrapolation of the space time dependence of $\tau_{butanol}$ to zero space time (within about 30%), which is a more conventional way to evaluate the intrinsic time constant. An estimate of the intrinsic turnover frequency per active site, TOF, is the reciprocal of $\tau_{butanol}^{0}$, which in this case is $1/(25\ s) = 0.04\ s^{-1}$ for butanol formation from ethanol coupling over MgO. This turnover frequency for butanol formation is quite similar to the value reported by Tsuchida et al. ($0.030\ s^{-1}$) for ethanol coupling over MgO at 658 K and 20 % conversion [55]. Although the basis of their turnover frequency was the number of CO_2 adsorption sites at 523 K, which is a somewhat arbitrary choice, their overall magnitude matches quite well the one determined here from isotopic transient analysis, which does not require an independent determination of active site density.

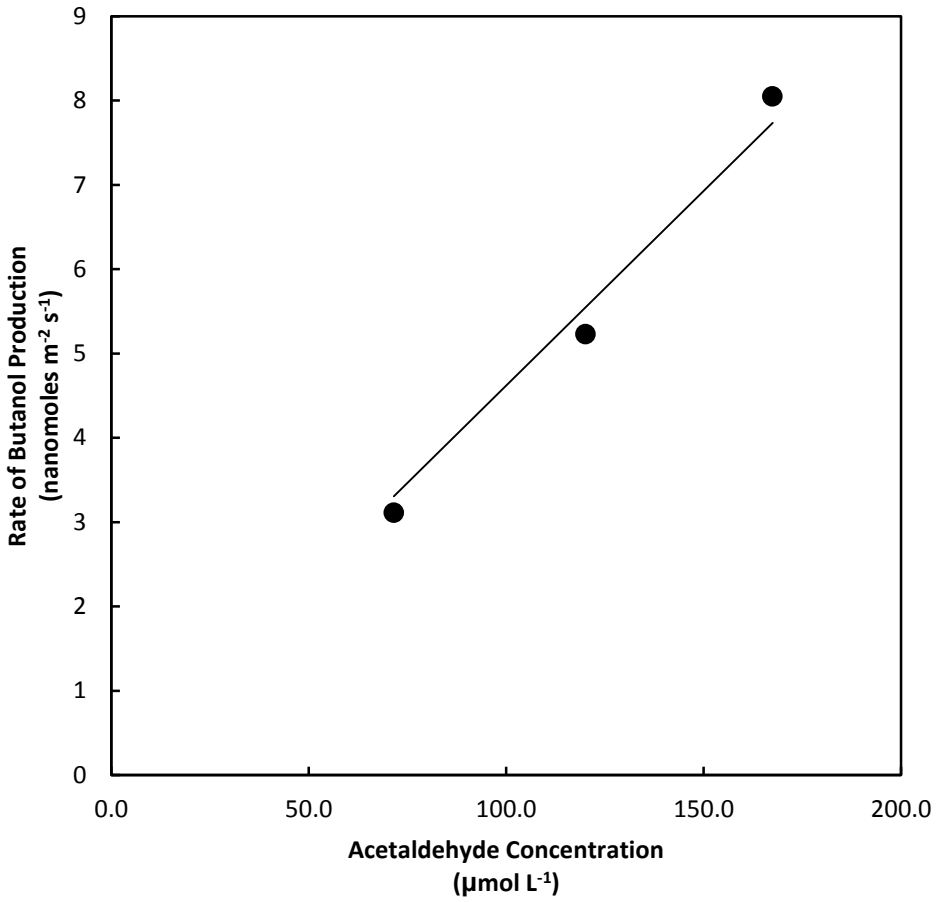

Figure 4.6. Correlation of butanol production rate to the exit concentration of acetaldehyde measured at three different flow rates during the differential conversion of ethanol at 673 K over MgO at 1.3 atm.

CO_2 Adsorption Microcalorimetry

The coverage of surface intermediates leading to butanol ranged between 2.8 x 10^{-7} and 6.6 x 10^{-7} mol m^{-2}, which is about an order of magnitude lower then ethanol coverage during the same reaction. If the Guerbet coupling of ethanol proceeds through a sequential reaction path in which aldol condensation of acetaldehyde is a key step, then base sites are likely to be important.

Thus, microcalorimetry of CO_2 adsorption was used to characterize the basic adsorption sites on the MgO used in this study.

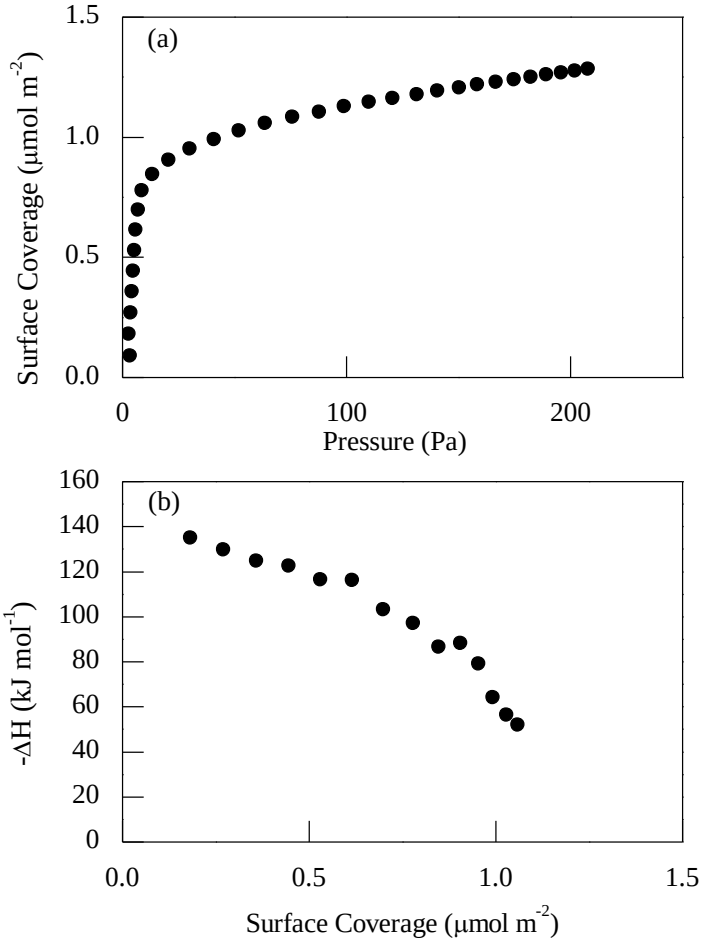

Figure 4.7. Adsorption microcalorimetry of carbon dioxide on MgO at 303 K. (a) adsorption isotherm of CO_2 on MgO ; (b) differential heat of adsorption of CO_2 on MgO determined from microcalorimetry.

Results from adsorption of carbon dioxide onto the MgO catalyst are presented in Figure 4.7. The adsorption isotherm in Figure 4.7a revealed a rapid rise in uptake at low pressure,

consistent with chemisorption of CO_2 on the MgO surface, whereas the low uptake at higher pressures signifies a weaker interaction with the surface typical of physisorption. The chemisorption uptake of CO_2 on the UBE MgO, calculated by extrapolating the physisorption regime of the isotherm at 303 K to zero pressure, was 1.0×10^{-6} mol m^{-2}. Figure 4.7b summarizes the differential heat of adsorption as a function of CO_2 coverage on the MgO catalyst. The initial heat of adsorption ($-\Delta H_{ads}$) was 135 kJ mol^{-1}, which is consistent with a fairly strong interaction with the surface, but weakens to about 50 kJ mol^{-1} at the saturation coverage of 1.0×10^{-6} mol m^{-2}.

The coverage of ethanol and intermediates leading to butanol during the Guerbet reaction (Tables 4.2 and 4.3, respectively) can be compared to the amount of strongly held CO_2 ($-\Delta H_{ads} >$ 50 kJ mol^{-1}) on MgO. During the Guerbet reaction at 673 K, the coverage of ethanol was found to be five times greater than the CO_2 adsorption capacity, but about half of the number of exposed Mg-O pairs at the catalyst surface. Evidently, the adsorption of ethanol on the metal oxide surface does not require strongly basic sites, presumably because ethanol can be easily activated to form adsorbed ethoxy and hydrogen at 673 K. The surface coverage of intermediates leading to butanol during the Guerbet reaction was substantially lower than the CO_2 adsorption capacity, which might suggest that strong basic sites facilitate the formation of butanol, presumably through an aldol condensation type coupling reaction.

Diffuse Reflectance FT-IR Spectroscopy of Adsorbed Ethanol

To corroborate the results from isotopic transient analysis, DRIFTS of ethanol adsorbed onto MgO was performed. Figure 4.8 presents the IR spectra of adsorbed ethanol during stepwise temperature-programmed desorption (STPD) in the DRIFTS cell. Two regions are shown in the figure are from 3300 to 2650 and from 1300 to 1000 cm^{-1}, which correspond to the CH_2/CH_3 and C-C-O stretching regions, respectively, for ethanol and adsorbed ethoxide. The STPD of ethanol was performed to calibrate the major adsorption modes and the relative strength of adsorption. Two IR peaks in the C-C-O stretching region were observed. One peak at 1066-1058 cm^{-1} corresponds closely to the gas phase C-C-O stretch in ethanol and is attributed to molecularly adsorbed ethanol. It should be noted that there is also a contribution from one mode of the C-C-O stretch from dissociatively adsorbed ethanol at a similar position. A second major peak observed at 1132-1119 cm^{-1} is attributed solely to deprotonated ethanol, or ethoxide species, coordinated to a cationic Mg surface atom. These peak assignments correspond well to previously reported studies of adsorbed ethanol [76,177]. By 673 K in the STPD experiment (Figure 4.8c), nearly all of all the molecularly-adsorbed ethanol had desorbed from the MgO, leaving signatures of the two C-C-O modes of ethoxide at 1122 and 1058 cm^{-1}. The CH_2 and CH_3 modes are also shown in the region 3300-2650 cm^{-1}. The two peaks at 2953 and 2920 cm^{-1} are attributed to CH_3 stretches in ethoxide whereas the peak at 2847 cm^{-1} is attributed to a CH_2 stretch in ethoxide. The observed CH_2 and CH_3 stretches from adsorbed ethoxide are red shifted from corresponding CH_2 and CH_3 stretches of gas phase ethanol. Most of the ethoxide desorbed from the catalyst by 713 K.

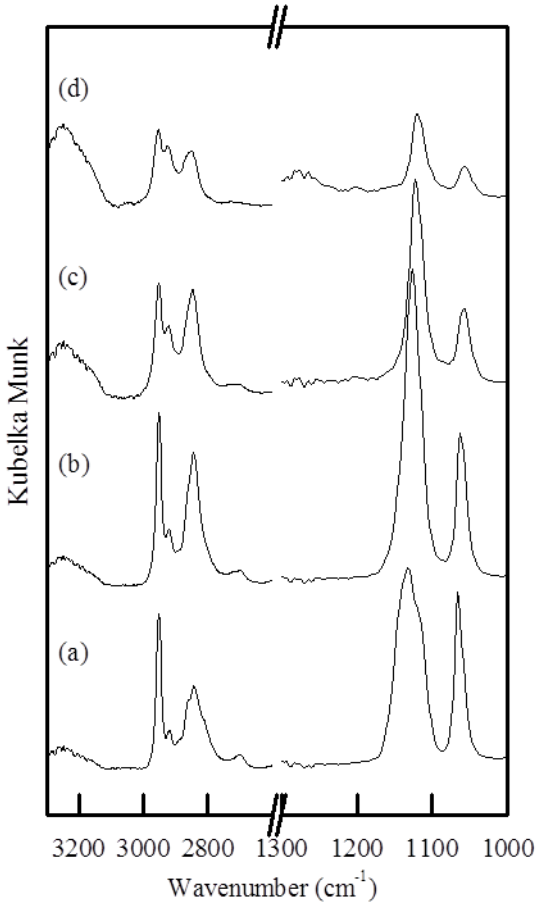

Figure 4.8. DRIFTS of ethanol adsorbed on MgO at room temperature followed by heating in He to: (a) 473 K, (b) 573 K, (c) 673 K, and (d) 713 K. Spectra are offset for clarity.

Figure 4.9 shows three IR spectra recorded at 673 K in flowing ethanol with various solid substrates and various backgrounds. The purpose of the experiments in Figure 4.9 was to interrogate the adsorbed species on MgO in the presence of flowing ethanol at 673 K in an effort to mimic the conditions of the Guerbet reaction. The spectrum in Figure 4.9a presents essentially the gas phase signal from ethanol at 673 K since MgO was not present in the cell. (Figure 4.9b and c are the spectrum for ethanol flowing over MgO at 673 K and the spectrum of adsorbed species on MgO with the gas phase subtracted, respectively.) The gas phase ethanol spectrum in Figure 4.9a reveals two CH_3 stretches at 2981 and 2969 cm^{-1} and one CH_2 stretch at 2909 cm^{-1}.

The stretches observed in this same region in Figure 4.9c, which involves the species adsorbed on MgO in the flowing gas mixture but with the contributions from the gas phase ethanol subtracted, are 2952, 2925, and 2845 cm^{-1}. Those peak positions correspond to the stretches, two CH_3 and one CH_2, observed in the STPD of adsorbed ethoxide (Figure 4.8c), within the resolution of the spectrometer. The observed red shifts of the CH_3 and CH_2 stretches from the gas phase agree with predicted red shifts of Branda et al. for ethoxide on MgO [76]. In that work, red shifts of 25-40 cm^{-1} are expected for the CH_3 stretches upon dissociative adsorption and we observed shifts of 29 and 44 cm^{-1}. Likewise, Branda et al. predicted a 25 – 130 cm^{-1} shift for CH_2 upon adsorption and we recorded a red shift of 64 cm^{-1} [76].

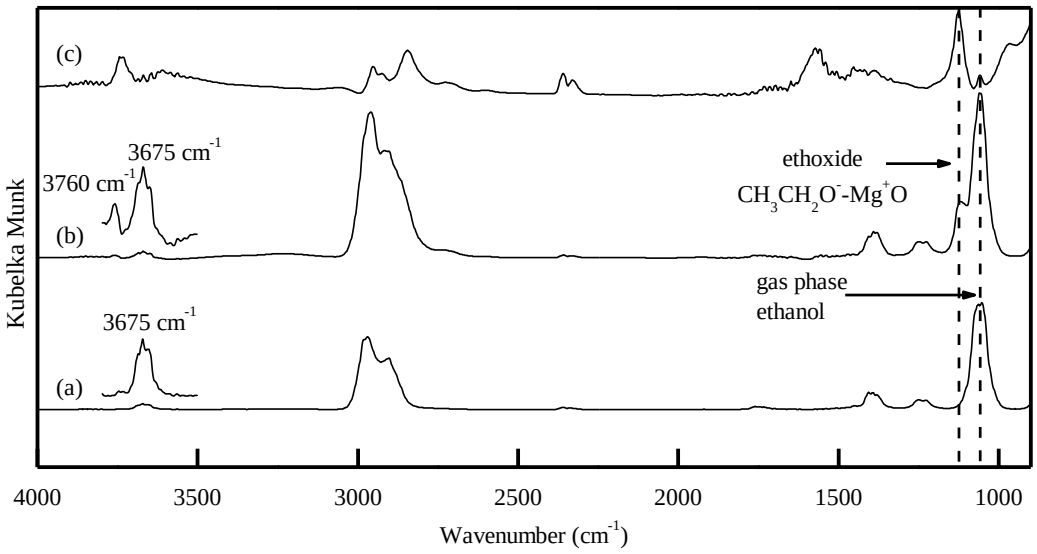

Figure 4.9. DRIFTS of ethanol in He at 673 K in the presence of: (a) KBr, with KBr in He at 673 K as a background; (b) MgO in 95 wt.% KBr, with MgO in 95 wt.% KBr in He at 673 K as a background; (c) MgO in 95 wt.% KBr, with KBr in ethanol and He at 673 K as a background. Spectra are offset for clarity.

The C-C-O region in Figure 4.9a shows features exclusively from the gas phase C-C-O stretches, whereas Figure 4.9b contains contributions from ethanol in the gas phase (1060 cm^{-1}) as well as from surface ethoxide (1120 cm^{-1}). When the gas phase spectrum of ethanol was removed, Figure 4.9c, the two C-C-O stretches associated with surface bound ethoxide were clearly revealed, indicating that under Guerbet reaction conditions adsorbed ethoxide is the major adsorbed species identified by DRIFTS on the MgO surface.

Since results in Figure 4.9 were obtained at ethanol coupling conditions, a feature associated with adsorbed aldol intermediates such as the C=C stretch present in crotonol or crotonaldehyde (which should appear near 1523 cm^{-1} [88]) might be expected. However, no IR feature was observed in that region in Figure 4.9b. Although there are stretches observed in that region in Figure 4.9c, the background for that particular scan was gas phase ethanol and KBr, so residual surface carbonates on MgO would still be present in the spectrum. The lack of a C=C stretch in the 1500-1600 cm^{-1} region of Figure 4.9b suggests very little ethanol coupling must have occurred during the DRIFTS experiment, presumably because of the very low conversion of ethanol in the cell. A very small amount of acetaldehyde is detected in Figure 4.9a and b (1711 cm^{-1}), which is consistent with a very low conversion of ethanol observed in the DRIFTS cell.

Information on the surface hydroxyls can be elucidated in the region from 3000 to 3700 cm^{-1}. Figure 4.9b shows the influence of ethanol adsorption on MgO since the background used for that spectrum consisted of the thermally-pretreated MgO surface. The OH stretch of ethanol was observed at 3675 cm^{-1} and the stretch of surface OH groups on MgO was seen at 3760 cm^{-1}. The band position of the surface OH groups on MgO agrees well with that Fouad et al. [88]. The small increase in the surface OH stretch in Figure 4.9b was likely the result of ethanol

dissociative chemisorption, but we cannot rule out the potential role of water produced from ethanol dehydration. Figure 4.9c cannot be used to evaluate the OH stretching region since the background contribution from MgO was not subtracted (only gas phase ethanol and KBr were removed).

Implications for the Guerbet reaction on MgO.

The results from isotopic transient analysis of the Guerbet reaction of ethanol, CO_2 adsorption microcalorimetry and DRIFTS of adsorbed ethanol provide a consistent picture of the Guerbet reaction of ethanol on MgO. First, the selectivity of the reaction as a function of reactant flow rate suggests that acetaldehyde is a reaction intermediate for the formation of butanol. Indeed, the observed rate of butanol formation was correlated strongly to the acetaldehyde concentration in the gas phase (Figure 4.6). Those results are consistent with the idea that the C-C bond forming step in the Guerbet coupling reaction is an aldol condensation step, which is well known to occur on basic catalysts. However, aldol addition reactions occur very readily on MgO, as illustrated by many earlier published papers in the area [37,40,42–44,62,79,90,93,178,179]. For example, the TOF for acetone addition over MgO at 273 K is 0.05 s^{-1}, based on the results from Zhang et al. [43], assuming a base site density on MgO of 1.0 x 10^{-6} mol m^{-2} (as seen in Figure 4.7). Thus, aldol condensation proceeds at reasonable rates even at temperatures as low as 273 K. In an attempt to explore the aldol condensation of acetone over MgO at similar gas phase concentrations and temperatures as those used here for Guerbet coupling, we observed many coupling products and very rapid deactivation of the catalyst. The

presence of ethanol in the gas phase evidently preserves the catalyst activity by inhibiting access of the aldehyde intermediates to the active sites on MgO and/or lowering the base strength of the surface oxide by forming surface hydroxide. Our results from isotopic transient analysis, CO_2 adsorption and DRIFTS confirm that the coverage of adsorbed ethanol, primarily as ethoxide, is nearly 50% of the exposed Mg-O surface sites and well beyond the adsorption capacity of chemisorbed CO_2, a typical probe of basic metal oxides. In contrast, the coverage of reactive intermediates leading to butanol during ethanol coupling at 673 K is nearly an order of magnitude lower than that of the adsorbed ethoxide (see Tables 4.2 and 4.3). Thus, we speculate that Guerbet coupling of ethanol on MgO occurs on a primarily ethoxide covered surface through a sequence of steps that involves dehydrogenation to acetaldehyde, aldol condensation to form C4 compounds, followed by hydrogenation or hydrogen transfer to the butanol final product. The high coverage of ethoxide provides a ready source of atomic hydrogen on the surface as well as inhibits the subsequent aldol condensation of C4 intermediates to C6 and heavier compounds that would deactivate the catalyst at 673 K. Since aldol condensation occurs readily on MgO, even at room temperature, the high temperatures required for Guerbet coupling are needed to dehydrogenate the ethoxide to the acetaldehyde intermediate, which is consistent with other works that show adding a hydrogen transfer catalyst allows the reaction to occur at lower temperatures [25–29,95,162,163,180].

Conclusions

The Guerbet coupling of gas phase ethanol to butanol was catalyzed by MgO at 673 K. The coverage of adsorbed ethoxide, which was identified by in situ DRIFTS, was determined

from isotopic transient analysis to be 5 x 10^{-6} mol m^{-2}, which is about half of the exposed Mg-O pairs based on the measured surface area of the catalyst assuming a surface atom density equivalent to that on the (100) plane of MgO. The surface coverage of intermediates leading to butanol ranged from 2.8 x 10^{-7} to 6.6 x 10^{-7} mol m^{-2}, depending on the conversion of ethanol. Since the primary product from the reaction over MgO was acetaldehyde, we concluded that butanol is a secondary product of acetaldehyde conversion, presumably through a C-C bond-forming aldol condensation step. The coverage of reaction intermediates leading to butanol was below the surface base site density evaluated by CO_2 adsorption, which was measured to be 1.0 x 10^{-6} mol m^{-2}. The intrinsic turnover frequency of the catalytic cycle on MgO leading to the formation of butanol at 673 K was determined from isotopic transient analysis to be 0.040 s^{-1}. The rather low turnover frequency of this reaction at 673 K is likely related to the difficulty associated with dehydrogenating ethanol to acetaldehyde over MgO.

Acknowledgment

This work was supported by the Chemical Sciences, Geosciences and Biosciences Division, Office of Basic Energy Sciences, Office of Science, U.S. Department of Energy, grant no. DE-FG02-95ER14549.

Chapter 5: Sodium Modification of Zirconia Catalysts for Ethanol Coupling to 1-Butanol

This chapter was accepted for publication in the Journal of Energy Chemistry as: J.T. Kozlowski, R.J. Davis, "Sodium Modification of Zirconia Catalysts for Ethanol Coupling to 1-Butanol".

Introduction

Interest in the conversion of ethanol to more valuable products has increased because the recent expansion in the production of ethanol from biobased feedstocks. One proposed process to upgrade ethanol is through coupling to form 1-butanol, also known as the Guerbet reaction of ethanol. Butanol can be more attractive than ethanol since it has a higher energy density, is less hydrophilic, and is used as a chemical intermediate, solvent or additive in many commercial products [30]. Marcel Guerbet first published on the alcohol coupling reaction in the 1890s [1], and ethanol coupling has been patented since the 1930's [3,4]. Coupling of short chain alcohols over heterogeneous catalysts has been the focus of recent works as well [29,31,32,46,55,69,74,180,181], in part due to a desire to produce chemicals and fuels from renewable feedstocks.

Heterogeneously-catalyzed ethanol coupling to 1-butanol via the Guerbet reaction [31,55,181] as well as ethanol conversion to butadiene [53] and isobutene [56] are known to be influenced by the acid-base character of the solid catalyst. One material that has been used with little success in ethanol coupling reactions is zirconia [46,66] even though it has well-recognized acid-base bifunctionality. Indeed, zirconia has been used successfully to catalyze a wide variety

of reactions including the Meerwein-Ponndorf-Verley reduction of an aldehyde or ketone with an alcohol [106,133,182–184], aldol condensation [90,160], alcohol dehydration and alcohol dehydrogenation [185,186]. Additional applications of zirconia catalysts can be found in a review on the topic by Yamaguchi [115]. One particular pair of reactions that is related to some of the steps in ethanol coupling is the dehydration or dehydrogenation of an alcohol such as 2-propanol. Results from alcohol probe reactions have indicated a propensity for zirconia to catalyze the dehydration of alcohols to form olefins more rapidly than the dehydrogenation of alcohols to form aldehydes or ketones [185,186]. For more information on catalytic probe reactions of alcohols see the review by Lauron-Pernot [144].

Zirconia is not recognized as a catalyst for the production of butanol from ethanol since ethanol coupling likely involves ethanal as a key intermediate [29,31-34,54,55,69,70,155,161,163,181,187] and, as mentioned above, zirconia generally catalyzes alcohol dehydration at higher rates compared to dehydrogenation. Thus, one possible way to decrease the dehydration rate of ethanol over zirconia is to selectively remove, block or deactivate the acid sites responsible for dehydration by adding small amounts of alkali metal. For example, Cutrufello et al. synthesized zirconia samples with varying concentrations of alkali metal oxides and observed significant decreases in dehydration rates and increases in dehydrogenation rates with increasing alkali metal concentration [186].

In this work, the influence of sodium addition on the reactivity of zirconia for ethanol conversion was investigated. Acetone condensation was also used as a simple probe for a C-C bond forming reaction on zirconia. Since adsorption microcalorimetry of ammonia and carbon dioxide has been used previously as a method to evaluate surface acid and base sites and has been related to catalyst performance in alcohol dehydration and dehydrogenation [186], we have

also used adsorption microcalorimetry to study the effect of sodium on the acidic and basic character of zirconia surfaces.

Experimental Methods

Catalyst Synthesis

Samples of zirconia (Sigma-Aldrich, <100nm particle size) were used as received, and impregnated with aqueous solutions of the appropriate concentration of sodium carbonate (Sigma-Aldrich, 99.95%) to the point of incipient wetness. Impregnated samples were dried in air at 413 K for 24 h. All samples were pelletized to 106-180 μm before characterization and reactivity measurements.

Catalyst Characterization

The elemental analysis (Zr and Na) was performed by Galbraith Laboratories (2323 Sycamore Drive, Knoxville, TN 37921) using inductively coupled plasma optical emission spectrometry (ICP-OES).

The X-ray diffraction (XRD) patterns were recorded on a PANalytical X'pert diffractometer using Cu K-α radiation.

Adsorption of N_2 was performed on a Micromeritics ASAP 2020 automated adsorption system to obtain the BET surface area and cumulative pore volume of the catalysts after evacuation at 723 K for 4 h.

Adsorption microcalorimetry experiments were completed on the same home built instrument that has been described previously [80,109,124,151,156]. The instrument is a heat flow calorimeter with two cells that are inserted into a large aluminum block maintained at 303 K. One cell functioned as a sample cell and the other one served as a reference. A catalyst sample was first heated to 773 K under vacuum to a pressure less than 10^{-2} Pa. The sample was then cooled and allowed to thermally equilibrate with the system for 2 h prior to adsorption of carbon dioxide or ammonia. The initial dosing pressure of adsorbate ranged from 10 Pa to 600 Pa, and each dose was allowed to equilibrate with the sample for 15 min

Ethanol Coupling

Conversion of ethanol over the solid catalysts was carried out in a gas phase, downward flow, fixed bed reactor. A reactant stream of ethanol (Sigma-Aldrich, 99.5% purity anhydrous) and 5 wt.% octane (Sigma-Aldrich, 99.9% purity anhydrous) as an internal standard was pumped to a vaporizer containing glass beads and 3 Å molecular sieves to remove trace water from the ethanol feed. The ethanol and octane mixture was mixed with flowing N_2 (ultrahigh purity from Praxair, additionally purified by passage through a Supelco OMI-2 purifier) to give 6.8 mol% ethanol in the vapor stream. The vaporizer was maintained at 333 K and all gas lines were maintained at 473 K to avoid condensation of reactant, internal standard and products. The feed mixture flowed through the catalyst bed and then into a gas sampling valve for product analysis by online gas chromatography. The GC column was a Varian CP-Poraplot column, 25 m in length with an internal diameter of 0.32 mm. The reaction was performed between 136 to 170 kPa absolute and the temperature and flow rates were varied from 633 to 673 K and 0.39 to 2.1

$\mu mol_{ethanol}$ m^{-2} s^{-1}, respectively. Catalyst samples were pretreated in-situ at 773 K with 100 cm^3 min^{-1} of flowing purified N_2 for 1 h before the reaction was started.

Acetone Condensation

Acetone condensation was carried out in the same gas phase, downward flow, fixed bed reactor system. The feed to the reactor, 95 wt.% acetone (Sigma-Aldrich, ≥99.9%) and 5 wt. % hexane (Sigma-Aldrich, ≥97%) as an internal standard, was fed to a vaporizer at a rate of 0.01 to 0.04 cm^3 (liquid) min^{-1}. The reactant and internal standard was mixed with 50 to 200 cm^3 min^{-1} flowing He (ultrahigh purity from Praxair, additionally purified by passage through a Supelco OMI-2 purifier) to give 5.5 mol % acetone in the vapor stream. Acetone condensation was performed at ambient total pressure and the temperature was varied between 473 and 573 K. Product analysis was carried out with an Agilent 7890 GC equipped with a DB-WAX column.

Results and Discussion

The nominal loading of Na, the measured loading of Na by ICP-OES, the surface area and the cumulative pore volume for each of the prepared catalysts are presented in Table 5.1. The measured Na loadings were quite similar to the nominal values and the surface area and cumulative pore volume of the samples decreased slightly with increasing Na content, as expected.

Table 5.1. Sodium loading, surface area and cumulative pore volume of monoclinic ZrO_2 and Na/ZrO_2

Nominal Na (wt. %)	Observed $Na^{(a)}$ (wt. %)	Surface Area ($m^2\ g^{-1}$)	Cumulative Pore Volume ($cm^3\ g^{-1}$)
0	0.02	12.8	0.090
0.1	0.13	12.1	0.090
1	0.93	10.8	0.085

(a) Measured by ICP-OES

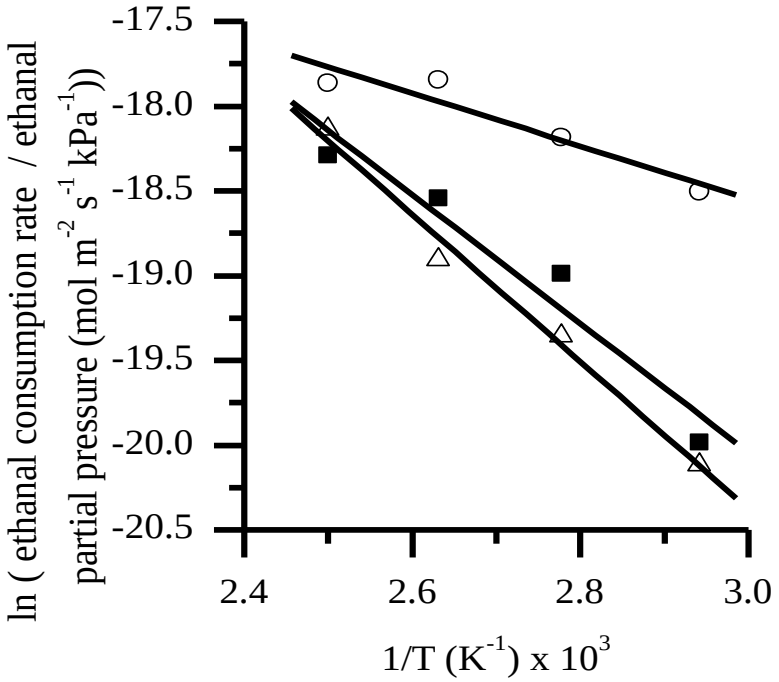

Figure 5.1. X-Ray diffraction patterns of the zirconia samples with 0 wt.% Na (a), 0.1 wt.% Na (b) and 1.0 wt.% Na (c).

The X-ray diffraction patterns for the three zirconia samples are shown in Figure 5.1. All of the materials have the characteristic peaks of monoclinic zirconia without any evidence for tetragonal zirconia. Addition of Na to the samples did not alter the monoclinic structure of zirconia. Monoclinic zirconia was chosen for this study over tetragonal zirconia since at the temperatures used for ethanol coupling (573 to 673 K), it is possible for the kinetically-trapped

tetragonal structure to partially transform into the thermodynamically-stable monoclinic structure.

The surface acid and base properties were evaluated by ammonia and carbon dioxide adsorption microcalorimetry. The adsorption isotherms and differential heats of adsorption for CO_2 on the various zirconia samples are presented in Figure 5.2. Addition of Na to ZrO_2 increased both the total uptake and the heat of adsorption of carbon dioxide. In contrast, the uptake and heat of adsorption of ammonia decreased upon addition of Na to the samples, as shown in Figure 5.3. A summary of the initial heat of adsorption and total uptake (determined by extrapolating the high pressure part of the isotherm to zero pressure) for carbon dioxide and ammonia adsorption is presented in Table 5.2. The addition of only 0.1 wt.% Na was sufficient to significantly affect the initial heats of adsorption of both CO_2 and NH_3, although the total uptakes of the probes were affected minimally. Addition of 1 wt.% Na essentially doubled the uptake of CO_2 and halved the uptake of NH_3, while also significantly affecting $-\Delta H_{ads}$. The adsorption of NH_3 on the sample with 1.0 wt.% Na likely involved hydrogen bonding of ammonia or formation of surface amide groups produced by the deprotonation of ammonia on strongly basic sites associated with Na. These modes of ammonia adsorption have been well documented on strongly basic materials [141,159,188]. In summary, the addition of Na from 0 to 1.0 wt. % Na formed a set of materials with a range of acid-base site densities and adsorption strengths.

Table 5.2. Summary of results from ammonia and carbon dioxide adsorption microcalorimetry

	CO_2 Adsorption		NH_3 Adsorption	
Na Content (wt.%)	Uptake[(a)] (μmol m^{-2})	Initial -ΔH (kJ mol^{-1})	Uptake[(a)] (μmol m^{-2})	Initial -ΔH (kJ mol^{-1})
0	1.4	104	3.3	126
0.1	1.8	137	3.3	98
1	3.6	158	1.7	91

(a) Uptake calculated by extrapolating the saturation conditions to zero pressure

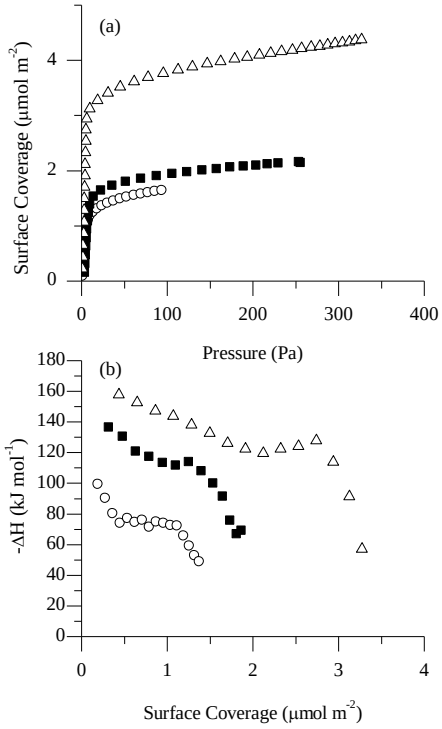

Figure 5.2. CO_2 adsorption microcalorimetry at 303 K on zirconia samples with nominal weight loadings of Na on ZrO_2 of 0 (○), 0.1 (■) and 1.0 (Δ) wt%. (a) adsorption isotherms and (b) differential heats of adsorption.

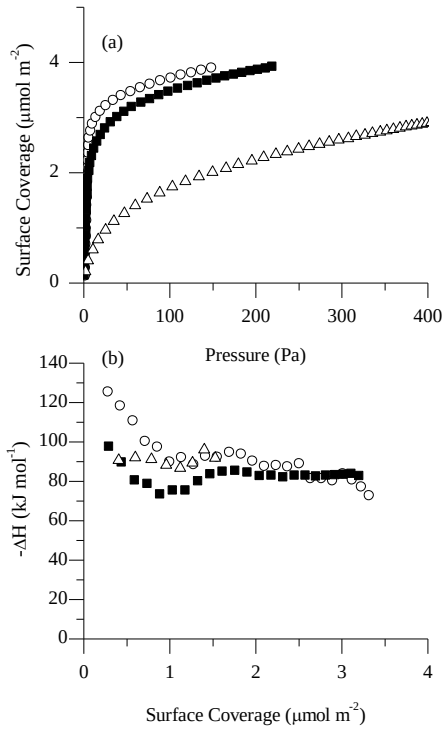

Figure 5.3. NH_3 adsorption microcalorimetry at 303 K on zirconia samples with nominal weight loadings of Na of 0 (○), 0.1 (■) and 1.0 (Δ) wt%. (a) adsorption isotherms and (b) differential heats of adsorption.

Ethanol conversions, rates of ethene, ethanal, butanol and crotonaldehyde production as well as ethanal concentrations at the reactor outlet are summarized in Table 5.3 for ethanol reactions at four different temperatures (613, 633, 653 and 673 K). The rate of ethene production was significantly inhibited over the 1.0 wt.% Na samples compared to pure zirconia at each temperature. In particular, the rate of dehydration over pure zirconia was approximately 20-30 times greater than over the 1.0 wt.% Na sample over the range of temperatures from 633 to 674 K (the rate over 1.0 wt. % Na/ZrO_2 was too low to measure at 613 K). In contrast, the rate of ethene production was not affected by adding 0.1 wt.% Na to pure zirconia.

Interestingly, the 1.0 wt.% Na sample showed a 50% decrease in NH_3 adsorption uptake and much lower $-\Delta H_{ads}$ compared to the pure zirconia sample, whereas the 0.1 wt.% Na/ZrO_2 sample had almost the same ammonia adsorption capacity as ZrO_2.

A different trend is observed in the ethanal production rates. The dehydrogenation rate to ethanal was slightly increased by addition of 1 wt.% Na to ZrO_2, although there was little influence of adding 0.1 wt.% Na. In this case, the 1.0 wt.% Na sample had 2.6 times as many CO_2 adsorption sites (related to base sites) as pure zirconia.

Table 5.3. Summary of ethanol reactions over Na containing zirconia at various temperatures[(a)]

Nominal Na Content (wt.%)	Temp. (K)	Ethanol Conv.[(b)]	Rate of Ethene Production (nmol m^{-2} s^{-1})	Rate of Ethanal Production (nmol m^{-2} s^{-1})	Ethanal Concentration (μmol L^{-1})[(c)]	Rate of Butanol Production (nmol m^{-2} s^{-1})	Rate of Crotonaldehyde Production (nmol m^{-2} s^{-1})
0	613	0.10	19	15	71	1.1	0.6
0.1	613	0.10	26	14	66	0.4	0.0
1	613	0.06	0.0	21	103	0	0
0	633	0.16	33	22	103	2.1	1.3
0.1	633	0.16	38	20	96	0.80	0.63
1	633	0.08	1.2	26	125	0.48	0.81
0	653	0.23	51	28	130	3.0	2.3
0.1	653	0.23	54	27	125	1.6	1.4
1	653	0.10	2.4	31	144	1.0	1.4
0	673	0.31	78	29	131	2.8	2.6
0.1	673	0.30	71	35	156	2.3	2.7
1	673	0.14	3.9	37	166	3.3	2.9

(a) Reactant flow rate: 0.39 $\mu mol_{ethanol}$ m^{-2} s^{-1}
(b) Conversion calculated by the sum of all products identified (ethene, ethanal, 1-butanol and crotonaldehyde)
(b) Concentration at the reactor outlet

The Arrhenius-type plots for dehydration and dehydrogenation are shown in Figures 5.4 and 5.5, respectively, and the activation energies for dehydration and dehydrogenation were calculated for the three samples and summarized in Table 5.4. The activation energy for dehydration over the pure zirconia (73 ± 6 kJ mol^{-1}) and 0.1 wt.% Na sample (58 ± 2 kJ mol^{-1}) were similar and significantly lower than 102 ± 9 kJ mol^{-1} calculated for 1.0 wt.% Na/ZrO_2. In Figure 5.5 the Arrhenius-type plot for the total dehydrogenation rate is shown. To calculate the total dehydrogenation rate, the ethanal production rate was added to the crotonaldehyde and butanol rates multiplied by two since the coupled products are produced from aldol condensation of ethanal. This analysis gave similar activation energies for ethanol dehydrogenation over the pure zirconia (58 ± 5 kJ mol^{-1}) and the 0.1 wt.% Na/ZrO_2 sample (65 ± 4 kJ mol^{-1}). The 1.0 wt.% Na/ZrO_2 sample showed a lower activation energy (38 ± 4 kJ mol^{-1}) for the dehydrogenation of ethanol.

Table 5.4. Activation energies for ethanol dehydration and dehydrogenation over ZrO_2 and Na/ZrO_2

Nominal Na Content (wt.%)	E_a (kJ mol^{-1})[(a)]	
	Dehydration	Dehydrogenation[(b)]
0	73 ± 6	58 ± 5
0.1	58 ± 2	65 ± 4
1	102 ± 9	38 ± 4

(a) Errors are standard errors associated with the linear fit of the transformed rate
(b) For all dehydrogenation reactions (ethanal production rate + 2 x rate of coupling)

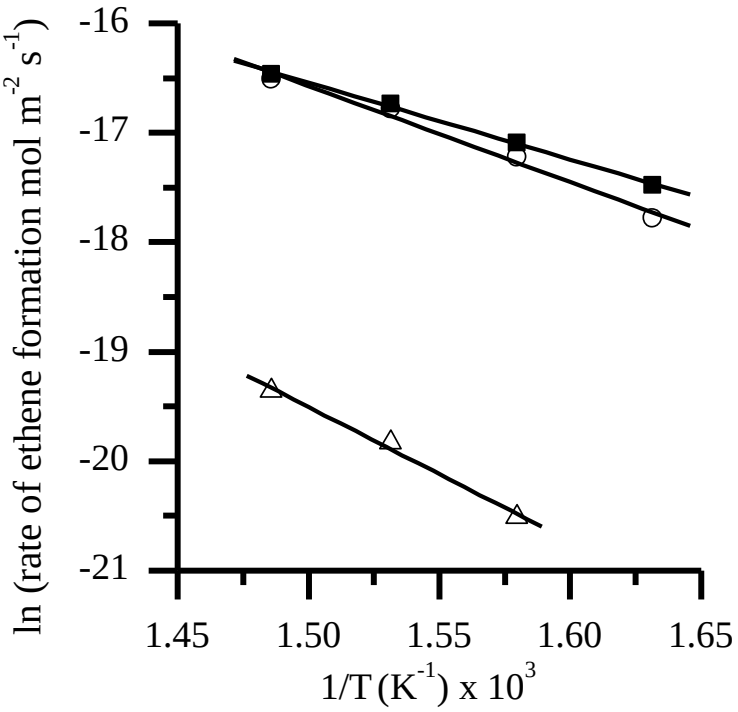

Figure 5.4. Arrhenius-type plot of the dehydration rate of ethanol over zirconia samples with nominal weight loadings of Na of 0 (○), 0.1 (■) and 1.0 (Δ) wt%. Solid lines represent a linear fits to the results.

The production rates of butanol and crotonaldehyde are also reported in Table 5.3. From 613-653 K, the 1.0 wt.% Na/ZrO_2 sample operated with a higher exit concentration of ethanal but exhibited lower production rates of coupled product compared to zirconia. Even at 673 K, the rates of coupling over the 1.0 wt.% Na/ZrO_2 sample were similar to those over pure zirconia, although the ethanal concentration was greater over the Na-loaded sample. This is interesting since the rate of coupling generally increases with increasing concentration of aldehyde [29]. Evidently, the sodium-doped sample was not as active for aldolization during ethanol coupling compared to pure zirconia.

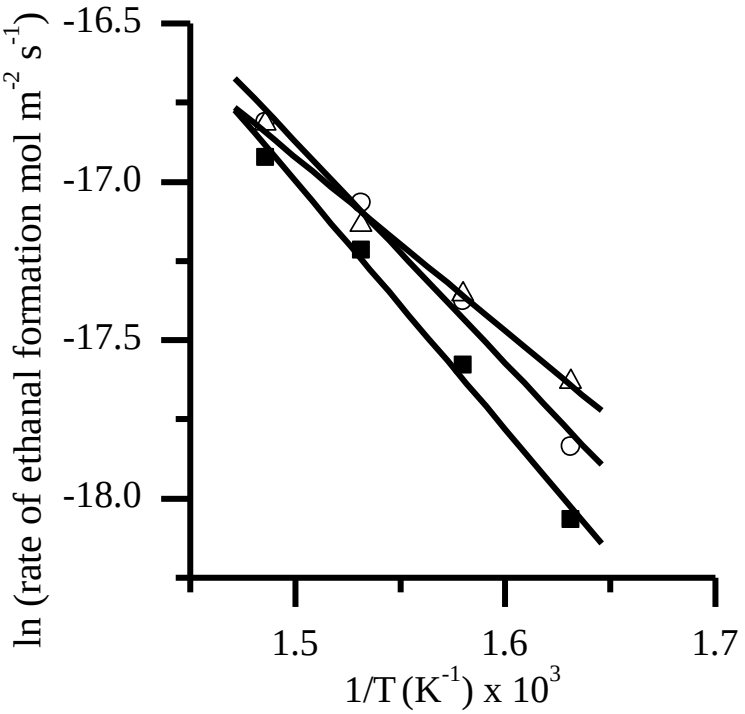

Figure 5.5. Arrhenius-type plot of the total dehydrogenation rate of ethanol over zirconia samples with nominal weight loadings of Na of 0 (○), 0.1 (■) and 1.0 (Δ) wt%. Solid lines represent a linear fits to the results

To further explore the role of Na addition to ZrO_2 on a C-C bond forming reaction, acetone condensation was performed at 473-573 K. Condensation of acetone was rapid at the higher temperatures used for ethanol coupling, so we chose to use lower reaction temperatures to minimize side reactions. Since ZrO_2 was stable in the acetone condensation reaction for hours on stream, the rates over ZrO_2 reported in Table 5.5 were calculated at the steady state. Mesityl oxide was the main condensation product over ZrO_2 with some formation of the heavier coupled products, mesitylene and isophorone. The 1 wt% Na/ZrO_2 was significantly more active for acetone condensation than ZrO_2 at 473 K (Table 5.5), but deactivated substantially with time on stream. The rate of acetone condensation decreased by 50% in the first 30 minutes and by more

than an order of magnitude over 12 h. We suspect the high rate of deactivation can be attributed to heavy products being deposited on the catalyst since the selectivity to isophorone (a further coupling product of mesityl oxide) was 44% at 473 K.

Table 5.5. Summary of results from acetone condensation over ZrO_2 and 1wt% Na/ZrO_2.

				Selectivity(%)[a]		
Nominal Na Content (wt.%)	Temperature (K)	Conversion (%)	Rate (nmol m^{-2} s^{-1})[b]	Mesityl Oxide	Mesitylene	Isophorone
0[c]	473	4.2	26	83	5	12
0[c]	523	5.5	34	78	3	18
0[c]	543	6.7	41	80	5	16
0[c]	573	10	62	80	12	8
1.0[d][e]	473	3.7	80	54	0	46
1.0[f][g]	473	32	90	56	0	44

(a) Selectivity calculated by moles of produced product
(b) Rate of acetone conversion
(c) Reactant Feed: 0.61 $\mu mol_{acetone}$ m^{-2} s^{-1}
(d) Initial rate only; rate of acetone condensation was 19 nmol m^{-2} s^{-1} after 0.63 h on stream
(e) Reactant Feed: 1.4 $\mu mol_{acetone}$ m^{-2} s^{-1}
(f) Initial rate only; rate of acetone condensation was 40 nmol m^{-2} s^{-1} after 0.69 h on stream
(g) Reactant Feed: 0.30 $\mu mol_{acetone}$ m^{-2} s^{-1}

Results from both ethanol coupling and acetone condensation need to be compared to explain the influence of Na on C-C bond forming reactions by ZrO_2. The lower rate of ethanol coupling over ZrO_2 after addition of Na might suggest the alkali metal disrupts the appropriate acid-base pairs on the surface that promote aldol condensation reactions. Indeed, bifunctional materials have been shown to be more active for aldolization [40,90,91] and dehydrogenation [31,87]. If this hypothesis were true, we would expect Na to negatively impact the rate of acetone condensation over zirconia, which clearly did not happen. Therefore, the influence of Na addition to ZrO_2 on the ethanol coupling rate is likely related to how Na affects other aspects

of the ethanol coupling reaction. Recent work in our lab utilizing isotopic transient methods and IR spectroscopy to study the coupling of ethanol over MgO at 673 K revealed a very high coverage of dissociated ethanol on the surface during reaction and very little coverage of reactive intermediates leading to coupling products [189]. The high coverage of ethoxide and surface hydroxide that was also likely to be present on ZrO_2 and Na-loaded ZrO_2 surfaces during ethanol coupling reactions likely inhibited C-C coupling reactions as was seen in the case with MgO [189]. We suspect that Na promotes aldol condensation on ZrO_2 catalysts (as observed in Table 5.5), but during the complex sequence of steps comprising the ethanol coupling reaction, the aldol condensation steps are more affected by the inventory of adsorbed ethoxide and hydroxide formed in situ rather than the Na present on the surface. Analysis of the apparent activation energies of the various reactions might support this speculation.

An Arrhenius-type plot for the aldol condensation of acetone over monoclinic zirconia is presented in Figure 5.6 and the apparent activation energy was calculated to be 18 ± 4 kJ mol^{-1}. One study by Rekoske and Barteau [190] found that the activation energy of ethanal condensation over titania was low as well, between 9 kJ mol^{-1} and 37 kJ mol^{-1}, depending on the deactivation level of the catalyst. Evidently, the apparent barrier for aldol condensation is generally quite low, which explains why acetone condensation was carried out over ZrO_2 at lower temperatures than those used for ethanol coupling. Rekoske and Barteau also observed the order of reaction with respect to ethanal to be between about 0.7 and 1 at 423 and 523 [190]. If a first order dependence on concentration was assumed for the ethanal condensation rate during ethanol coupling, an apparent activation energy for coupling can be calculated for the three samples in Table 5.3. The Arrhenius-type plot for the ethanal condensation rate is presented as Figure 5.7 and the apparent activation energies are summarized in Table 5.6. The

activation energy of ethanal condensation (13 ± 3 kJ mol^{-1}) over zirconia is similar to that of acetone condensation over the same material (18 ± 4 kJ mol^{-1}). As the sodium concentration increased to 1 wt%, the apparent activation energy for ethanal condensation increased substantially to 36 ± 3 kJ mol^{-1}. Since the increase in the apparent barrier of ethanal condensation during ethanol coupling is not consistent with the observed promotional influence of Na on acetone condensation, we suspect Na also modified the coverage of adsorbed intermediates such as hydroxide and ethoxide present during ethanol conversion.

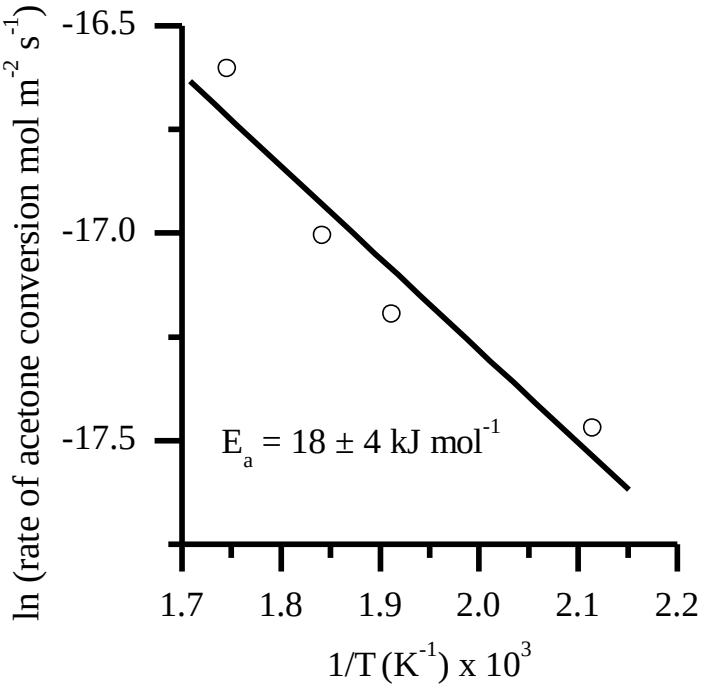

Figure 5.6. Arrhenius-type plot of the acetone coupling rate over zirconia (○). Solid lines represent a linear fit to the results with the error in the activation energy calculated from the standard error of the linear fit.

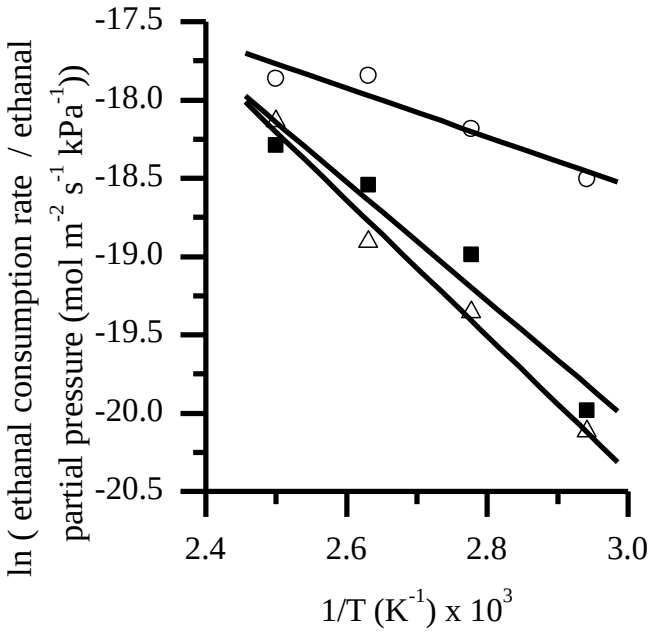

Figure 5.7. Arrhenius-type plot of ethanal condensation during the ethanol coupling reaction over zirconia samples with nominal weight loadings of Na of 0 (○), 0.1 (■) and 1.0 (Δ) wt%. Solid lines represent linear fits to the results.

Table 5.6. Apparent activation energy of ethanal condensation derived from rates of ethanol coupling over Na-loaded ZrO_2 samples.

Nominal Na Content (wt.%)	E_a[(a)] (kJ mol^{-1}) Aldol[(b)]
0	13 ± 3
0.1	31 ± 6
1	36 ± 6

(a) Errors are standard errors associated with the linear fit of the transformed rate
(b) Ethanal condensation activation energy

While the rates of dehydrogenation and aldol condensation during ethanol coupling reactions are not significantly increased by adding sodium, the selectivity towards coupled products is significantly improved. The selectivities to ethene, ethanal, crotonaldehyde and

butanol at 673 K are compared at similar conversions of ethanol in Table 5.7. Addition of Na to ZrO_2 inhibited the unproductive dehydration of ethanol to ethene, thus allowing for dehydrogenation and condensation reactions to occur with higher overall selectivity. The gain in selectivity to desired products is offset by their lower rate of formation caused by addition of Na.

Table 5.7. Selectivity of the products during ethanol coupling reactions at 673 K and at similar conversions

			Selectivity (C%)[(d)]			
Nominal Na (wt.%)	Ethanol Conversion Rate (nmol m^{-2} s^{-1})	Conversion (%)	Ethene	Ethanal	Crotonaldehyde	Butanol
0[(a)]	200	9.4	44	54	0.0	2.2
0.1[(b)]	160	9.6	32	63	2.5	2.7
1[(c)]	40	7.7	17	71	0.0	12

(a) Reactant flow rate: 2.1 $\mu mol_{ethanol}$ m^{-2} s^{-1}
(b) Reactant flow rate: 1.7 $\mu mol_{ethanol}$ m^{-2} s^{-1}
(c) Reactant flow rate: 0.52 $\mu mol_{ethanol}$ m^{-2} s^{-1}
(d) Carbon based selectivity

Conclusions

The addition of a small amount of sodium (1 wt.%) to monoclinic zirconia successfully decreased the density of acid sites and increased the density of base sites as measured by adsorption microcalorimetry of ammonia and carbon dioxide, respectively. This decrease in acid site density on 1.0 wt.% Na/ZrO_2 significantly decreased the rate of ethanol conversion to the unwanted product ethene by more than an order of magnitude, thereby shifting the selectivity to the desired coupling products. Although the 1.0 wt.% Na/ZrO_2 sample was slightly more active for dehydrogenation of ethanol to ethanal compared to zirconia, the ethanal condensation rate was actually inhibited by the added Na. In contrast, addition of Na to ZrO_2 promoted the rate of

acetone condensation. Since aldol condensation is an important step in the overall path for ethanol coupling, the influence Na on the inventory of adsorbed intermediates such as ethoxide and hydroxide likely dominate the reaction kinetics during the coupling reaction.

Acknowledgements

This work was supported by the Chemical Sciences, Geosciences and Biosciences Division, Office of Basic Energy Sciences, Office of Science, U.S. Department of Energy, grant no. DE-FG02-95ER14549.

Chapter 6: Conclusions and Future Directions

Acid-base bifunctional materials have many potential applications as catalysts for the upgrading and transformation of renewable feedstocks. Among the many reactions that occur over acid and base sites, four reactions were chosen for this study: transesterification of tributyrin with methanol, acetone condensation, acetone coupling and ethanol coupling. Transesterification of tributyrin to methanol was employed as a model reaction for the synthesis of biodiesel from triglycerides. The current catalysts for transesterification are typically soluble bases, so developing a solid catalyst might improve the recyclability of the catalyst as well as decrease the catalyst separation requirements. Alcohol coupling, also known as the Guerbet reaction, is a potentially important process to increase the value of short chain alcohols. In particular, ethanol has seen large increases in production rates from renewable feedstocks and could be upgraded to butanol by the Guerbet reaction. Finally, acetone coupling and condensation were used as model reactions to further understand the carbon-carbon bond forming step in the ethanol coupling reaction. To further the understanding of these important reactions, various bifunctional materials were synthesized, characterized and used in the reactions mentioned.

Mixed oxides of magnesia and zirconia have great potential for base catalyzed reactions. First, mixed oxides prepared by sol-gel synthesis were better mixed at the atomic level since the X-ray diffraction patterns revealed poor crystallinity compared to samples prepared by co-precipitation. However, the only significant promotional effect for transesterification was observed on a magnesia-rich mixed oxide (Mg:Zr 11:1) prepared by co-precipitation. The X-ray

pattern of this sample revealed phases of both MgO and ZrO_2, suggesting that perhaps the promotional effect occurred at the interface between phases. The influences of trace sodium and catalyst leaching on activity were ruled out by control experiments. In an attempt to relate surface properties to catalysis, DRIFTS of adsorbed CO_2 and CH_3OH were recorded on the most active mixed oxide, standard MgO and inactive ZrO_2. The DRIFTS of adsorbed CO_2 was not effective at distinguishing between the samples. However, DRIFTS of adsorbed CH_3OH showed very significant differences among the samples. Although the mixed oxide sample was primarily composed of magnesia, the DRIFTS of CH_3OH showed a different ratio of unidentate to bidentate modes. Moreover, the initial heat of CO_2 adsorption on the mixed oxide was greater than that on MgO.

A mixed oxide of Mg:Zr 11:1 that was prepared in a controlled precipitation had a higher surface exposure of zirconia than a material prepared traditionally by increasing the pH. Although the controlled precipitation method produced a more uniform distribution of zirconia, the larger surface exposure of zirconia caused an undesirable increase in the rate of ethanol dehydration, which is detrimental to the Guerbet coupling reaction. Since ZrO_2 was inactive for transesterification and low temperature coupling of acetone, the presence of small amounts of crystalline ZrO_2 on the surface of Mg:Zr 11:1 was not detrimental to those reactions. Interestingly, Mg:Zr 11:1 mixed oxides prepared by either method were substantially more active for transesterification and low temperature acetone coupling compared to MgO (on a surface area basis). The promotion of MgO-catalyzed reactions by the addition of Zr^{4+} was presumably the result of additional acid-base surface sites that facilitate those reactions.

In summary, both methods of preparation, i.e. controlled precipitation and rising pH precipitation, produced highly active mixed oxides for transesterification and acetone coupling.

However, if crystalline ZrO_2 at the surface of the oxide is detrimental to a reaction, the rising pH method of precipitation is the preferred synthesis procedure since crystalline ZrO_2 is buried below the interface.

The Guerbet coupling of gas phase ethanol to butanol was catalyzed by MgO at 673 K. The coverage of adsorbed ethoxide, which was identified by in situ DRIFTS, was determined from isotopic transient analysis to be 5×10^{-6} mol m^{-2}, which is about half of the exposed Mg-O pairs based on the measured surface area of the catalyst assuming a surface atom density equivalent to that on the (100) plane of MgO. The surface coverage of intermediates leading to butanol ranged from 2.8×10^{-7} to 6.6×10^{-7} mol m^{-2}, depending on the conversion of ethanol. Since the primary product from the reaction over MgO was ethanal, we concluded that butanol is a secondary product of ethanal conversion, presumably through a C-C bond-forming aldol condensation step. The coverage of reaction intermediates leading to butanol was below the surface base site density evaluated by CO_2 adsorption, which was measured to be 1.0×10^{-6} mol m^{-2}. The intrinsic turnover frequency of the catalytic cycle on MgO leading to the formation of butanol at 673 K was determined from isotopic transient analysis to be 0.040 s^{-1}. The rather low turnover frequency of this reaction at 673 K is likely related to the difficulty associated with dehydrogenating ethanol to ethanal over MgO.

The addition of a small amount of sodium (1 wt.%) to monoclinic zirconia successfully decreased the density of acid sites and increased the density of base sites as measured by adsorption microcalorimetry of ammonia and carbon dioxide, respectively. This decrease in acid site density on 1.0 wt.% Na/ZrO_2 significantly decreased the rate of ethanol conversion to the unwanted product ethene by more than an order of magnitude, thereby shifting the selectivity to the desired coupling products. Although the 1.0 wt.% Na/ZrO_2 sample was slightly more active

for dehydrogenation of ethanol to ethanal compared to zirconia, the ethanal condensation rate was actually inhibited by the added Na. In contrast, addition of Na to ZrO_2 promoted the rate of acetone condensation. Since aldol condensation is an important step in the overall path for ethanol coupling, the influence Na on the inventory of adsorbed intermediates such as ethoxide and hydroxide likely dominate the reaction kinetics during the coupling reaction.

Future Recommendations

New acid and base probes

Throughout this dissertation research, NH_3 and CO_2 were used as probe molecules to evaluate the acid and base site strength and density on various surfaces. While these two probe molecules are widely used, their usefulness to explain reactivity trends in ethanol coupling appears to be limited. Carbon dioxide for example forms a variety of surface species that are quite different than the moiety that forms from ethanol adsorption on basic oxides (ethoxide). While ethanol and methanol have been used as probes in DRIFTS studies to interrogate the surfaces, other alcohols or organic acids might provide more information about the strength, type and quantity of surface base sites. Ammonia also has limitations as a probe molecule since it can react with surface base sites. It could be advantageous to use a basic probe molecule that cannot be deprotonated and has a lower likelihood of hydrogen bonding, such as trimethy- or triethyl-amine.

In-situ analysis using DRIFTS

In Chapter 4, in-situ measurements of surface adsorption modes were completed over MgO. While this provided information about surface species present in this case, it could be expanded to compare other materials with different activity or selectivity in the various probe reactions. One interesting comparison would be MgO and ZrO_2. It may be informative to see if the tendency of a material to catalyze dehydration vs dehydrogenation could be related to the strength of the alkoxide surface bond. Additionally, co-feeding of gas phase acids and bases might be used to selectively poison different types of sites and correlate observations with changes in reactivity. Examples of these co-fed poisons could include:

- carbon dioxide to selectively bind to strong base sites (those that do not desorb CO_2 below reaction temperature)
- a stronger acid than carbon dioxide, such as acetic acid, to bind a larger percentage of the available base sites
- A molecule like 2,6-di-t-butylpyridine that can possibly only react with Brønsted acid sites (to help probe which sites are active for dehydration over MgO and ZrO_2)

Model dehydrogenation reaction

Much like acetone condensation is often used as a model for aldol condensation dehydrogenation of a model alcohol might be usedul to explore the catalysts. This type of study

would simplify determination of kinetic parameters like activation energies and orders of reaction for alcohol dehydrogenation. One such possible molecule would be neopentyl alcohol or 2,2-dimethylpropan-1-ol.

References

[1] M. Guerbet, Condensation de l'alcool isopropylique avec son dérivé sodé; formation du méthylisobutylcarbinol et du diméthyl-2.4-heptanol-6, C.R. Acad. Sci. Paris. (1899) 1002.

[2] A.J. O'Lenick, Guerbet chemistry, J. Surfactants Deterg. 4 (2001) 311–315.

[3] O. Fuchs, U.S. Patent 1,992,480, 1931.

[4] J.P. Wibaut, U.S. Patent 1,910,582, 1933.

[5] O. Fuchs, U.S. Patent 2,092,450, 1937.

[6] E.E. Burgoyne, U.S. Patent 2,645,667, 1951.

[7] R.E. Miller, G.E. Bennett, U.S. Patent 2,762,847, 1956.

[8] R.E. Miller, U.S. Patent 2,836,628, 1958.

[9] M.W. Farrar, W. Groves, U.S. Patent 2,971,033, 1961.

[10] G. Pregaglia, G. Gregorio, U.S. Patent 3,514,493, 1970.

[11] R. Clark, U.S. Patent 3,972,952, 1976.

[12] P.G. Abend, P. Leenders, U.S. Patent 4,011,273, 1977.

[13] M. Matsuda, M. Horio, U.S. Patent 4,518,810, 1985.

[14] J.R. Budge, S.V. Compton, U.S. Patent 4,681,868, 1986.

[15] A. Clark, F.E. Condon, U.S. Patent 2,593,009, 1952.

[16] J. Herzenberg, G. Cevidalli, A. Nenz, U.S. Patent 2,861,110, 1958.

[17] R.L. Poe, U.S. Patent 3,328,470, 1967.

[18] J.E. Yates, U.S. Patent 3,864,407, 1975.

[19] J.E. Yates, U.S. Patent 3,979,466, 1976.

[20] C.A. Carter, U.S. Patent 2,457,866, 1949.

[21] J.K. Wilkinsburg, J.G.D. Schulz, U.S. Patent 3,119,880, 1964.

[22] G. Pregaglia, G. Gregorio, F. Conti, U.S. Patent 3,479,412, 1969.

[23] N.L. Cull, J.K. Mertzweiller, U.S. Patent 2,829,177, 1958.

[24] K.W. Yang, X.Z. Jiang, W.C. Zhang, One-step Synthesis of n-Butanol from Ethanol Condensation over Alumina-supported Metal Catalysts, Chinese Chem. Lett. 15 (2004) 1497–1500.

[25] C. Carlini, A. Macinai, M. Marchionna, M. Noviello, A.M.R. Galletti, G. Sbrana, Selective synthesis of isobutanol by means of the Guerbet reaction: Part 3: Methanol/n-propanol condensation by using bifunctional catalytic systems based on nickel, rhodium and ruthenium species with basic components, J. Mol. Catal. A:Chem. 206 (2003) 409–418.

[26] C. Carlini, M. Di Girolamo, A. Macinai, M. Marchionna, M. Noviello, A.M.R. Raspolli Galletti, G. Sbrana, Selective synthesis of isobutanol by means of the Guerbet reaction: Part 2. Reaction of methanol/ethanol and methanol/ethanol/n-propanol mixtures over copper based/MeONa catalytic systems, J. Mol. Catal. A:Chem. 200 (2003) 137–146.

[27] C. Carlini, C. Flego, M. Marchionna, M. Noviello, A.M.R. Galletti, G. Sbrana, F. Basile, A. Vaccari, Guerbet condensation of methanol with n-propanol to isobutyl alcohol over heterogeneous copper chromite/Mg-Al mixed oxides catalysts, J. Mol. Catal. A:Chem. 220 (2004) 215–220.

[28] C. Carlini, M.D. Girolamo, M. Marchionna, M. Noviello, A.M.R. Galletti, G. Sbrana, Selective synthesis of isobutanol by means of the Guerbet reaction: Part 1. Methanol/n-propanol condensation by using copper based catalytic systems, J Mol. Catal. A:Chem. 184 (2002) 273–280.

[29] M.J.L. Gines, E. Iglesia, Bifunctional condensation reactions of alcohols on basic oxides modified by copper and potassium, J. Catal. 176 (1998) 155–172.

[30] Kirk-Othmer Publishing, Kirk-Othmer Encyclopedia of Chemical Technology, 5th ed., Wiley-Interscience, New York, 2004.

[31] J.I. Di Cosimo, C.R. Apesteguía, M.J.L. Ginés, E. Iglesia, Structural requirements and reaction pathways in condensation reactions of alcohols on Mg_yAlO_x catalysts, J. Catal. 190 (2000) 261–275.

[32] S. Ogo, A. Onda, K. Yanagisawa, Selective synthesis of 1-butanol from ethanol over strontium phosphate hydroxyapatite catalysts, Appl. Catal. A:Gen. 402 (2011) 188–195.

[33] V. Nagarajan, Kinetics of a complex reaction system preparation of n-butanol from ethanol in one step, Indian J. Technol. 9 (1971) 380–386.

[34] V. Nagarajan, N.R. Kuloor, Catalytic Preparation of n-Butanol from Ethanol in One Step, Indian J. Technol. 4 (1966) 46–54.

[35] A.S. Ndou, N.J. Coville, Self-condensation of propanol over solid-base catalysts, Appl. Catal. A:Gen. 275 (2004) 103–110.

[36] S. Veibel, J. Nielsen, On the mechanism of the Guerbet reaction, Tetrahedron. 23 (1967) 1723–1733.

[37] J.F. Sanz, J. Oviedo, A. Márquez, J.A. Odriozola, M. Montes, Adsorption of Acetone onto MgO: Experimental and Theoretical Evidence for the Presence of a Surface Enolate, Angew. Chem. Int. Edit. 38 (1999) 506–509.

[38] S.E. Davis, B.N. Zope, R.J. Davis, On the mechanism of selective oxidation of 5-hydroxymethylfurfural to 2,5-furandicarboxylic acid over supported Pt and Au catalysts, Green Chem. 14 (2012) 143–147.

[39] S. Abelló, F. Medina, D. Tichit, J. Pérez-Ramírez, J.C. Groen, J.E. Sueiras, P. Salagre, Y. Cesteros, Aldol condensations over reconstructed Mg-Al hydrotalcites: structure-activity relationships related to the rehydration method., Chem. Eur. J. 11 (2005) 728–39.

[40] M.J. Climent, A. Corma, V. Fornés, R. Guil-Lopez, S. Iborra, Aldol Condensations on Solid Catalysts: A Cooperative Effect between Weak Acid and Base Sites, Adv. Synth. Catal. 344 (2002) 1090–1096.

[41] J.I. Di Cosimo, V.K. Díez, C.R. Apesteguía, Base catalysis for the synthesis of α,β-unsaturated ketones from the vapor-phase aldol condensation of acetone, Appl. Catal. A:Gen. 137 (1996) 149–166.

[42] G. Zhang, H. Hattori, K. Tanabe, Aldol condensation of acetone/acetone d6 over magnesium oxide and lanthanum oxide, Appl. Catal. 40 (1988) 183–190.

[43] G. Zhang, H. Hattori, K. Tanabe, Aldol Addition of Acetone, Catalyzed by Solid Base Catalysts: Magnesium Oxide, Calcium Oxide, Strontium Oxide, Barium Oxide, Lanthanum (III) Oxide and Zirconium Oxide, Appl. Catal. 36 (1988) 189–197.

[44] J. Oviedo, J.F. Sanz, Ab initio study of the adsorption of acetone and keto-enol equilibrium on the MgO(100) surface, Surf. Sci. 397 (1998) 23–33.

[45] C. Yang, Z.Y. Meng, Bimolecular condensation of ethanol to 1-butanol catalyzed by alkali cation zeolites, J. Catal. 142 (1993) 37–44.

[46] A.S. Ndou, N. Plint, N.J. Coville, Dimerisation of ethanol to butanol over solid-base catalysts, Appl. Catal. A:Gen. 251 (2003) 337–345.

[47] W.J. Toussaint, J. Lee Marsh, Manufacture of Butadiene From Alcohol, in: G.S. Whitby (Ed.), Synthetic Rubber, Wiley: New York, 1954: pp. 86–104.

[48] Y. Kitayama, M. Satoh, T. Kodama, Preparation of large surface area nickel magnesium silicate and its catalytic activity for conversion of ethanol into buta-1, 3-diene, Catal. Lett. (1996) 95–97.

[49] Y. Kitayama, A. Michishita, Catalytic activity of fibrous clay mineral sepiolite for butadiene formation from ethanol, J. Chem. Soc. Chem. Commun. (1981) 401–402.

[50] V. Gruver, A. Sun, J. Fripiat, Catalytic properties of aluminated sepiolite in ethanol conversion, Catal. Lett. 34 (1995) 359–364.

[51] H. Niiyama, S. Morii, E. Echigoya, Butadiene Formation from Ethanol over Silica-Magnesia Catalysts, B. Chem. Soc. Jpn. 45 (1972) 655–659.

[52] S. Kvisle, A. Aguero, R.P.A. Sneeden, Transformation of ethanol into 1,3-butadiene over magnesium oxide/silica catalysts, Appl. Catal. 43 (1988) 117–131.

[53] M.D. Jones, C.G. Keir, C. Di Iulio, R.A.M. Robertson, C. V. Williams, D.C. Apperley, Investigations into the conversion of ethanol into 1,3-butadiene, Catal. Sci. Technol. 1 (2011) 267–272.

[54] S. Ordóñez, E. Díaz, M. León, L. Faba, Hydrotalcite-derived mixed oxides as catalysts for different C–C bond formation reactions from bioorganic materials, Catal. Today. 167 (2010) 71–76.

[55] T. Tsuchida, J. Kubo, T. Yoshioka, S. Sakuma, T. Takeguchi, W. Ueda, Reaction of ethanol over hydroxyapatite affected by Ca/P ratio of catalyst, J. Catal. 259 (2008) 183–189.

[56] J. Sun, K. Zhu, F. Gao, C. Wang, J. Liu, Direct Conversion of Bio-ethanol to Isobutene on Nanosized $Zn_xZr_yO_z$ Mixed Oxides with Balanced Acid-Base Sites, J. Am. Chem. Soc. 133 (2011) 11096–11099.

[57] T. Nishiguchi, T. Matsumoto, H. Kanai, K. Utani, Y. Matsumura, W. Shen, S. Imamura, Catalytic steam reforming of ethanol to produce hydrogen and acetone, Appl. Catal. A:Gen. 279 (2005) 273–277.

[58] J. Bussi, S. Parodi, B. Irigaray, R. Kieffer, Catalytic transformation of ethanol into acetone using copper-pyrochlore catalysts, Appl. Catal. A:Gen. 172 (1998) 117–129.

[59] T. Nakajima, H. Nameta, S. Mishima, I. Matsuzaki, K. Tanabe, A highly active and highly selective oxide catalyst for the conversion of ethanol to acetone in the presence of water vapour, J. Mater. Chem. 4 (1994) 853–858.

[60] F. Haga, T. Nakajima, K. Yamashita, S. Mishima, Effect of crystallite size on the catalysis of alumina-supported cobalt catalyst for steam reforming of ethanol, React. Kinet. Catal. Lett. 63 (1998) 253–259.

[61] T. Nakajima, T. Yamaguchi, K. Tanabe, Efficient synthesis of acetone from ethanol over ZnO-CaO catalyst, J. Chem. Soc. Chem. Commun. (1987) 394.

[62] S. Lippert, W. Baumann, K. Thomke, Secondary reactions of the base-catalyzed aldol condensation of acetone, J. Mol. Catal. 69 (1991) 199–214.

[63] J.M. Christensen, P.A. Jensen, N.C. Schiødt, A.D. Jensen, Coupling of Alcohols over Alkali-Promoted Cobalt-Molybdenum Sulfide, ChemCatChem. 2 (2010) 523–526.

[64] J. Nunan, C. Bogdan, K. Klier, K. Smith, Higher alcohol and oxygenate synthesis over cesium-doped Cu/ZnO catalysts, J. Catal. 116 (1989) 195–221.

[65] M. Xu, E. Iglesia, Carbon–Carbon bond formation pathways in CO hydrogenation to higher alcohols, J. Catal. 131 (1999) 125–131.

[66] W. Ueda, T. Kuwabara, T. Ohshida, Y. Morikawa, A low-pressure guerbet reaction over magnesium oxide catalyst, J. Chem. Soc. Chem. Commun. (1990) 1558–1559.

[67] W. Ueda, T. Ohshida, T. Kuwabara, Y. Morikawa, Condensation of alcohol over solid-base catalyst to form higher alcohols, Catal. Lett. 12 (1992) 97–104.

[68] P. Kustrowski, D. Sulkowska, L. Chmielarz, A. Rafalskalasocha, B. Dudek, R. Dziembaj, Influence of thermal treatment conditions on the activity of hydrotalcite-derived Mg-Al oxides in the aldol condensation of acetone, Microporous Mesoporous Mater. 78 (2005) 11–22.

[69] J.I. Di Cosimo, V.K. Díez, M. Xu, E. Iglesia, C.R. Apesteguía, Structure and Surface and Catalytic Properties of Mg-Al Basic Oxides, J. Catal. 178 (1998) 499–510.

[70] D.L. Carvalho, R.R. de Avillez, M.T. Rodrigues, L.E.P. Borges, L.G. Appel, Mg and Al mixed oxides and the synthesis of n-butanol from ethanol, Appl. Catal. A:Gen. 415-416 (2012) 96–100.

[71] C. Kibby, W. Hall, Dehydrogenation of alcohols and hydrogen transfer from alcohols to ketones over hydroxyapatite catalysts, J. Catal. 31 (1973) 65–73.

[72] S. Ogo, A. Onda, K. Yanagisawa, Hydrothermal synthesis of vanadate-substituted hydroxyapatites, and catalytic properties for conversion of 2-propanol, Appl. Catal. A:Gen. 348 (2008) 129–134.

[73] C. Kibby, W. Hall, Studies of acid catalyzed reactions: XII. Alcohol decomposition over hydroxyapatite catalysts, J. Catal. 29 (1973) 144–159.

[74] Ndou, A.S. Ndou, N.J. Coville, Self-condensation of propanol over solid-base catalysts, Appl. Catal. A:Gen. 275 (2004) 103–110.

[75] P.E. Hathaway, M.E. Davis, Base catalysis by alkali modified zeolites: III. Alkylation with methanol, J. Catal. 119 (1989) 497–507.

[76] M.M. Branda, A.H. Rodríguez, P.G. Belelli, N.J. Castellani, Ethanol adsorption on MgO surface with and without defects from a theoretical point of view, Surf. Sci. 603 (2009) 1093–1098.

[77] H. Petitjean, K. Tarasov, F. Delbecq, P. Sautet, J.M. Krafft, P. Bazin, M.C. Paganini, E. Giamello, M. Che, H. Lauron-Pernot, G. Costentin, Quantitative Investigation of MgO Brønsted Basicity: DFT, IR, and Calorimetry Study of Methanol Adsorption, J. Phys. Chem. C. 114 (2010) 3008–3016.

[78] M.M. Branda, P.G. Belelli, R.M. Ferullo, N.J. Castellani, Proton abstraction ability of MgO: a DFT cluster model study of the role of surface geometry, Catal. Today. 85 (2003) 153–165.

[79] M. Bailly, C. Chizallet, G. Costentin, J. Krafft, H. Lauron-Pernot, M. Che, A spectroscopy and catalysis study of the nature of active sites of MgO catalysts: Thermodynamic Brønsted basicity versus reactivity of basic sites, J. Catal. 235 (2005) 413–422.

[80] J.T. Kozlowski, M.T. Aronson, R.J. Davis, Transesterification of tributyrin with methanol over basic Mg:Zr mixed oxide catalysts, Appl. Catal. B:Environ. 96 (2010) 508–515.

[81] V.K. Díez, C.R. Apesteguía, J.I. Di Cosimo, Acid-base properties and active site requirements for elimination reactions on alkali-promoted MgO catalysts, Catal. Today. 63 (2000) 53–62.

[82] Y. Shinohara, H. Satozono, T. Nakajima, S. Suzuki, S. Mishima, Study of the Interaction of Ethanol with Bronsted and Lewis Acid Sites on Metal Oxide Surfaces Using the DV-Xα Method, J. Chem. Software. 4 (1998) 41–50.

[83] V.A. Ivanov, J. Bachelier, F. Audry, J.C. Lavalley, Study of the Meerwein—Pondorff—Verley reaction between ethanol and acetone on various metal oxides, J. Mol. Catal. 91 (1994) 45–59.

[84] J. Ruiz, C. Jiménez-Sanchidrián, Heterogeneous Catalysis in the Meerwein-Ponndorf-Verley Reduction of Carbonyl Compounds, Curr. Org. Chem. 11 (2007) 1113–1125.

[85] J.N. Kondo, K. Ito, E. Yoda, F. Wakabayashi, K. Domen, An ethoxy intermediate in ethanol dehydration on Brønsted acid sites in zeolite., J. Phys. Chem. 109 (2005) 10969–10972.

[86] M.A. Aramendía, V. Borau, C. Jiménez, J.M. Marinas, A. Porras, F.J. Urbano, Magnesium Oxides as Basic Catalysts for Organic Processes Study of the Dehydrogenation–Dehydration of 2-Propanol, J. Catal. 161 (1996) 829–838.

[87] E. Iglesia, D.G. Barton, J.A. Biscardi, M.J.L. Gines, S.L. Soled, Bifunctional pathways in catalysis by solid acids and bases, Catal. Today. 38 (1997) 339–360.

[88] N.E. Fouad, P. Thomasson, H. Knözinger, Surface reactions of acetone, acetylene and methylbutynol on a yttrium-modified magnesium oxide catalyst, Appl. Catal. A:Gen. 196 (2000) 125–133.

[89] C. Ma, G. Liu, Z. Wang, Y. Li, J. Zheng, W. Zhang, M. Jia, Aldol condensation of acetone over Mg–Al mixed oxides catalyst prepared by a citric acid route, React. Kinet. Catal. Lett. 98 (2009) 149–156.

[90] J. Tai, R.J. Davis, Synthesis of methacrylic acid by aldol condensation of propionic acid with formaldehyde over acid–base bifunctional catalysts, Catal. Today. 123 (2007) 42–49.

[91] I. Sádaba, M. Ojeda, R. Mariscal, J.L.G. Fierro, M.L. Granados, Catalytic and structural properties of co-precipitated Mg–Zr mixed oxides for furfural valorization via aqueous aldol condensation with acetone, Appl. Catal. B:Environ. 101 (2011) 638–648.

[92] C.J. Barrett, J.N. Chheda, G.W. Huber, J.A. Dumesic, Single-reactor process for sequential aldol-condensation and hydrogenation of biomass-derived compounds in water, Appl. Catal. B:Environ. 66 (2006) 111–118.

[93] J. Lercher, H. Noller, G. Ritter, Acetone on magnesia. An infrared and temperature programmed desorption study, J. Chem. Soc. Faraday Trans. 1 (1981) 621–628.

[94] Sasol, Density Tables for Sasol Solvents and Sasol Acrylates Products in the range 0 ^{o}C to 40 ^{o}C, (2009) 6.

[95] C. Carlini, M. Marchionna, M. Noviello, A.M.R. Galletti, G. Sbrana, F. Basile, A. Vaccari, Guerbet condensation of methanol with n-propanol to isobutyl alcohol over heterogeneous bifunctional catalysts based on Mg–Al mixed oxides partially substituted by different metal components, J. Mol. Catal. A:Chem. 232 (2005) 13–20.

[96] M. Di Serio, M. Ledda, M. Cozzolino, G. Minutillo, R. Tesser, E. Santacesaria, Transesterification of Soybean Oil to Biodiesel by Using Heterogeneous Basic Catalysts, Ind. Eng. Chem. Res. 45 (2006) 3009–3014.

[97] M. Diasakou, A. Louloudi, N. Papayannakos, Kinetics of the non-catalytic transesterification of soybean oil, Fuel. 77 (1998) 1297–1302.

[98] F. Ma, M.A. Hanna, Biodiesel production: a review, Bioresour. Technol. 70 (1999) 1–15.

[99] J. Van Gerpen, Biodiesel processing and production, Fuel Process. Technol. 86 (2005) 1097–1107.

[100] A.C. Pinto, L.L.N. Guarieiro, M.J.C. Rezende, N.M. Ribeiro, E.A. Torres, W.A. Lopes, P.A. de P. Pereira, J.B. de Andrade, Biodiesel: an overview, J. Brazil Chem. Soc. 16 (2005) 1313–1330.

[101] F. Figueras, M.L. Lakshmi, B.M. Choudary, Solid Base Catalysts in Organic Synthesis, Curr. Org. Chem. 10 (2006) 1627–1637.

[102] N. Barakos, S. Pasias, N. Papayannakos, Transesterification of triglycerides in high and low quality oil feeds over an HT2 hydrotalcite catalyst, Bioresource Technol. 99 (2008) 5037–5042.

[103] Y. Xi, R. Davis, Influence of water on the activity and stability of activated MgAl hydrotalcites for the transesterification of tributyrin with methanol, J. Catal. 254 (2008) 190–197.

[104] G. Vicente, M. Martínez, J. Aracil, Integrated biodiesel production: a comparison of different homogeneous catalysts systems, Bioresource Technol. 92 (2004) 297–305.

[105] Z. Shi, L. Xu, S. Da, Y. Feng, Study of the magnesia additive on the characterization of zirconia–magnesia composite sphere, Microporous Mesoporous Mater. 94 (2006) 34–39.

[106] D.E. López, J.G. Goodwin Jr., D.A. Bruce, E. Lotero, Transesterification of triacetin with methanol on solid acid and base catalysts, Appl. Catal. A:Gen. 295 (2005) 97–105.

[107] A.L. McKenzie, C.T. Fishel, R.J. Davis, Investigation of the surface structure and basic properties of calcined hydrotalcites, J. Catal. 138 (1992) 547–561.

[108] C.T. Fishel, R.J. Davis, Use of catalytic reactions to probe Mg-Al mixed oxide surfaces, Catal. Lett. 25 (1994) 87–95.

[109] E.J. Doskocil, S.V. Bordawekar, R.J. Davis, Alkali–Support Interactions on Rubidium Base Catalysts Determined by XANES, EXAFS, CO_2 Adsorption, and IR Spectroscopy, J. Catal. 169 (1997) 327–337.

[110] M.A. Aramendía, V. Borau, C. Jiménez, Catalytic hydrogen transfer from 2-propanol to cyclohexanone over basic Mg-Al oxides, Appl. Catal. A:Gen. 255 (2003) 301–308.

[111] M.A. Aramendía, V. Borau, C. Jiménez, A. Marinas, J.M. Marinas, J.R. Ruiz, F.J. Urbano, Magnesium-containing mixed oxides as basic catalysts: base characterization by carbon dioxide TPD-MS and test reactions, J. Mol. Catal. A: Chem. 218 (2004) 81–90.

[112] J. Li, R.J. Davis, On the use of 1-butene double-bond isomerization as a probe reaction on cesium-loaded zeolite X, Appl. Catal. A:Gen. 239 (2003) 59–70.

[113] M. Tu, R.J. Davis, Cycloaddition of CO_2 to Epoxides over Solid Base Catalysts, J. Catal. 199 (2001) 85–91.

[114] L.C. Meher, D. Vidya Sagar, S. Naik, Technical aspects of biodiesel production by transesterification—a review, Renew. Sust. Energ. Rev. 10 (2006) 248–268.

[115] T. Yamaguchi, Application of ZrO_2 as a catalyst and a catalyst support, Catal. Today. 20 (1994) 199–217.

[116] R. Sree, N.S. Babu, P.S. Prasad, N. Lingaiah, Transesterification of edible and non-edible oils over basic solid Mg/Zr catalysts, Fuel Process. Technol. 90 (2009) 152–157.

[117] M.L. Rojas-Cervantes, L. Alonso, J. Diaz-Teran, A.J. Lopez-Peinado, R.M. Martin-Aranda, V. Gomez-Serrano, Basic metal–carbons catalysts prepared by sol–gel method, Carbon. 42 (2004) 1575–1582.

[118] J.N. Chheda, J.A. Dumesic, An overview of dehydration, aldol-condensation and hydrogenation processes for production of liquid alkanes from biomass-derived carbohydrates, Catal. Today. 123 (2007) 59–70.

[119] M.A. Aramendía, V. Boráu, C. Jiménez, A. Marinas, J.M. Marinas, J.A. Navio, J.R. Ruiz, F.J. Urbano, Synthesis and textural-structural characterization of magnesia, magnesia-titania and magnesia-zirconia catalysts, Colloid. Surface A. 234 (2004) 17–25.

[120] D. Ciuparu, A. Ensuque, F. Bozon-Verduraz, Pd catalysts supported on MgO, ZrO_2 or MgO-ZrO_2: Preparation, characterization and study in hexane conversion, Appl. Catal. A:Gen. 326 (2007) 130–142.

[121] H. Gocmez, H. Fujimori, Synthesis and characterization of ZrO_2–MgO solid solutions by citrate gel process, Mater. Sci. Eng. B. 148 (2008) 226–229.

[122] S. Liu, X. Zhang, J. Li, N. Zhao, W. Wei, Y. Sun, Preparation and application of stabilized mesoporous MgO–ZrO_2 solid base, Catal. Commun. 9 (2008) 1527–1532.

[123] T. Settu, Characterisation of MgO-ZrO_2 precursor powders prepared by in-situ peptisation of coprecipitated oxalate gel, Ceram. Int. 26 (2000) 517–521.

[124] S.V. Bordawekar, E.J. Doskocil, R.J. Davis, Microcalorimetric study of CO_2 and NH_3 adsorption on Rb-and Sr-modified catalyst supports, Langmuir. 14 (1998) 1734–1738.

[125] D. Bianchi, T. Chafik, M. Khalfallah, S.J. Teichner, Intermediate species on zirconia supported methanol aerogel catalysts. IV. Adsorption of carbon dioxide, Appl. Catal. A:Gen. 123 (1994) 89–110.

[126] V. Bolis, G. Magnacca, G. Cerrato, C. Morterra, Microcalorimetric and IR-spectroscopic study of the room temperature adsorption of CO_2 on pure and sulphated t-ZrO_2, Thermochim. Acta. 379 (2001) 147–161.

[127] B. Bachiller-Baeza, I. Rodriguez-Ramos, A. Guerrero-Ruiz, Interaction of Carbon Dioxide with the Surface of Zirconia Polymorphs, Langmuir. 14 (1998) 3556–3564.

[128] G. A. H. Mekhemer, S. A. Halawy, M. A. Mohamed, M.I. Zaki, Qualitative and Quantitative Assessments of Acid and Base Sites Exposed on Polycrystalline MgO Surfaces: Thermogravimetric, Calorimetric, and in-Situ FTIR Spectroscopic Study Combination, J. Phys. Chem. B. 108 (2004) 13379–13386.

[129] K.T. Jung, A.T. Bell, Effects of catalyst phase structure on the elementary processes involved in the synthesis of dimethyl carbonate from methanol and carbon dioxide over zirconia, Top. Catal. 20 (2002) 97–105.

[130] F. Khairallah, A. Glisenti, Synthesis, characterization and reactivity study of nanoscale magnesium oxide, J. Mol. Catal. A: Chem. 274 (2007) 137–147.

[131] R. Vidruk, M. V Landau, M. Herskowitz, M. Talianker, N. Frage, V. Ezersky, Grain boundary control in nanocrystalline MgO as a novel means for significantly enhancing surface basicity and catalytic activity, J. Catal. 263 (2009) 196–204.

[132] I. Sádaba, M. Ojeda, R. Mariscal, R. Richards, M.L.L. Granados, Mg–Zr mixed oxides for aqueous aldol condensation of furfural with acetone: Effect of preparation method and activation temperature, Catal. Today. 167 (2010) 77–83.

[133] K. Tanabe, T. Yamaguchi, Acid-base bifunctional catalysis by ZrO_2 and its mixed oxides, Catal. Today. 20 (1994) 185–197.

[134] M.A. Aramendía, V. Borau, C. Jiménez, J.M. Marinas, J.R. Ruiz, F.J. Urbano, Influence of the preparation method on the structural and surface properties of various magnesium oxides and their catalytic activity in the Meerwein-Ponndorf-Verley reaction, Appl. Catal. A:Gen. 244 (2003) 207–215.

[135] M.A. Aramendía, V. Boráu, C. Jiménez, J.M. Marinas, A. Marinas, A. Porras, F.J. Urbano, Synthesis and Characterization of ZrO_2 as Acid–Basic Catalysts: Reactivity of 2-Methyl-3-butyn-2-ol, J. Catal. 183 (1999) 240–250.

[136] S. Huber, H. Knözinger, Adsorption of CH-acids on magnesia: An FTIR-spectroscopic study, J. Mol. Catal. A: Chem. 141 (1999) 117–127.

[137] D. Cornu, H. Guesmi, J. Krafft, H. Lauron-Pernot, Lewis Acido-Basic Interactions between CO_2 and MgO Surface: DFT and DRIFT Approaches, J. Phys. Chem. C. 116 (2012) 6645–6654.

[138] M. Bensitel, O. Saur, J. Lavalley, Use of methanol as a probe to study the adsorption sites of different MgO samples, Mater. Chem. Phys. 28 (1991) 309–320.

[139] M.A. Hasan, M.I. Zaki, L. Pasupulety, A spectroscopic investigation of isopropanol and methylbutynol as infrared reactive probes for base sites on polycrystalline metal oxide surfaces, J. Mol. Catal. A: Chem. 178 (2002) 125–137.

[140] C. Pighini, T. Belin, J. Mijoin, P. Magnoux, G. Costentin, H. Lauron-Pernot, Microcalorimetric and thermodynamic studies of CO_2 and methanol adsorption on magnesium oxide, Appl. Surf. Sci. 257 (2011) 6952–6962.

[141] A. Auroux, A. Gervasini, Microcalorimetric study of the acidity and basicity of metal oxide surfaces, J. Phys. Chem. 94 (1990) 6371–6379.

[142] C. Chizallet, M.L. Bailly, G. Costentin, H. Lauron-Pernot, J.M. Krafft, P. Bazin, J. Saussey, M. Che, Thermodynamic brønsted basicity of clean MgO surfaces determined by their deprotonation ability: Role of Mg^{2+}–O^{2-} pairs, Catal. Today. 116 (2006) 196–205.

[143] A.O. Menezes, P.S. Silva, E.P. Hernández, L.E.P. Borges, M.A. Fraga, Tuning surface basic properties of nanocrystalline MgO by controlling the preparation conditions., Langmuir. 26 (2010) 3382–3387.

[144] H. Lauron-Pernot, Evaluation of Surface Acido-Basic Properties of Inorganic-Based Solids by Model Catalytic Alcohol Reaction Networks, Catal. Rev. 48 (2006) 315–361.

[145] J.M. Montero, P. Gai, K. Wilson, A.F. Lee, Structure-sensitive biodiesel synthesis over MgO nanocrystals, Green Chem. 11 (2009) 265.

[146] K. Zhu, J. Hu, C. Kübel, R. Richards, Efficient preparation and catalytic activity of MgO(111) nanosheets, Angew. Chem. Int. Ed. 45 (2006) 7277–81.

[147] H. Kawakami, Y. Satohiro, Theoretical approach to the basicity of alkaline-earth metal oxide catalysts, J. Chem. Soc., Faraday Trans. (1984) 921–932.

[148] R. Kakkar, P.N. Kapoor, K.J. Klabunde, Theoretical Study of the Adsorption of Formaldehyde on Magnesium Oxide Nanosurfaces: Size Effects and the Role of Low-Coordinated and Defect Sites, J. Phys. Chem. B. 108 (2004) 18140–18148.

[149] C.A. Ferretti, S. Fuente, R. Ferullo, N. Castellani, C.R. Apesteguía, J.I. Di Cosimo, Monoglyceride synthesis by glycerolysis of methyl oleate on MgO: Catalytic and DFT study of the active site, Appl. Catal. A:Gen. 413-414 (2012) 322–331.

[150] J.L. Anchell, K. Morokuma, A.C. Hess, An electronic structure study of H_2 and CH_4 interactions with MgO and Li-doped MgO clusters, J. Chem. Phys. 99 (1993) 6004.

[151] S.V. Bordawekar, R.J. Davis, Probing the basic character of alkali-modified zeolites by CO_2 adsorption microcalorimetry, butene isomerization, and toluene alkylation with ethylene, J. Catal. 189 (2000) 79–90.

[152] Y. Xi, R.J. Davis, Influence of textural properties and trace water on the reactivity and deactivation of reconstructed layered hydroxide catalysts for transesterification of tributyrin with methanol, J. Catal. 268 (2009) 307–317.

[153] Y. Xi, R.J. Davis, Glycerol-intercalated Mg-Al Hydrotalcite As a Potential Solid Base Catalyst for Transesterification, Clay. Clay Miner. 58 (2010) 475–485.

[154] P. Thomasson, O.S. Tyagi, H. Knözinger, Characterisation of the basicity of modified MgO-catalysts, Appl. Catal. A:Gen. 181 (1999) 181–188.

[155] T. Tsuchida, S. Sakuma, T. Takeguchi, W. Ueda, Direct Synthesis of n -Butanol from Ethanol over Nonstoichiometric Hydroxyapatite, Ind. Eng. Chem. 45 (2006) 8634–8642.

[156] S.V. Bordawekar, E.J. Doskocil, R.J. Davis, Influence of support composition on the structure and reactivity of strontium base catalysts, Catal. Lett. 44 (1997) 193–199.

[157] Y. Xi, R.J. Davis, Intercalation of ethylene glycol into yttrium hydroxide layered materials., Inorg. Chem. 49 (2010) 3888–95.

[158] Y. Zhao, W. Li, M. Zhang, K. Tao, A comparison of surface acidic features between tetragonal and monoclinic nanostructured zirconia, Catal. Commun. 3 (2002) 239–245.

[159] A.A. Tsyganenko, D.V. Pozdnyakov, V.N. Filimonov, Infrared Study of Surface Species Arising from Ammonia Adsorption Oxide Surfaces, J. Mol. Struct. 29 (1975) 299–318.

[160] M. Zaki, M. Hasan, L. Pasupulety, Surface reactions of acetone on Al_2O_3, TiO_2, ZrO_2, and CeO_2: IR spectroscopic assessment of impacts of the surface acid-base properties, Langmuir. 17 (2001) 768–774.

[161] M. León, E. Díaz, S. Ordóñez, Ethanol catalytic condensation over Mg–Al mixed oxides derived from hydrotalcites, Catal. Today. 164 (2011) 436–442.

[162] C. Carlini, M.D. Girolamo, A. Macinai, M. Marchionna, M. Noviello, A.M.R. Galletti, G. Sbrana, Synthesis of isobutanol by the Guerbet condensation of methanol with n-propanol in the presence of heterogeneous and homogeneous palladium-based catalytic systems, J. Mol. Catal. A-Chem. 204 (2003) 721–728.

[163] M.N. Dvornikoff, M.W. Farrar, Condensation of alcohols, J. Org. Chem. 22 (1957) 540–542.

[164] T.C. Hsiao, S.D. Lin, Methanol to Long-chain Oxygenates Over Mg/Al Mixed Oxides Supported Cu Catalysts, Catal. Lett. 119 (2007) 72–78.

[165] P. Biloen, Transient kinetic methods, J. Mol. Catal. 21 (1993) 17–24.

[166] C.O. Bennett, Understanding Heterogeneous Catalysis Through the Transient Method, in: A.T. Bell, L.L. Hegedus (Eds.), Catalysis Under Transient Conditions, ACS Symposium Series; American Chemical Society, Washington, D.C., 1982: pp. 1–32.

[167] J. Happel, Transient Tracing, Chem. Eng. Sci. 33 (1978) 1567–1568.

[168] M. Depontes, G.H. Yokomizo, A.T. Bell, A Novel Method for Analyzing Transient-Response Data Obtained in Isotopic Tracer Studies of CO Hydrogenation, J. Catal. 104 (1987) 147–155.

[169] S.L. Shannon, J.G. Goodwin, Characterization of Catalytic Surfaces by Isotopic-Transient Kinetics during Steady-State Reaction, Chem. Rev. 95 (1995) 677–695.

[170] J.T. Calla, R.J. Davis, Oxygen-exchange reactions during CO oxidation over titania- and alumina-supported Au nanoparticles, J. Catal. 241 (2006) 407–416.

[171] J.T. Calla, M.T. Bore, A.K. Datye, R.J. Davis, Effect of alumina and titania on the oxidation of CO over Au nanoparticles evaluated by 13C isotopic transient analysis, J. Catal. 238 (2006) 458–467.

[172] J.T. Calla, R.J. Davis, Investigation of alumina-supported Au catalyst for CO oxidation by isotopic transient analysis and X-ray absorption spectroscopy., J. Phys. Chem. B. 109 (2005) 2307–14.

[173] S. Siporin, R. Davis, W. Raróg-Pilecka, D. Szmigiel, Z. Kowalczyk, Isotopic transient analysis of ammonia synthesis over Ba or Cs-promoted Ru/carbon catalysts, Catal. Lett. 93 (2004) 61–65.

[174] S.E. Siporin, R.J. Davis, Isotopic transient analysis of ammonia synthesis over Ru/MgO catalysts promoted by cesium, barium, or lanthanum, J. Catal. 222 (2004) 315–322.

[175] B.C. McClaine, R.J. Davis, Importance of Product Readsorption during Isotopic Transient Analysis of Ammonia Synthesis on Ba-Promoted Ru/BaX Catalyst, J. Catal. 211 (2002) 379–386.

[176] B.C. McClaine, R.J. Davis, Isotopic Transient Kinetic Analysis of Cs-Promoted Ru/MgO during Ammonia Synthesis, J. Catal. 210 (2002) 387–396.

[177] R.N. Spitz, J.E. Barton, M.A. Barteau, R.H. Staley, A.W. Sleight, Characterization of the surface acid-base properties of metal oxides by titration/displacement reactions, J. Phys. Chem. 1 (1986) 4067–4075.

[178] W. Ji, Y. Chen, H.H. Kung, Vapor phase aldol condensation of acetaldehyde on metal oxide catalysts, Appl. Catal. A:Gen. 161 (1997) 93–104.

[179] J. Li, J. Tai, R.J. Davis, Hydrocarbon oxidation and aldol condensation over basic zeolite catalysts, Catal. Today. 116 (2006) 226–233.

[180] K. Koda, T. Matsu-ura, Y. Obora, Y. Ishii, Guerbet Reaction of Ethanol to n-Butanol Catalyzed by Iridium Complexes, Chem. Lett. 38 (2009) 838–839.

[181] S. Ogo, A. Onda, Y. Iwasa, K. Hara, A. Fukuoka, K. Yanagisawa, 1-Butanol synthesis from ethanol over strontium phosphate hydroxyapatite catalysts with various Sr/P ratios, J. Catal. 296 (2012) 24–30.

[182] S. Axpuac, M.A. Aramendía, J. Hidalgo-Carrillo, A. Marinas, J.M. Marinas, V. Montes-Jiménez, F.J. Urbano, V. Borau, Study of structure–performance relationships in Meerwein–Ponndorf–Verley reduction of crotonaldehyde on several magnesium and zirconium-based systems, Catal. Today. 187 (2012) 183–190.

[183] J.F. Miñambres, M.A. Aramendía, A. Marinas, J.M. Marinas, F.J. Urbano, Liquid and gas-phase Meerwein–Ponndorf–Verley reduction of crotonaldehyde on ZrO_2 catalysts modified with Al_2O_3, Ga_2O_3 and In_2O_3, J. Mol. Catal. A: Chem. 338 (2011) 121–129.

[184] F.J. Urbano, M.A. Aramendía, A. Marinas, J.M. Marinas, An insight into the Meerwein–Ponndorf–Verley reduction of α,β-unsaturated carbonyl compounds: Tuning the acid–base properties of modified zirconia catalysts, J. Catal. 268 (2009) 79–88.

[185] M. Angeles Aramendía, V. Boráu, C. Jimenez, J.M. Marinas, A. Porras, F.J. Urbano, Synthesis and characterization of ZrO_2 as an acid–base catalyst Dehydration–dehydrogenation of propan-2-ol, J Chem. Soc. Faraday Trans. 93 (1997) 1431–1438.

[186] M. Cutrufello, I. Ferino, R. Monaci, E. Rombi, V. Solinas, Acid-base properties of zirconium, cerium and lanthanum oxides by calorimetric and catalytic investigation, Top. Catal. 19 (2002) 225–240.

[187] I. Marcu, D. Tichit, F. Fajula, N. Tanchoux, Catalytic valorization of bioethanol over Cu-Mg-Al mixed oxide catalysts, Catal. Today. 147 (2009) 231–238.

[188] S. Coluccia, E. Garrone, E. Borello, Infrared spectroscopic study of molecular and dissociative adsorption of ammonia on magnesium oxide, calcium oxide and strontium oxide, J. Chem. Soc., Faraday Trans. 79 (1983) 607.

[189] T.W. Birky, J.T. Kozlowski, R.J. Davis, Isotopic Transient Analysis of the Ethanol Coupling Reaction over Magnesia, J. Catal. In Press, DOI: 10.1016/j.jcat.2012.11.014.

[190] J.E. Rekoske, M.A. Barteau, Kinetics, Selectivity, and Deactivation in the Aldol Condensation of Acetaldehyde on Anatase Titanium Dioxide, Ind. Eng. Chem. Res. 50 (2011) 41–51.

Appendix A: Copper Containing Mixed Oxides

One possible way to increase the activity for ethanol coupling reactions would be to include copper, a known catalyst for dehydrogenation, in the material. The inclusion of copper in Mg and Zr mixed oxides was accomplished using a controlled precipitation method.

Synthesis Procedure

Two pumps were employed to feed two precursor solutions to the continuously stirred Labmax reactor. The first pump fed 1M NaOH solution, whereas the second pump fed the metal salt solution of appropriate concentrations of $MgNO_3$ $6H_2O$, $ZrO(NO_3)_2$ $5.4H_2O$, and $Cu(NO_3)_2$ $3H_20$. For example a 11:1:1 ratio of Mg:Zr:Cu in the final solid required a solution of 76.47 g magnesium nitrate, 6.05 g zirconyl nitrate and 4.41 g copper nitrate dissolved in 500 mL of deionized water. This metal salt solution was fed to the Labmax reactor, which had an initial volume of 400 mL of Deionized water with NaOH added to obtain an initial pH of 11, at a rate of 4.5 g min^{-1}. The solution was fed continuously until 390 grams had been pumped into the reactor. The NaOH solution was also fed to control the solution pH in the reactor to a constant value of 10.5. This pH of 10.5 was used rather than the pH of 10 in the prior work to provide a constant pH for precipitation. At a control pH of 10 the solution pH could not adequately controlled and large swings in pH were observed as the metal salt solution was added. The final solid catalyst was removed with vacuum filtration from the solution and the resulting solid was washed with deionized water. This washing procedure was repeated several times until the conductivity of the filtrate was below 0.05 mS m^{-1}.

Mg:Zr:Cu mixed oxide catalysts made include Mg:Zr:Cu predicted ratios of:

1. 11:1:1
2. 11:1:0.2
3. 11:0:1
4. 11:0:0.2
5. 0:1:1
6. 0:1:0.2

Additionally, the 0:1:0.2 Mg:Zr:Cu sample was impregnated with 5 wt.% sodium identically to how the zirconia samples were impregnated in Chapter 5. These samples were characterized using BET, XRD, and SEM. The characterization results along with a brief discussion of the catalysis is provided below.

Table A-1. Surface area and FHI identification number for the copper containing materials.

Mg:Zr:Cu Ratio	Surface Area (m^2 g^{-1})	FHI Number
11:1:1	-	10099
11:1:0.02	-	10100
11:0:1	149	10307
11:0:0.2	143	10308
0:1:1	132	10332
0:1:0.2	168	10334

SEM images of the materials showed little copper in the Mg:Cu samples (see Figure A-1). However, visual analysis (blue/black in Mg/Cu cases and green/blue when Zr is present with Cu) confirmed that Cu was incorporated into all samples. The Mg samples with both zirconia and copper showed that the copper preferentially segregated to the zirconia regions of the samples. One example of this segregation is shown in Figure A-2. The XRD pattern showed no copper phase in any of the samples and by visual color indication the zirconia and copper samples probably had some phase mixing (Cu can incorporate into ZrO_2 lattice at about 20 mol.%). All of the XRD patterns and SEM images can be found in the stored lab data under there FHI numbers specified above.

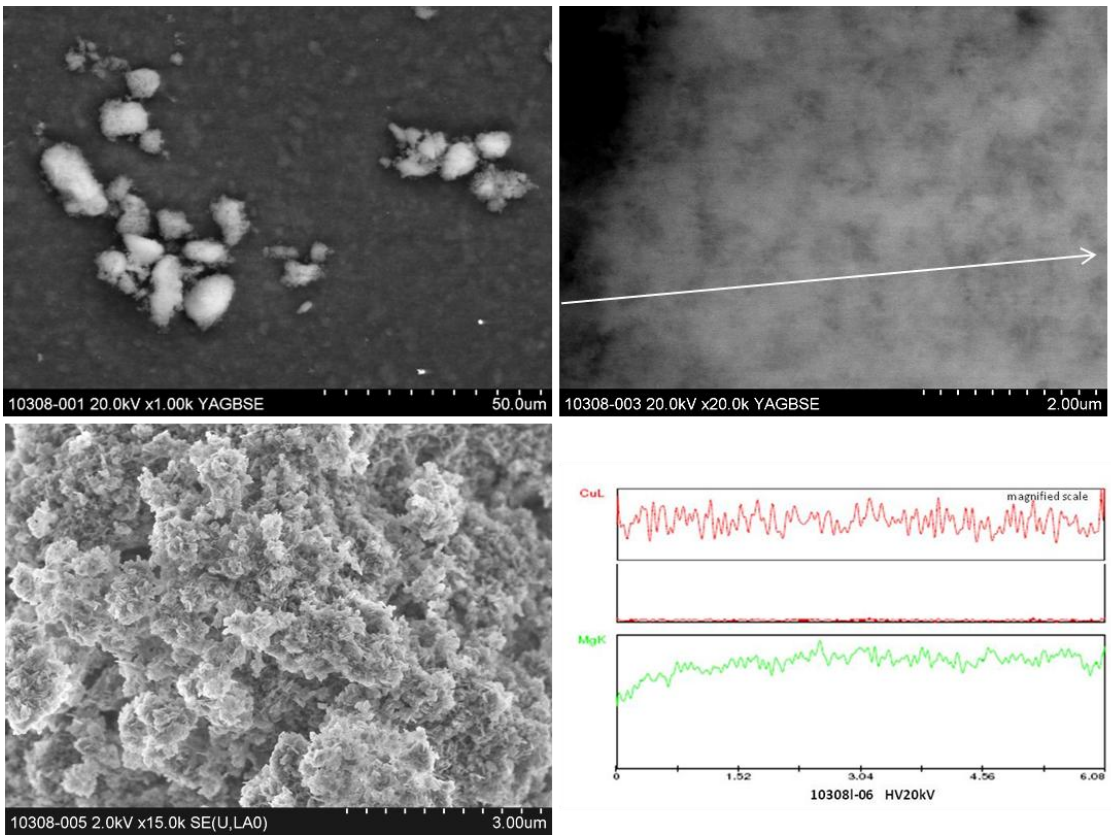

Figure A-1. SEM images and EDS line scans for the 11:0:0.2 sample.

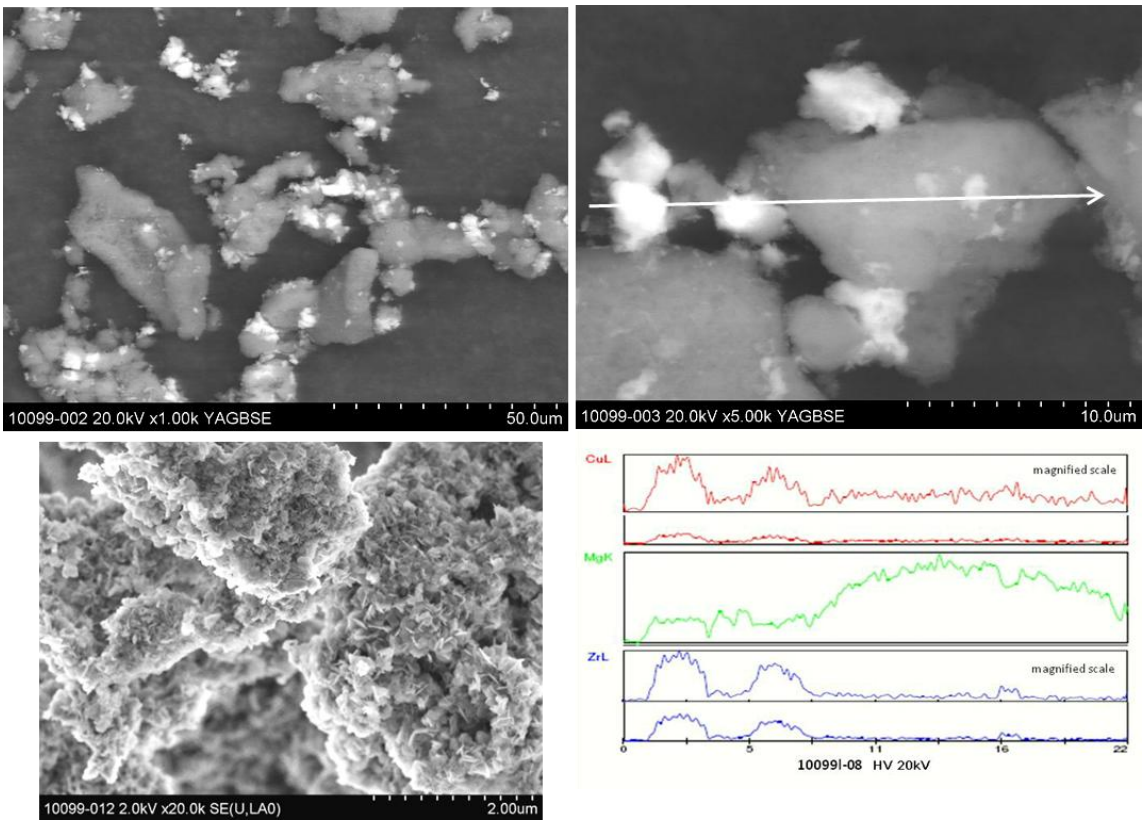

Figure A-2. SEM images and EDS line scans for the 11:1:1 sample.

Copper containing MgO (Mg:Cu 11:0.2) and ZrO_2 (Zr:Cu 1:0.2) samples were used in the ethanol coupling reaction with a reduction in flowing H_2 for 1 h at 523 K. The production rates for ethene, ethanal, crontonaldehyde and butanol are presented in Table A-2. For the copper containing MgO sample (11:0:0.2) it showed similar rates of product production compared to a pure MgO sample (Chapter 3). The addition of Na drastically lowered the dehydration rate of the Cu/ZrO_2 sample which is similar to what was observed in Chapter 5. All rates of copper containing materials were very similar to those observed over samples without the copper.

Table A-2. Ethanol reaction rates to ethene, ethanal and butanol.

Catalyst	Temperature (K)	Ethene Production Rate (nmol m^{-2} s^{-1})	Ethanal Production Rate (nmol m^{-2} s^{-1})	Crotonaldehyde Production Rate (nmol m^{-2} s^{-1})	Butanol Production Rate (nmol m^{-2} s^{-1})
11:0:0.2	673	2.1	9.4	0.4	1.5
0:1:0.2	613	25	11	0	0
0:1:0.2 + 5 wt.% Na	673	4.4	12	0	0

Appendix B: TEM images of Mg:Zr mixed oxides

Transmission electron microscopy of the rising pH precipitation of Mg:Zr mixed oxides was completed at FHI by Lide Yao. This technique was used since it has been postulated that one possible modification of MgO might occur at the MgO-ZrO_2 grain boundaries. Several example images are presented below. Not many definitive conclusions can be drawn, other than the zirconia looks to be amorphous along several of the grain boundaries. It does not look as clear cut a modification as Vidruk et al. observed.[131]

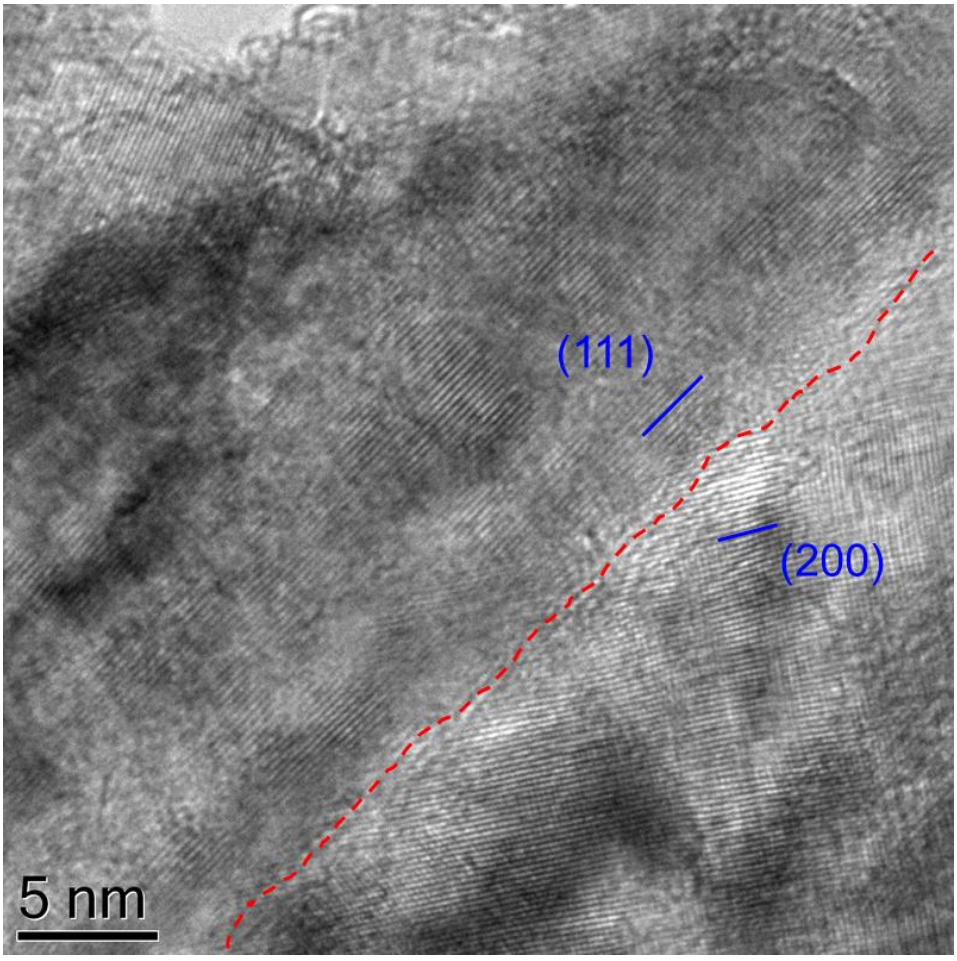

Figure B-1. TEM image of a MgO-MgO grain boundary in a pure MgO sample prepared by rising pH precipitation

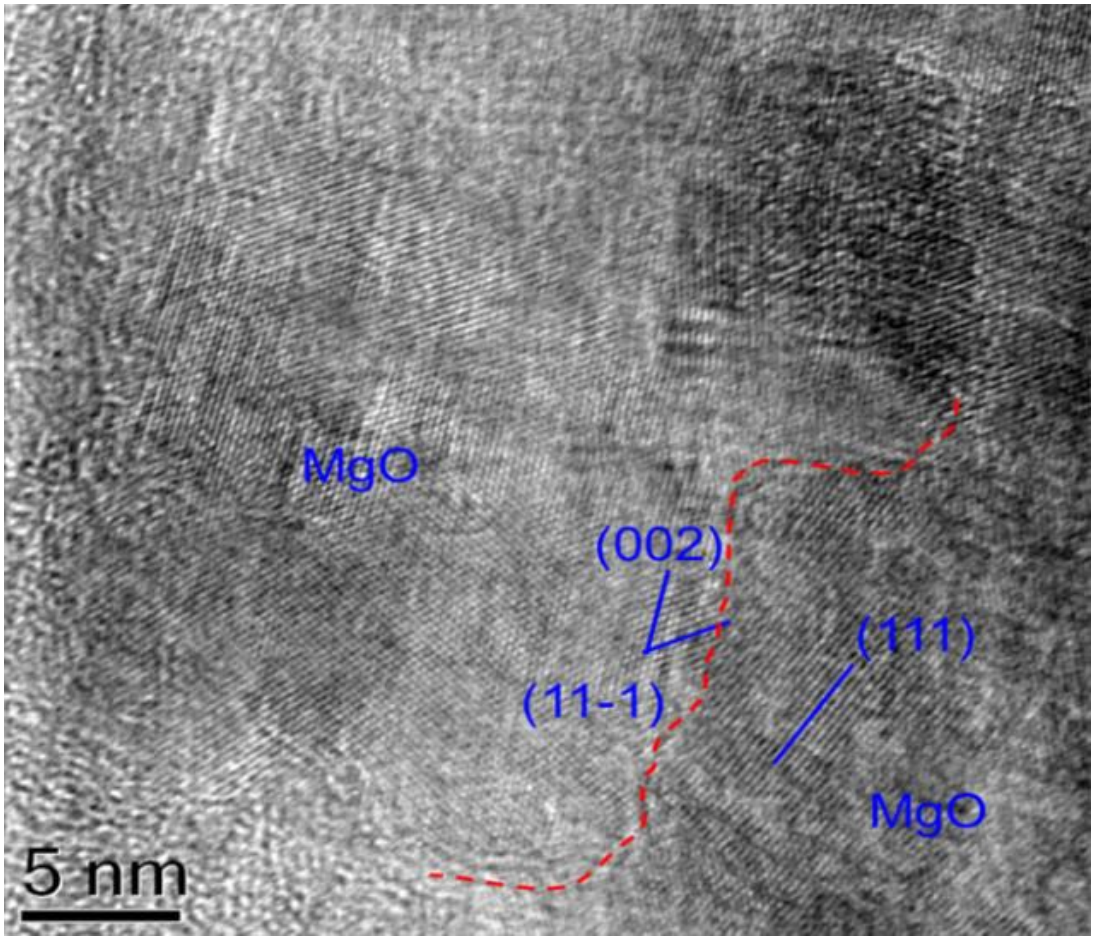

Figure B-2. TEM image of a MgO-MgO grain boundary in the Mg:Zr 11:1 mixed oxide prepared by rising pH precipitation

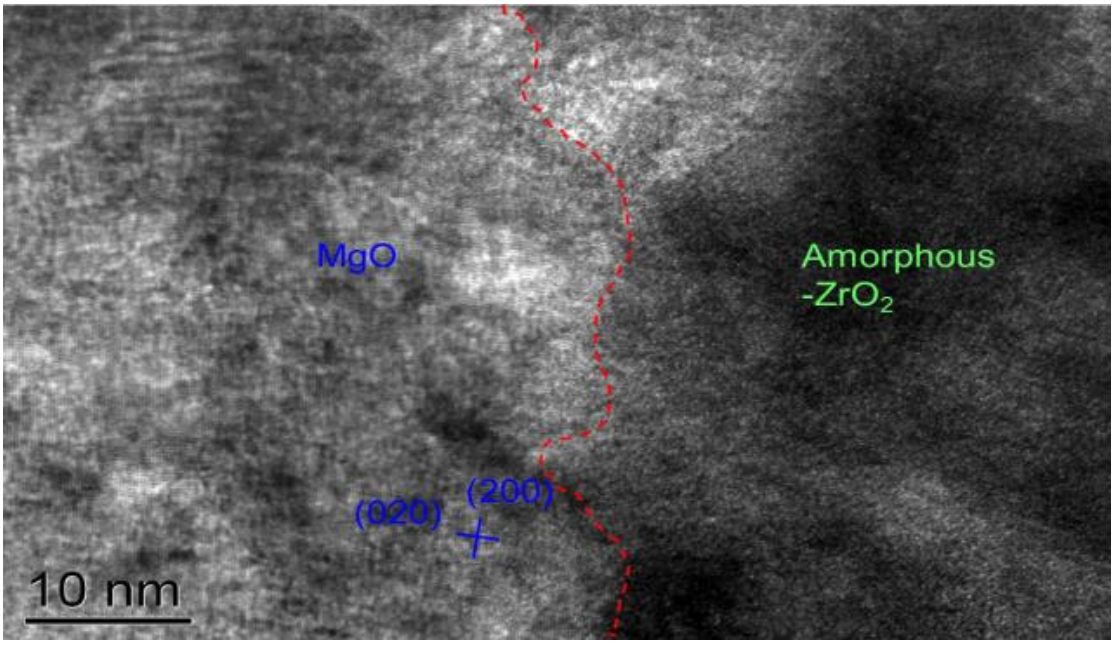

Figure B-3. TEM image of a MgO-ZrO_2 grain boundary in the Mg:Zr 11:1 mixed oxide prepared by rising pH precipitation

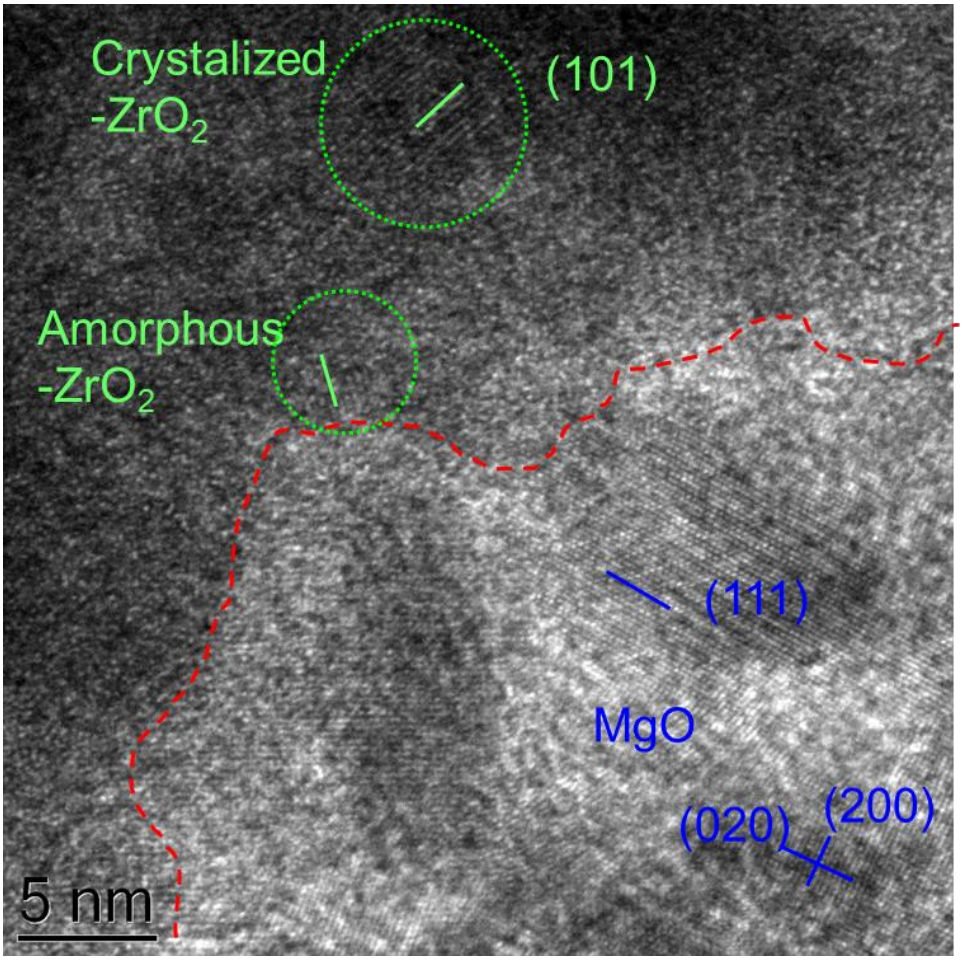

Figure B-4. TEM image of a MgO-ZrO_2 grain boundary in the Mg:Zr 11:1 mixed oxide prepared by rising pH precipitation

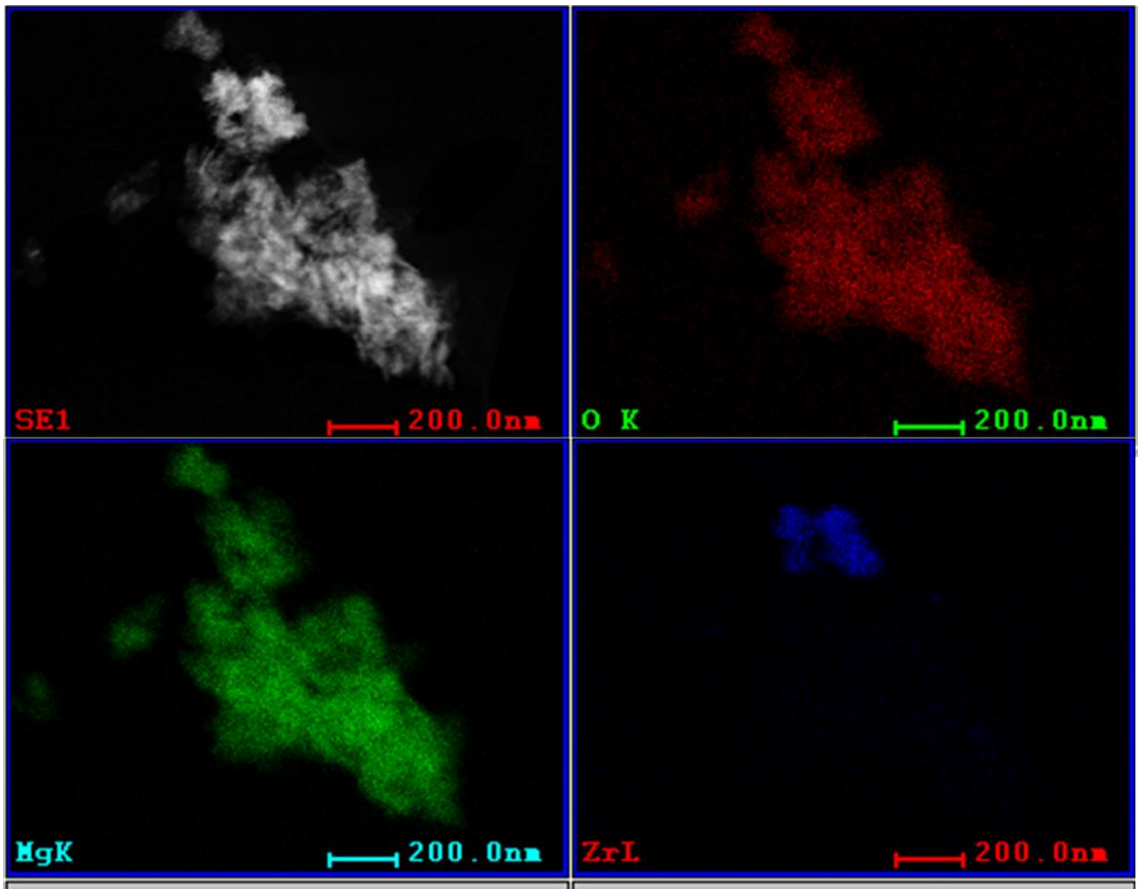

Figure B-5. Elemental mapping of one particle in Mg:Zr 11:1 mixed oxide prepared by rising pH precipitation

Finally, to confirm that 773 K was an appropriate temperature to perform the calcination TGA-DSC was performed on the controlled precipitation Mg:Zr 11:1 mixed oxide catalyst (Figure B-6). Little weight loss due to adsorbed carbonates or water was observed above 773 K and no exothermic or endothermic crystal transformation was observed. The results from DSC as well as a mass spec analysis of the desorbed products can be found in the saved data on the external drive in the Davis Lab.

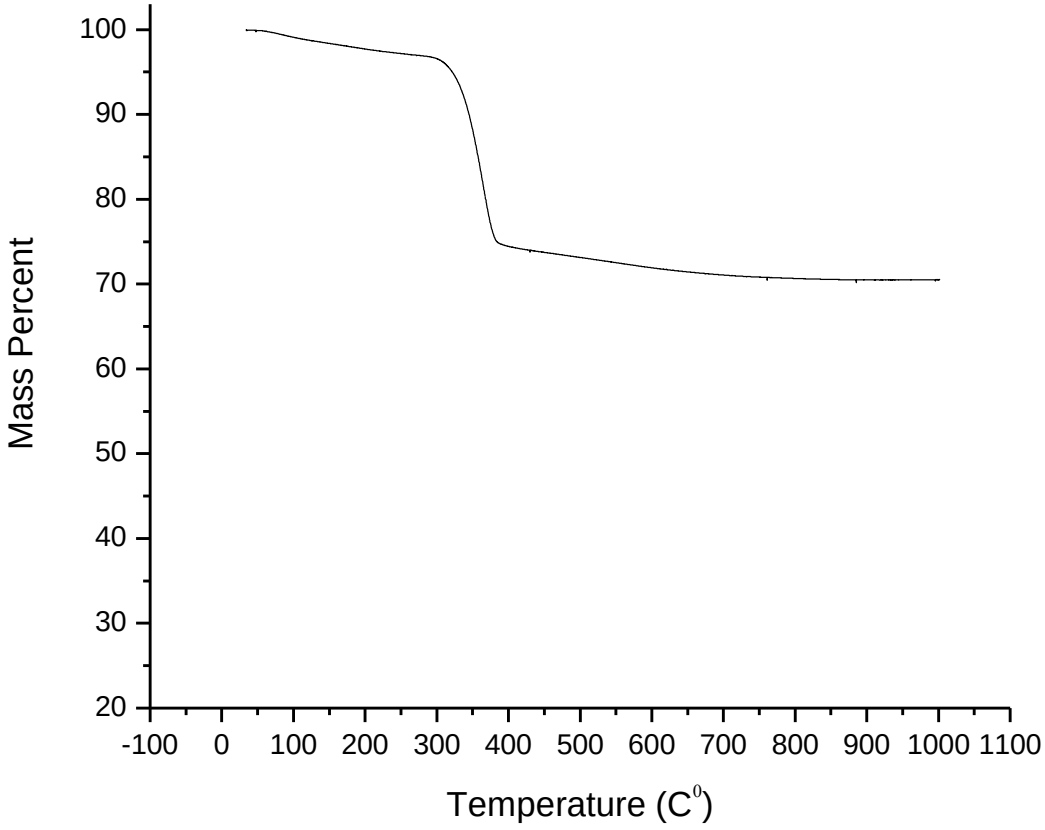

Figure B-6. TGA of Mg:Zr 11:1 mixed oxide in inert atmosphere.